

**Insight into the Intermolecular Interactions and
Functionality of the Recombinant PEX19-PEX26 Complex**

Dissertation

der Mathematisch-Naturwissenschaftlichen Fakultät
der Eberhard-Karls-Universität Tübingen
zur Erlangung des Grades eines
Doktors der Naturwissenschaften
(Dr. rer. nat.)

vorgelegt von
Erman Koçak
aus Çorum, Türkei

Tübingen

2019

Gedruckt mit Genehmigung der Mathematisch-Naturwissenschaftlichen
Fakultät der Eberhard-Karls-Universität Tübingen

Tag der mündlichen Qualifikation: 22.08.2019

Dekan: Prof. Dr. Wolfgang Rosenstiel

1.Berichterstatter Prof. Dr. Gabriele Dodt

2.Berichterstatter Prof. Dr. Dirk Schwarzer

„HAYATTA EN HAKİKİ MÜRŞİT İLİMDİR“

„THE TRUEST SPIRITUAL GUIDE IN LIFE IS SCIENCE“

MUSTAFA KEMAL ATATÜRK

For Ali, Cemil, Emine and Ersoy

I hereby declare, that I have authored the work filed for doctorate with the title "Insight into the Intermolecular Interactions and Functionality of the Recombinant PEX19-PEX26 Complex" myself, only used the sources and auxiliary materials cited and have labelled as such places adopted literally or with regards to content. I affirm under penalty of perjury that these statements are true and that I have concealed nothing. I am aware that the submission of a false affirmation under penalty of perjury is punishable by imprisonment of up to three years or a fine

Tübingen, July 18, 2019

Erman Koçak

Table of Contents

1. Summary	1
2. Introduction	3
2.1 Peroxisomes	3
2.1.1 Major metabolic pathways in peroxisomes	3
2.1.2 Peroxisomal matrix protein import.....	5
2.1.3 Peroxisomal membrane protein import	7
2.1.4 Peroxisome origin and biogenesis	9
2.1.5 Peroxisome biogenesis disorders	10
2.2 Tail-anchored membrane proteins	13
2.2.1 Tail-anchored membrane protein import into peroxisomes.....	14
2.2.1.1 PEX26	15
2.2.1.2 PEX3.....	17
2.2.1.3 PEX19.....	18
2.2.2 Tail-anchored membrane protein import into the ER	19
2.2.3 Tail-anchored membrane protein into mitochondria.....	20
2.3 Mass spectrometry analysis	21
2.3.1 Native mass spectrometry.....	22
2.3.2 Protein cross-linking coupled with mass spectrometry	24
3. Aims of the work	26
4. Materials and methods	27
4.1 Buffers, reagents and solutions	27
4.2 Molecular biology	27
4.2.1 Plasmids.....	27
4.2.2 Cloning and transformation	27

4.3 Protein analysis	30
4.3.1 Protein overproduction and purification.....	30
4.3.2 Bicinchoninic acid protein assay	32
4.3.4 Sodium dodecyl sulphate polyacrylamide gel electrophoresis.....	33
4.3.5 Western blot analysis	34
4.3.6 Native mass spectrometry.....	36
4.3.7 Protein cross-linking of nPEX3 and PEX19-PEX26	37
4.3.8 Protein digestion for mass spectrometry.....	38
4.3.9 Mass spectrometry analysis of nPEX3 and PEX19-PEX26	39
4.4 Cell culture experiments	39
4.4.1 Transformation of PEX26-deficient human fibroblasts.....	40
4.4.2 Immunostaining of fibroblasts	41
4.4.3 Immunofluorescence microscopy analysis.....	42
4.5 LUV Integration	42
4.5.1 Protein labelling of nPEX3 ^T and PEX19-PEX26	42
4.5.2 Preparation of large unilamellar vesicles (LUVs)	43
4.5.3 Dynamic light scattering analysis of LUVs	44
4.5.4 LUV-protein integration assay.....	44
4.5.5 Flow cytometry-based LUV-protein integration assay.....	46
4.5.6 Carbonate extraction of nPEX3 ^T and PEX26	46
5. Results	48
5.1. Optimizing the purification conditions of the PEX19-PEX26 complex.....	48
5.2. Purification of the recombinant PEX19-PEX26 complex.....	52
5.3. Ternary complex of co-expressed nPEX3, PEX19 and PEX26	55
5.4. Ternary complex of purified nPEX3 and PEX19-PEX26.....	57

5.5. Native MS analysis of the recombinant PEX19-PEX26 complex.....	62
5.6. XL-MS analysis of the PEX19-PEX26 complex	69
5.7. Complementation of PEX26-deficient fibroblasts.....	73
5.8. Flow cytometry analysis of PEX26 associations with LUVs.....	77
5.9. Carbonate extraction of LUV-associated PEX26	83
6. Discussion.....	88
6.1. Recombinant PEX26 and PEX19 form a binary complex	88
6.2. Native-MS confirms the binary PEX19-PEX26 complex.....	91
6.3. XL-MS reveals the interacting segments of the PEX19-PEX26 complex	92
6.4. The PEX19-PEX26 complex complemented PEX26-deficient cells	96
6.5. Flow cytometry indicates nPEX3 ^T -dependent PEX26 association with LUVs ..	97
6.6. Carbonate extraction confirms PEX26 insertion into the LUV membrane	99
7. Outlook	101
8 References	102
9. Appendix	117
Acknowledgments	124
Curriculum Vitae	125
Zusammenfassung	126

List of Abbreviations

AAA	ATPases associated with various cellular activities
ABCD	ATP-binding cassette subfamily D
Alexa488	Alexa Fluor™ 488 C ₅ - Maleimide
APS	Ammonium persulfate
ATP	Adenosine triphosphate
2-ME	2-mercaptoethanol
CG	Complementation group
CHO	Chinese Hamster Ovary
CoA	Coenzyme A
DMEM	Dulbecco's modified Eagle's medium
DNA	Deoxyribonucleic acid
dNTP	Deoxynucleotide triphosphate
DOL	Degree of labelling
DTT	Dithiothreitol
ECL	Enhanced chemoluminescence
<i>E. coli</i>	<i>Escherichia coli</i>
EDTA	Ethylenediaminetetraacetate
Egg PC	L- α -phosphatidylcholine (Chicken)
Egg PE	L- α -phosphatidylethanolamine (Chicken)
ER	Endoplasmic reticulum
ESI-MS	Electrospray ionization mass spectrometry
FCS	Fetal calf serum
FIS1	Fission protein 1
GET	Guided entry of tail-anchored proteins
GFP	Green fluorescent protein
HEPES	4-(2-hydroxyethyl)-1-piperazineethanesulfonic acid
HPLC	High performance liquid chromatography
HRP	Horseradish peroxidase
IPTG	Isopropyl-thiogalactopyranoside
IRD	Infantile Refsum disease
LB	Luria Bertani
LUV	Large unilamellar vesicles
MALDI-TOF	Matrix-assisted laser desorption/ionization time of flight mass spectrometry
MCS	Multiple cloning site
MOM	Mitochondrial outer membrane
MWCO	Molecular weight cut-off

NALD	Neonatal adrenoleukodystrophy
NHS	<i>N</i> -Hydroxysuccinimide
Ni-DGS	2-dioleoyl-sn-glycero-3-[(<i>N</i> -(5-amino-1-carboxypentyl) iminodiacetic acid) succinyl] (nickel salt)
OD600	Optical density at 600 nm
ORF	Open reading frame
PAGE	Polyacrylamide gel electrophoresis
PBD	Peroxisomal biogenesis disorder
PBS	Phosphate buffered saline
PCR	Polymerase chain reaction
PEG	Polyethylene glycol
PEX	Peroxin
PMP	Peroxisomal membrane protein
(m)PTS	(membrane) peroxisomal targeting sequence
PVDF	Polyvinylidene fluoride
rbs	Ribosomal binding site
RCDP	Rhizomelic chondrodysplasia punctata
ROS	Reactive oxygen species
SDS	Sodium dodecyl sulphate
SEC	Size exclusion chromatography
TA	Tail-anchored
TCEP	Tris-(2-carboxyethyl)phosphine
TEMED	Tetramethylethylenediamine
TEV	Tobacco etch virus
TIM	Translocase of the inner mitochondrial membrane
TMD	Transmembrane domain
TNT	Transcription and translation
TOC	Translocase of the outer membrane of chloroplasts
TOM	Translocase of the outer mitochondrial membrane
TPR	Tetratricopeptide repeat
TRIS	Tris-(hydroxymethyl)aminomethane
VLCFA	Very long chain fatty acid
WB	Western blotting
YFP	Yellow fluorescent protein
ZS	Zellweger syndrome

1. Summary

Peroxisomal membrane proteins (PMPs) function in various *mode of actions* as membrane receptors or docking proteins. They are mainly employed in the import of metabolites or matrix proteins as well as in the export machinery of the matrix protein receptor PEX5. PEX3 as one of *class II* PMPs serves as a docking protein on the peroxisome membrane for PEX19. Lack of PEX3 or PEX19 results in the absence of peroxisomes, as well as of peroxisomal remnants and in the degradation or mislocalisation of PMPs to other organelles such as mitochondria. PEX19 is a chaperone-like receptor protein recruiting *class I* PMPs that are employed in transport of metabolites like PMP22, PMP34 and PMP70 or are components of the docking-translocation complex (DTM) like PEX2, PEX10, PEX12 and PEX13. Besides that, PEX19 is also essential for the PEX26 import into the peroxisomal membrane, a protein that is one of the components of the receptor export module (REM). PEX26 as one of these tail-anchored (TA) *class I* PMPs is essential for the export of PEX5, recruiting the AAA-ATPase (PEX1-PEX6) to the peroxisomal membrane forming the REM. Depletion of the AAA-ATPase in *HeLa* cells results in accumulation of monoubiquitinated PEX5, thus in impaired matrix protein import. Phenotypically, deficiency of PEX26 was reported in all CG8-patients (Complementation Group 8) suffering from Zellweger syndrome which is referred to as the most severe peroxisomal biogenesis disorder. Overexpression of *PEX26*-cDNA in *E. coli* resulted in highly insoluble or aggregated PEX26. In contrast, its co-expression with *PEX19* revealed a stable and soluble binary complex. Here we could successfully overexpress *PEX19* and *PEX26* as a binary complex through a two-promoter *E. coli* system without using any denaturing agent for the solubilisation. This provided us with an *in vitro* native-like complex that could be analysed by using two different methods, size exclusion chromatography and native-MS. Furthermore, we elucidated the interacting domains of this binary complex by XL-MS employing the cross-linking reagent BS³. This revealed the proximity of the domains that are able to interact with each other in the native-like complex of PEX19-PEX26. Regarding functionality, we showed that this binary complex was able to restore matrix protein import *in vivo* in PEX26-deficient fibroblasts re-establishing the REM. Last but not least, we successfully integrated PEX26 into liposomal membranes employing Ni-NTA-LUVs (large unilamellar vesicles) which were previously coupled with nPEX3^T (Thx-His₆-Thr-TEV-nPEX3). Following this, flow cytometry analysis revealed that PEX26 can be effectively

integrated into these LUVs by nPEX3^T. The membrane association of PEX26 could be tested using carbonate extraction, which confirmed PEX26 integration into LUVs.

2. Introduction

2.1 Peroxisomes

Peroxisomes were firstly discovered by Rhodin using electron microscopy in 1954, and initially named them as microbodies. He has described the characteristics of peroxisomes as cytoplasmic bodies present in tubular mouse kidney cells, which comprises a granular matrix surrounded with a single membrane^[1]. The microbodies were firstly isolated and named by a following study as peroxisomes due to their important association through catalase with the H₂O₂ metabolism^[2].

Today we know that peroxisomes in human cells can metabolize up to 50 different reactions participating in the biosynthesis of plasmalogens and bile acids or in degradation, such as in ROS metabolism and β -oxidation^[3-4]. They vary in size (100 to 1000 nm), abundance and most importantly in content according to their homeostatic state and the originated organs or organisms^[5-6]. Therefore, a functional peroxisome contains various enzymes such as catalase as well as other proteins of the mentioned metabolisms, which are called peroxisomal matrix proteins. They need to be transported from the cytosol into peroxisomes post translationally utilizing the matrix protein import machinery, that is formed by peroxins. Peroxins are essential factors for peroxisome biogenesis and maintenance. So far, there are 36 peroxins that were identified^[7]

2.1.1 Major metabolic pathways in peroxisomes

The Human genome contains around 85 genes, which encode for peroxisomal proteins. Peroxisomal metabolic pathways in human encompass at least 50 different enzymatic reactions, which are processed by mostly peroxisomal proteins^[8]. Furthermore, 36 genes in yeast (20 and 23 homologs in mammals and plants, respectively) encode for peroxins i.e. essential factors for peroxisomal biogenesis and maintenance^[7] (see Figure 2.1). However, some of the proteins included in peroxisomes are also common in mitochondria, such as enzymes in fatty acid β -oxidation. These enzymes are encoded by different genes; but they catalyse similar reactions with distinct substrate specificities.

Major metabolic pathways in human peroxisomes consist of catabolic pathways such as α - and β -oxidation of fatty acids as well as glyoxylate detoxification, while anabolic pathways comprise biosynthesis of bile acids, ether lipids and cholesterol^[3] (see Figure 2.1).

In humans, fatty acid catabolism in peroxisomes and mitochondria differ from each other regarding the chain-length of fatty acids they prefer to metabolize. Therefore, peroxisomes can metabolise fatty acids through β -oxidation, which contains 22 carbons or more ($n \geq 22$), called very long chain fatty acids (VLCFA), as well as branched-chain fatty acids such as phytanic acid through α -oxidation. In contrast, mitochondria can only metabolise fatty acids containing 18 carbons or less by β -oxidation^[9].

VLCFA encompass a few percent of the total fatty acid content of the cells^[10]. They are synthesized in the ER and transported by ABCD (ATP-binding cassette subclass D) transporters into peroxisomes. Their catabolism by β -oxidation in peroxisomes result in the shortened fatty acids ($n-2$), that are metabolized further either to bile acids, plasmalogens or they are transferred to mitochondria for further degradation by β -oxidation (see Figure 2.1). β -oxidation of VLCFA results in cleavage of two carbons from the VLCFA through the enzymatic catalysis cycles of dehydrogenation (Acyl-CoA Oxidase), hydration (Enoyl-CoA Hydratase), dehydrogenation (3-Hydroxyacyl-CoA Dehydrogenase) and thiolytic cleavage (3-Ketoacyl-CoA Thiolase) respectively in both organelles. The first dehydrogenation step, which is catalysed by Acyl-CoA Oxidase results in formation of FADH_2 in peroxisomes and mitochondria. In addition, FADH_2 is reduced reacting with O_2 forming H_2O_2 in peroxisomes, which is further degraded in peroxisomal catalase to H_2O and O_2 . In contrast, FADH_2 is metabolised in oxidative phosphorylation in mitochondria, so that the electrons from FADH_2 participates in ATP synthesis^[11-12].

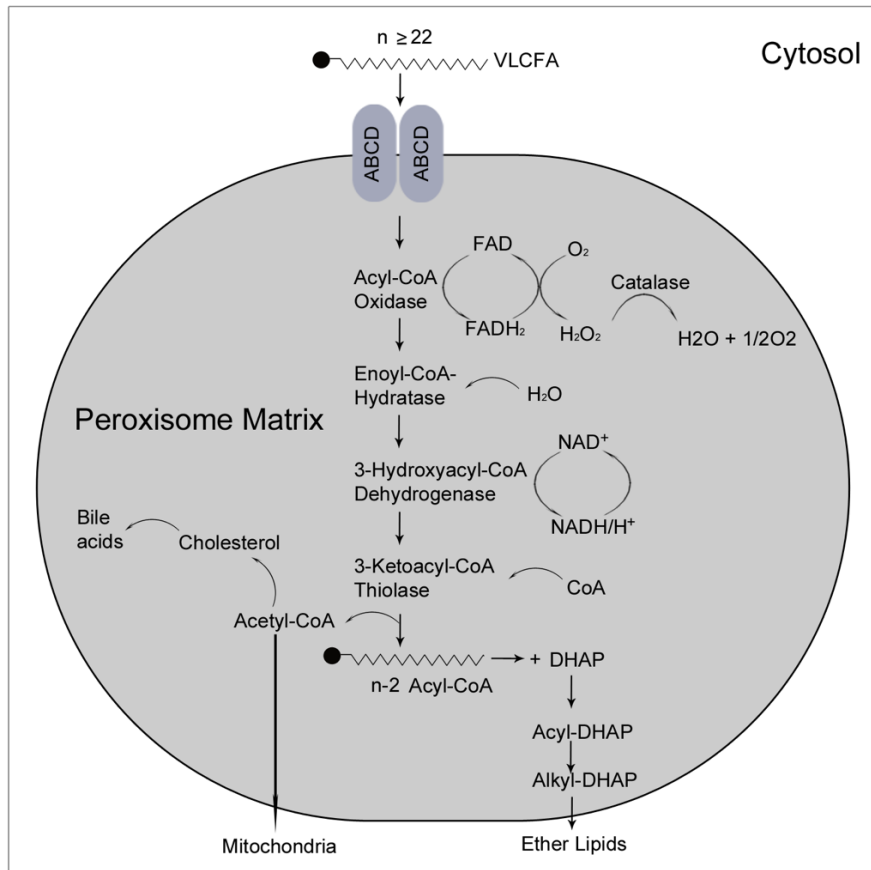


Figure 2.1: Major metabolic pathways in human peroxisomes

Some of the representative enzymatic reactions, that are processed mostly by peroxisomal proteins. After their synthesis in ER, very-long chain fatty acids (VLCFAs, $n \geq 22$) enter into peroxisomes through ABCD (ATP-binding cassette subclass D) transporters. β -oxidation of VLCFA results in cleavage of two carbons ($n - 2$) from the VLCFA through the enzymatic catalysis cycles of dehydrogenation (Acyl-CoA Oxidase), hydration (Enoyl-CoA Hydratase), dehydrogenation (3-Hydroxyacyl-CoA Dehydrogenase) and thiolytic cleavage (3-Ketoacyl-CoA Thiolase), respectively. Duve *et al.* (1965) called these organelles peroxisomes as they use catalase to degrade H_2O_2 that is generated by oxidases. Catalase and 3-Ketoacyl-CoA thiolase are examples for PTS1 and PTS2 proteins, respectively which are imported into peroxisomes in a PEX5- or PEX7-dependent way^[13]. Figure adapted from reference [3]

2.1.2 Peroxisomal matrix protein import

A general and current model describes the highly conserved and similar basic steps for peroxisomal matrix protein import, which can vary among organisms regarding the peroxins involved in this pathway (see Figure 2.2). Peroxisomal matrix protein import is essential for mature i.e. functional peroxisomes and comprises transport of cargo proteins such as enzymes or proteins into peroxisomes, which are newly synthesized and released from polyribosomes to cytosol. If these cargo proteins include a C-terminal tripeptide with following combination and order called PTS1; S/A/C-K/R/L-L/M, they are imported in a PEX5-dependent pathway. Whereas, the cargo proteins with a

N-terminal consensus sequence called PTS2 as following; R/K-L/V/I-X₅-H/Q-L/A, are transported in a PEX7-dependent way with its co-receptor, a long splice isoform of PEX5 (PEX5L) in mammals^[14-15]. In contrast, PEX18, PEX20 and PEX21 serve as co-receptor for PEX7 in yeast^[16-18]. In addition, PEX13, PEX14, PEX17 (not in higher eukaryotes) and PEX33 (*N. crassa*) form docking/translocation machinery (DTM) in peroxisomal membrane for these two cytosolic receptor proteins PEX5 (or PEX5L) or PEX7, in which PEX14 facilitates the formation of cargo-translocation channel in association with PEX5^[19]. Furthermore, PEX2 and two other peroxins; PEX10 and PEX12 form a RING (Really Interesting New Gene) finger complex, which participates in the ubiquitination of the cytosolic matrix protein receptor PEX5 before its exit back to the cytosol^[20]. Ubiquitination of PEX5 is processed by PEX12 (ligase) and PEX4 (ubiquitin conjugation, not in higher eukaryotes) that docks PEX22 (not in higher eukaryotes) in peroxisomal membrane. In addition, PEX8 (not in higher eukaryotes) conjugates the two machineries, DTM and RING finger complex serving as a bridge^[21] (see Figure 2.2).

The recycling of PEX5 (or PEX5L) from the peroxisomal membrane back to the cytosol after cargo release, is undertaken by the receptor export complex (REM). REM is an assembly of a hetero hexameric complex of PEX1 and PEX6 that is formed by trimers of PEX1-PEX6 complex dimers and its membrane receptor PEX26 (see Figure 2.2)^[22-23]. Mode of action of this hetero hexameric complex comprises the steps of unfolding the ubiquitinated PEX5 (or PEX5L) in an ATP-dependent manner, which ends up either their dislocation and recycling to cytosol or in degradation through the 26S proteasome^[24].

Moreover, a functioning peroxisomal matrix protein import (or export) machinery requires peroxisomal membrane proteins (PMPs) integrated in the peroxisomal membrane.

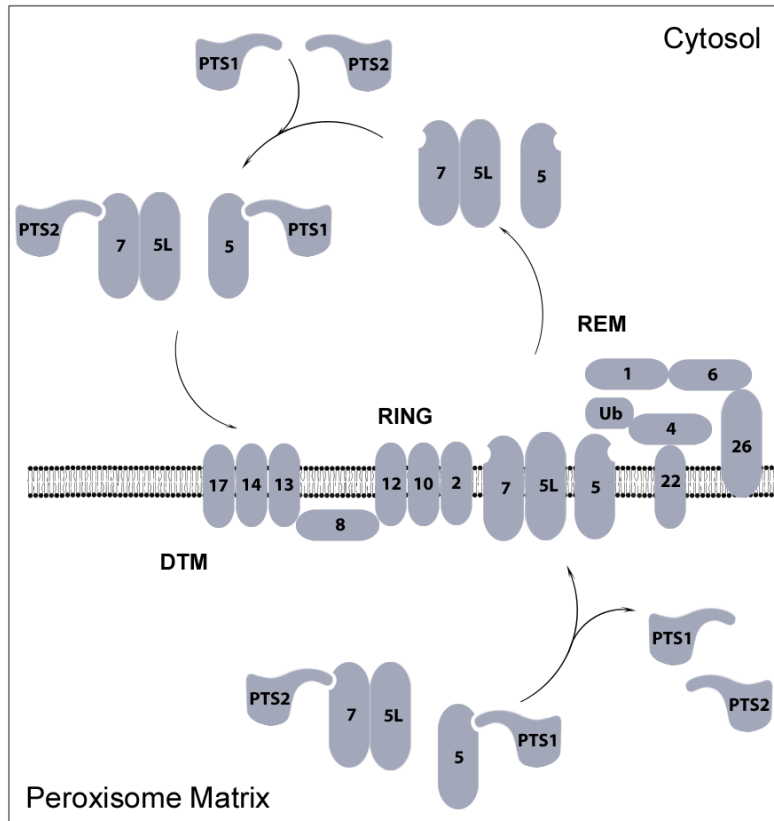


Figure 2.2: A suggested current model of the peroxisomal matrix protein import pathway. Current suggested peroxisomal matrix protein import model facilitates two different routes based on the presence of cargo motifs PTS1 and PTS2. PTS1 containing cargo proteins are harvested by PEX5, while PTS2 containing ones are captured by PEX7, that requires PEX5L (a splice variant of PEX5) as a co-receptor. Both of the cargo-receptor complexes are directed to import into peroxisomes through the DTM, that consists of PEX13, PEX14 and PEX17. After cargo release into peroxisomal matrix, both, the PEX5L-PEX7 receptor complex and PEX5 are directed to ubiquitination through the RING finger complex and PEX4 and PEX12 (ubiquitin-conjugation and ligase enzymes, respectively). Subsequently to ubiquitination, the receptor proteins are recycled back to the cytosol in an ATP-dependent manner through the REM complex that is assembled from a PEX1-PEX6 heteromeric complex and this membrane receptor PEX26. This model suggests the basic steps of peroxisomal matrix protein import, which can vary among organisms. Accordingly, the import in *S. cerevisiae* involves PEX18, PEX20 and PEX21 that serve as co-receptor for PEX7 instead of PEX5L and PEX15 instead PEX26 in human. *N.crassa* utilizes PEX33 instead of PEX17. Furthermore, PEX22, PEX8, PEX4 and PEX17 are not involved in higher eukaryotes. Figure adapted from reference [38]

2.1.3 Peroxisomal membrane protein import

PEX3 and PEX19 form the peroxisomal membrane protein (PMP) import machinery (MPIM) in which PEX3 serves as peroxisomal membrane receptor for the cytosolic PMP receptor, PEX19 (see Figure 2.3). The MPIM facilitates the import of mPTS-containing peroxisomal membrane proteins (PMPs), that are harvested by PEX19. This comprises also the tail-anchored PMPs^[25-27]. PMPs have distinct *mode of actions* like ones that are involved in peroxisomal membrane import complexes DTM and

RING (PEX13, PEX14, PEX2, PEX10, PEX12) and the ones that are involved in the REM (PEX26, PEX1, PEX6)^[24]. Furthermore, PEX3, as a *class II* PMP, is PEX19-independent and binds PMP-loaded PEX19 through its 20 aa long alpha-helical segments (aa 14-33)^[28].

In principle, PMPs are synthesized on free polyribosomes in cytosol and post-translationally imported into peroxisome membrane following two distinct routes, which are distinguished according to their PEX19 dependencies as *class I* and *II*^[26,29]. Peroxisomal *class I* membrane proteins employ a membrane targeting signal (mPTS) like PEX2, PEX11, PEX13, PEX16, PMP22, PMP34, PMP70 and PEX26, which is recognized by PEX19 (see Figure 2.3)^[25-26]. In contrast, *class II* PMPs are PEX19-independent and follow an ER or mitochondria-associated route to reach peroxisomes, such as PEX22, PEX16 and PEX3 (see Figure 2.3)^[26,29-30]. However, PEX19 is not completely selective as a peroxisome specific cytosolic receptor and is able to import membrane proteins such as FIS1 into peroxisomes, which promotes fission in both organelles: mitochondria and peroxisomes^[31]. In addition, a recent study has reported that PEX19 participates in the TA protein import into mitochondria^[32].

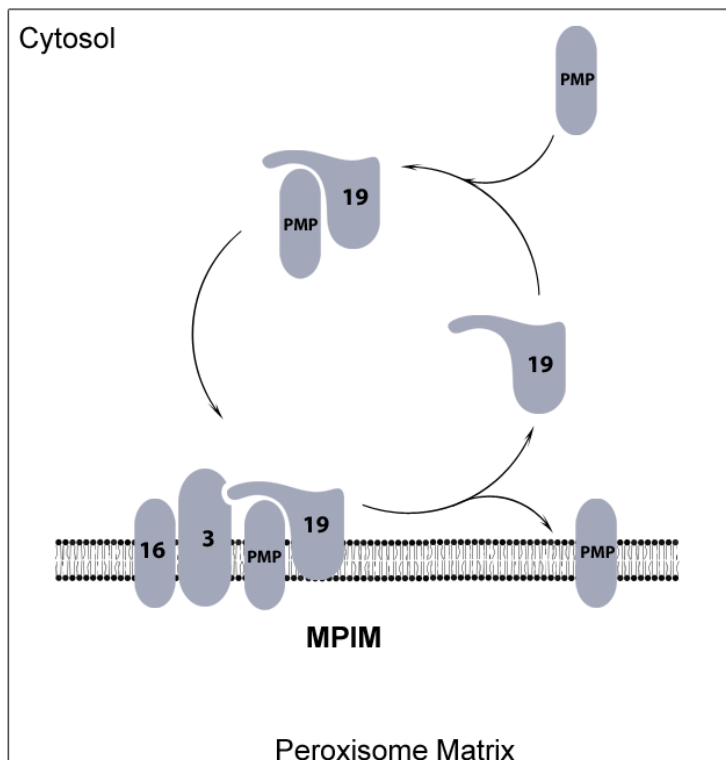


Figure 2.3: A current model for *class I* peroxisomal membrane protein import

The peroxisomal membrane proteins such as PMP70 follows an PEX19-dependent post-translational route to peroxisomal membrane. PEX19 exhibits a chaperone-like activity stabilising the PMPs during their translation in the cytosol. This prevents their aggregation in the cytosol^[33]. PEX19 recognizes PMPs through their putative membrane targeting signal (mPTS). The mPTS can vary in length and sequence and may locate to different regions of

the PMPs, contrary to the PTS1 and PTS2 in matrix protein import^[25,34]. After recognition, the cargo-loaded PEX19 binds to its membrane receptor PEX3 on the peroxisomal membrane through its 20 aa long alpha-helical segments (aa 14-33)^[28]. The PMPs are released from PEX19 and inserted into membrane without ATP requirement. PEX3 as a *class II* PMP is not PEX19-dependent and follows a mitochondria and ER-dependent route towards peroxisomes. Figure adapted from reference [38]

2.1.4 Peroxisome origin and biogenesis

Regarding the phylogenetic origin of the peroxisomes, Gabaldón et al. (2010) reported that 39% (*S. cerevisiae*) and 58% (*R. norvegicus*) of peroxisomal proteins have eukaryotic origin. In addition, 36 peroxins are also included in this group. In contrast, 13-18% of peroxisomal proteins, mainly consist of enzymes, have their origin in alpha-proteobacteria^[35]. Moreover, peroxisomes demonstrate more the autonomous characteristics like division and growth, presence of their own protein import machinery and post-translational protein import, indicating an endosymbiotic origin. Contrary to this, their characteristics, like lack of a peroxisomal genome and their *de novo* biogenesis are considerable features that indicate peroxisomes derive from other organelles^[35-36].

Yet, previous studies showed that deficiency or non-functional mutations of one of three peroxins, PEX3, PEX16 and PEX19 cause absence of both peroxisomes as well as of peroxisomal remnants in mammalian cells^[37]. Furthermore, complementation studies with these peroxins showed that peroxisomes can be formed *de novo*^[38]. Accordingly, most of the PMPs are mistargeted to mitochondria or degraded in PEX3 and PEX19-deficient mammalian cells, whereas they were mislocalised to the ER in non-functional *PEX3* and *PEX19* mutant yeast cells. Moreover, overexpressed PEX16 targeted to the ER in mammalian PEX16 mutant cells, where this gives rise to *de novo* formation of peroxisomes through ER derived vesicles (see Figure 2.4)^[39]. These pre-peroxisomal vesicles can further import PMPs post-translationally from the cytosol and can form mature peroxisomes^[40]. A recent study showed that peroxisomes might be formed *de novo* through fusion of pre-peroxisomal vesicles which originates from both organelles, mitochondria and the ER^[30] (see Figure 2.4). Accordingly, PEX3-YFP is targeted to mitochondria in the absence of peroxisomes, which gives rise to (pre-peroxisomal) vesicles from mitochondria. These vesicles fused with PEX16 containing vesicles from the ER to form peroxisomes, that are able to import PMPs and subsequently the matrix proteins forming mature peroxisomes (see Figure 2.4).

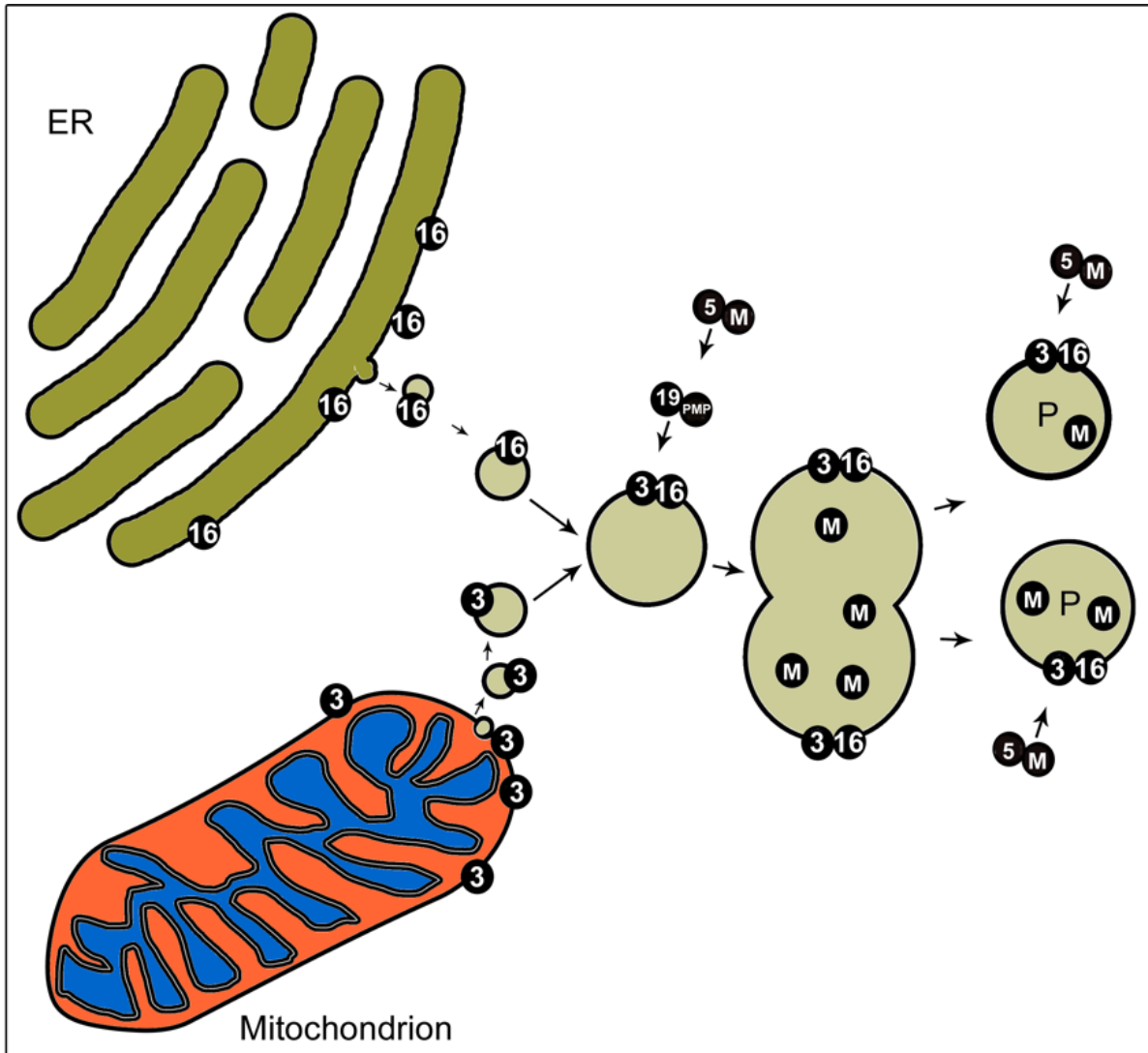


Figure 2.4 Mature peroxisomes originate from both organelles, mitochondria and ER

Three peroxins, PEX3 (3), PEX16 (16) and PEX19 (19) are essential for the biogenesis of peroxisomes in mammalian cells. Their deficiency or non-functional mutations result in the absence of both peroxisomes (P) as well as of peroxisomal remnants. Sugiura et al. (2017) suggest that peroxisomes might be formed *de novo* through fusion of pre-peroxisomal vesicles which originate from both organelles, mitochondria and the ER. Mature peroxisomes are formed from these pre-peroxisomal vesicles (contain either PEX3 or PEX16) subsequently to post-translational PMP and matrix (M) protein import from the cytosol^[40]. Figure adapted from reference [39]

2.1.5 Peroxisome biogenesis disorders

Peroxisome biogenesis disorders comprises several phenotypes that are given with a descending severity and average survival time, respectively: Zellweger Syndrome (ZS, 6 months), Neonatal Adrenoleukodystrophy (NALD, longer than 6 months, early childhood), Infantile Refsum Disease (IRD 3-11 years) and Rhizomelic Chondrodysplasia Punctate (RCDP between one year and young adulthood)^[41-42]. In general, all these disorders have a similar molecular background, in which the

mutations in one of the PEX genes are responsible for biogenesis defects and result in the absence or in dysfunctional peroxisomes, as a consequence; the accumulation of VLCFA. The accumulation of VLCFA has been observed in almost all tissues of patients^[43]. Accordingly, the most apparent symptoms of ZS are characterized as craniofacial dysmorphism, vision and hearing impairment and hypotonia, whereas those of NALD and IRD are loss of hearing and vision and developmental delay. Furthermore, RCDP patients demonstrate skeletal-abnormalities, post-natal growth deficiency and intellectual disabilities^[41,44]. The genotypes of ZS, NALD, IRD and RCDP are classified in 14 complementation groups depending on the responsible PEX genes (Table 2.1)^[45]. The complementation groups CG8, CG12 and CG14 are relevant for this work, due to their association with the characterized mutations of PEX3, PEX19 and PEX26 respectively.

Table 2.1: 14 Complementation groups of PBD in mammals

CG	Peroxin	PBD	Peroxisomes Absent(A)/Present(P)	Function
1	PEX1	ZS, NALD, IRD	P	REM
2	PEX5	ZS, NALD	P	DTM
3	PEX12	ZS, NALD, IRD	P	RING
4(6)	PEX6	ZS, NALD	P	REM
7(5)	PEX10	ZS, NALD	P	RING
8	PEX26	ZS, NALD, IRD	P	REM
9	PEX16	ZS	A	ER PMP Recruitment
10	PEX2	ZS, IRD	P	RING
11	PEX7	RCDP	P	DTM
12	PEX3	ZS	A	MPIM
13	PEX13	ZS, NALD	P	DTM
15	PEX14	ZS	P	DTM
14	PEX19	ZS	A	MPIM
16	PEX11	ZS	P	Fission

The data represents the complementation groups (CG) of peroxisomal biogenesis disorders (PBD) based on the original classification (CG 1-14) of the Kennedy Krieger Institute (Baltimore, USA)^[45]. It contains the complementation groups, their associated peroxins and phenotypes as Zellweger Syndrome (ZS), Neonatal Adrenoleukodystrophy (NALD), Infantile Refsum Disease (IRD) and Chondrodysplasia Punctate (RCDP). In addition to this, the presence (P) or absence (A) of peroxisomes in these CGs and the association of these peroxins with machineries described in section 2.3

Complementation group 8 (CG8) is one of the 14 complementation groups, which displays all three of the PBD phenotypes that show an association with *PEX26* gene;

genotypically autosomal recessive; ZS, NALD and IRD^[41]. The genotypes of the fibroblasts of 18 NALD patients revealed that more than half of the PEX26 mutations are missense mutations and addressed to the N-half of PEX26. In addition, all these mutations involve crucial amino acids for the interactions with PEX6. Moreover, 39% of all missense mutations are represented by R98W in PEX26^[23]. A CHO mutant cell line ZP167, that also involves *PEX26* deficiency, isn't able to form functional peroxisomes but peroxisomal remnants. Expression of *PEX26* originated from human kidney cDNA library in one of the transformants of ZP164 was able to form peroxisomes showing the same phenotype as in wild-type CHO-K1 cells. Furthermore, *PEX26* expression in fibroblasts from NALD patients (*PEX26* mutation R98W) was able to restore catalase import (PTS1)^[46]. In addition, the steady state level of the PTS1 receptor PEX5 was equally and severely reduced in all three, PEX1, PEX6 and PEX26-deficient cells (CG8) ^[47], whereas the PEX26 steady state level decreased 5-fold in PEX1, PEX5 and PEX6-deficient cells (PEX13 was an endogenous control)^[23]

Complementation Group 12 (CG12) shows the characteristic phenotype of ZS, that classified as most severe ones under PBDs and points out an association with *PEX3* gene. Sequencing analysis of isolated *PEX3*-cDNAs from fibroblasts of CG12 patients are lack of 98 bp at exon 11 of *PEX3*, that translated as PEX3 with a 32 aa-truncation^[48]. Consequently, phenotype of this cell line shows diffused and cytosolic co-localisation of catalase and no detectable peroxisomal remnants according to antibody staining analysis of this cell line using anti-catalase and PMP70 respectively^[48,70]. *PEX3* overexpression in this cell line complement impaired peroxisome biogenesis while restoring both catalase (PTS1) and 3-ketoacyl-CoA thiolase (PTS2) imports into peroxisomes^[48].

Complementation Group 14 is also phenotypically characterized by the most severe PBD ZS in which fibroblasts of CG14 patients lack functional peroxisomes and also peroxisomal remnants. Additionally, CG14 resembles a CHO mutant (ZP119) that exhibits PEX19 deficiency, thus impaired matrix and membrane protein import. Phenotype complementation assays using ZP119 indicates that *PEX19* cDNAs from human liver library is able to restore in both ZP119 cell line and CG14 fibroblasts matrix and membrane protein import confirming the *PEX19* gene association of CG14 in these cells^[49].

2.2 Tail-anchored membrane proteins

Tail-anchored (TA) membrane proteins comprise 3-5% of all proteins. Their main characteristics are described by a C-terminus that includes a targeting signal and a luminal anchor and a single transmembrane segment, which is translated lastly^[50]. Subcellular localisation of the TA proteins are mostly the ER, the outer membrane of mitochondria or plastids or peroxisomes^[51]. Depending on the import mechanism, they are imported co- or post-translationally to the target organelles. Based on this, they are captured by organelle-specific cytosolic receptors during or after their exit from ribosomes to prevent aggregation as well as mistargeting. Recent studies suggested that a positively charged C-terminal tail sequence is essential for the correct localisation of mitochondrial and peroxisomal TA proteins^[52]. Furthermore, it was suggested that a highly positive charge in the C-terminal tail significantly differentiated peroxisomal TA proteins from those of the ER or the mitochondria in mammals^[53]. Accordingly, in case of reduction of the positive charge on tail segments, peroxisomal TA proteins such as ABCD5 are mislocalised gradually to mitochondria and the ER, respectively^[54]. Whereas an increase of the positive charge in tail segments in TA proteins such as GDAP1 (mitochondrial fission, MOM or cytosol), FIS1-SR (organelle fission, peroxisomal or mitochondrial outer membrane) and FALDH-PO (fatty acid oxidation, ER membrane) resulted in an interaction with PEX19 and changed the location from mitochondria or the ER to peroxisomes^[54]. In contrast, an increase in hydrophobicity of TMD segments directed peroxisomal TA proteins to the ER membrane. However, increasing hydrophobicity of the PEX26 TMS by mutation of three positively charged amino acids to leucine gave rise to a GET3 (Guided Entry of Tail-anchored proteins factor 3) interaction rather than to a peroxisomal integration^[55]. Therefore, targeting of TA proteins is influenced by two factors including the hydrophobicity of the TMS and the charge of the tail segments^[87]. ER TA proteins are characterized by a significantly higher TMS hydrophobicity and lower tail charge, while mitochondrial TA proteins have lower TMS hydrophobicity but higher tail charge. However, peroxisomal TA proteins showed a significantly higher tail charge and a moderate hydrophobicity^[52]. Accordingly, the hydrophobicity of TA protein in the ER, mitochondria and peroxisomes can be ranked as ER > mitochondria > peroxisomes and the charge level of the tail as peroxisomes > mitochondria > ER^[54,56-57].

2.2.1 Tail-anchored membrane protein import into peroxisomes

TA-PMP import into peroxisomal membrane comprises three main steps which are proceeded in an ATP-independent manner;

Firstly, TA-PMPs are recognized through their mPTS and stabilized by PEX19 in the cytosol to prevent aggregation. In this step, PEX19 stabilizes TA-PMPs already at the stage of translation functioning as a *chaperone-like* protein, in which mainly its rigid C-terminal half (aa 161-283) is involved^[25,58]. This C-terminal half is sufficient for the TA-PMP recognition and stabilization.

Secondly, the cargo loaded PEX19 docks to PEX3 complexing with a 20 aa long alpha-helical segments of PEX19 (aa 14-33) on the peroxisomal membrane, where the insertion of the *class I* PMPs takes place^[28]. It was also reported that the PEX19 docking to PEX3 (in the second step) is coupled with conformational changes on three regions of PEX19 and the whole PEX3, despite of any ATP requirement^[59]. In this assembly, the cargo loaded PEX19 and PEX3 form a hydrophobic pocket at the peroxisomal membrane, where the TA protein is located^[71] (see Figure 2.5).

Thirdly, the hydrophobicity in this pocket which is built through the adjacent hydrophobic residues of PEX3 and PEX19 as well as hydrophobic surface of PEX3 on the peroxisomal membrane promote the TA PMP release and insertion into the membrane through an unusual membrane intercalation without ATP requirement^[55, 60-61] (see Figure 2.5).

PEX26 is one of the examples of peroxisomal TA proteins, which is inserted into the peroxisome membrane in this manner. PEX26 is a TA and *class I* PMP and comprises two different predicted regions in the C-terminal segment described as PEX19-binding site I (BSI: aa 248-270) and PEX19-binding site II (BSII: aa 276-296). The former one overlaps with PEX26-TMS (aa 252-269) while the latter overlaps with the luminal segment^[62].

All three steps; PEX19 recognition/stabilization, docking and insertion of PMPs don't require ATP hydrolysis, but the PEX19-guided PMP import mechanism still remains poorly understood, especially the exact interacting segments of the proteins are not well characterized (see Figure 2.5).

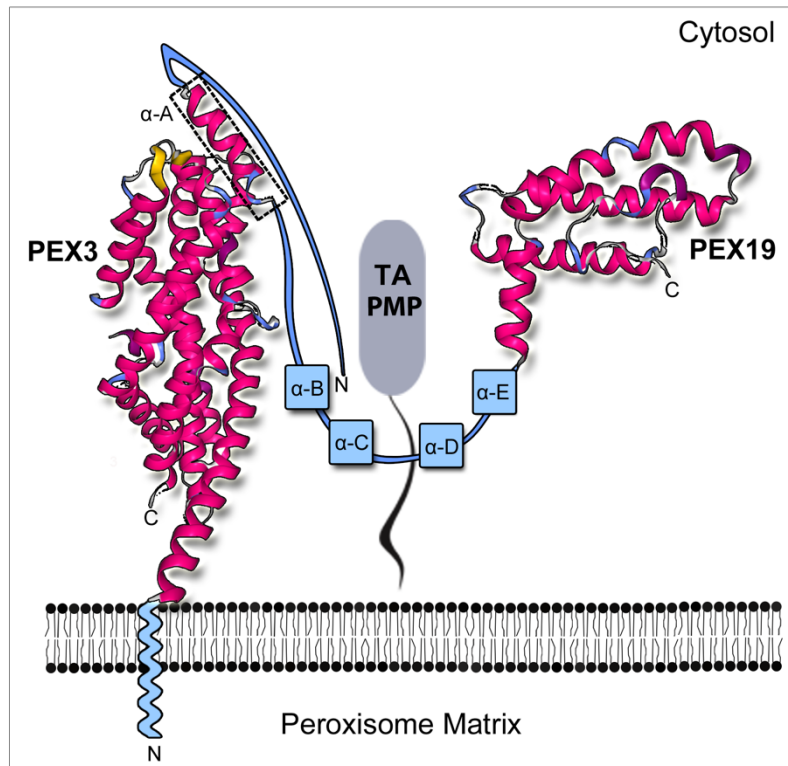


Figure 2.5 Model of the TA PMP import into the peroxisomal membrane.

The represented model shows the crystal structure of PEX3₄₁₋₃₇₃ in complex with the alpha-A in complexing with a peptide of PEX19₁₄₋₃₃ (PBD: 3MK4)^[28,136] (left) and the rigid core of PEX19₁₆₁₋₂₈₃ (PBD: 2WL8)^[58,136] (right). In addition to this, the four putative and characterized segments of PEX19, alpha-B, -C, -D and -E, which are highly conserved in human, yeast and *N.crassa*, are also included in this model^[55]. After TA-PMP recognition, the cargo loaded PEX19 binds to its membrane receptor PEX3 on the peroxisomal membrane through its 20 aa long alpha-helical segments (aa 14-33)^[28]. The TA-PMPs are released from PEX19 and inserted into the membrane without ATP requirement. PEX3 as a *class II* PMP is not PEX19-dependent and follows a mitochondria- and ER-dependent route towards peroxisomes^[30]. *Class I* PMPs such as TA-PEX26, follow a PEX19-dependent pathway as represented. The purple-coloured segments present the known structures of PEX3 and PEX19, while the blue segments illustrate unsolved structural elements of all three proteins.

2.2.1.1 PEX26

The PEX26 gene is located in chromosome 22 and comprises 13.1 kb, from which 6 exons of full length PEX26 are transcribed. Translation of PEX26 starts in the second exon resulting in a 34 kDa (305 aa) hydrophilic protein with a singular carboxy-terminal hydrophobic transmembrane segment^[121]. Alternative splicing of PEX26 expresses a PEX26-isoform which lacks amino acids 223-271 of full length PEX26, but still can bind PEX19 and can recruit the PEX1-PEX6 heteromeric complex to the membrane^[63]. Alignment of PEX26 with its orthologs from *M. musculus*, *R. norvegicus*, *G. gallus*, *D. rerio*, *F. rubripes* and *T. nigriviridis* indicates low sequence similarity (the highest ones:

D. rerio: 30% and *T. nigriviridis*: 32%). Furthermore, sequence similarity of PEX26 and its yeast homolog PEX15 shows 12% amino acid identity overall^[23]. Nevertheless, they are both TA PMPs and follow distinct pathways to reach peroxisomes. PEX15 is targeted to peroxisomes in an ER-dependent manner through GET pathway^[140]. Furthermore, an ER-dependent targeting of PEX26 to peroxisomes through GET pathway in yeast is also reported^[139]. Contrary to this, PEX26 is targeted to peroxisomes via a cytosolic receptor; PEX19 in an ATP-independent manner, despite the existence of a GET-homologue TRC40 complex in mammals^[62,64]. Analysis using siRNA-PEX19 knockdown in *HeLa* cells resulted in mislocalisation of PEX26 to mitochondria. In addition, cell free import analysis showed that the TA-PMP PEX26 is PEX19-dependent and already stabilised by PEX19 at the stage of translation in the cytosol^[64].

Peroxisomal TA proteins are distinguished from those of mitochondria by a higher TMS hydrophobicity and increased helical composition, as well as by more charged amino acids in the TMS^[65-67]. The PEX26 C-terminal segment consists of two distinctive regions, a highly hydrophobic transmembrane (aa 252-269) segment and a hydrophilic luminal segment (aa 270-305), that define the subcellular localisation of PEX26^[68]. Increasing hydrophobicity of TMS by mutation of three positively charged amino acids to leucine gave rise to a GET3 interaction rather than peroxisomal integration^[55]. Additionally, reduction of positively charged amino acids in the luminal segment by replacing them with serines resulted in a decreased peroxisomal localisation^[64].

Analysis using post nuclear supernatants (PNS) of a ZP167 cell line expressing PEX26-HA resulted in co-sedimentation of PEX26-HA with catalase, PEX14 and PMP70, indicating that PEX26 had a peroxisomal localisation. Furthermore, treatment of these fractions of ZP167 by sonication in 1M NaCl and 0.3 M Na₂CO₃ confirmed that PEX26 is an integral protein, classified as Type II transmembrane protein^[46,51]. Additionally, Triton-X100 treated wild-type CHO cells expressing Flag-PEX26 confirmed the colocalisation of PEX26 with PEX14. Further treatment of ZP167 cells expressing PEX26-HA with digitonin (25 µg/mL) and afterwards with 0.1% Triton revealed that the C-terminus of PEX26 is exposed to the peroxisomal matrix. Last but not least, treatment of this PNS with proteinase K showed that the N-Terminus of PEX26 is directed to the cytosol, as it was seen in digitonin-treated wild-type CHO cells expressing Flag-PEX26^[46].

2.2.1.2 PEX3

The Human *PEX3* gene is located in chromosome 6 and comprises 39.8 kb, from which 12 exons are transcribed in human. *PEX3* translation starts at the first exon and results in a 42.1 kDa-protein consisting of 373 amino acids^[121]. Alignments of *PEX3* with its orthologs from *S. cerevisiae* (441 aa), *P. pastoris* (455 aa) and *H. polymorpha* (457 aa) revealed 15% 19% and 18% identity score respectively^[121]. Fluorescence microscopy analysis indicated that the fibroblasts, which were transfected separately with C- or N-terminal *myc*-tagged *PEX3*, showed co-localisation of anti-*myc* with anti-catalase antibodies, indicating a peroxisomal *PEX3* localisation^[69]. Confirming this, the same transformants are further analysed with peroxisomal marker proteins PMP69 and PMP70, which colocalised with *myc*-tagged *PEX3* as well. Regarding the topology of *PEX3*, these transformants were additionally permeabilized using 25 µg/mL digitonin and stained with monoclonal anti-*myc* antibodies^[69]. Accordingly, the fibroblasts, which are transfected with C-terminal *myc*-tagged *PEX3*, showed no antibody staining against anti-*myc*, confirming a luminal C-terminus of *PEX3*. However, those which were transfected with N-terminal *myc*-tagged *PEX3*, were successfully stained, indicating a cytosol exposed N-terminal topology of *PEX3*^[69]. *PEX3* is relatively hydrophilic protein with a very hydrophobic N-terminal transmembrane segment comprising the first 33 residues regarding its GRAVY index at -0.154^[124]. In accordance with this, purification of full length *PEX3* resulted in formation of inclusion bodies which were even toxic for the *E. coli* overexpression strain^[28]. In contrast, truncated variants of *PEX3* (C235S) comprising the aa residues 26-373 and 41-373 could be purified using the affinity tag, *His*₆ and the stabilising tag *Thioredoxin*. Furthermore, the truncated variant of *PEX3* comprising the aa residues 41-373 in complex with a *PEX19*-derived peptide (aa 14-33) could be crystallized and the structure could be solved by X-ray analysis. Accordingly, crystal structure analysis of *PEX3* revealed a model (PDB; 3MK4)^[136] for truncated *PEX3* (aa 41-373, C235S) with a structural organisation consisting of ten alpha helices (Table 2.1)^[28]. Its alpha-3 forms the major axis for five segments consisting of 9 alpha helices and five loops. The *PEX19*-derived peptide has an amphipathic secondary structural organisation binding to a groove at the cytosolic apex of *PEX3*. Participating segments in this interaction are given in Table 2.1^[28]. In addition, surface analysis of the *PEX3* crystal structure indicated another hydrophobic groove near of N-terminal alpha-1 comprising Ile49, Met67, Met72, Ile135, and Ile140. Since alpha-1 follows transmembrane segment of

PEX3(aa 1-33), this groove indicates a proximity to the peroxisomal membrane suggesting a contribution of this helix to peroxisomal membrane protein insertion, in which hydrophobicity is main driving force^[71].

Table 2.1 Interacting segments of sPEX3 (PEX3₄₁₋₃₇₃) and PEX19^{Pep} (PEX19₁₄₋₃₃) and their portion in their complex structure

sPEX3 Segments	Residues in sPEX3 (aa 41-373)	Residues in PEX19 (aa 14-33)	Interaction	Portion
$\alpha 2$ and $\alpha 3$	Thr90, Leu93, Lys94, Lys100, Leu101, Trp104 and Leu107	Leu22, Ala25, Leu26, and Phe29	Hydrophobic	42%
Loop between $\alpha 4$ and $\alpha 5$	Leu196	Leu18, Leu21 and Leu22	Hydrophobic	
Loop between $\alpha 4$ and $\alpha 5$	Lys197	Asp15 and Glu17	Salt bridge	31%
Loop between $\alpha 4$ and $\alpha 5$	Lys197	Leu18	Hydrophobic	
$\alpha 8$ near $\alpha 8$	Lys324	Asp28 and Ser24	Salt bridge	27%
$\alpha 8$	Pro321	Leu21 and Leu2	Hydrophobic	
$\alpha 8$	Pro327	Phe29	Hydrophobic	
$\alpha 8$	Ile326 and Asn330	Phe29	Hydrophobic	
$\alpha 8$	Ala323	Leu21, Leu22 and Ala25	Hydrophobic	

The data present encompasses the interacting segments of sPEX3 (PEX3₄₁₋₃₇₃) and PEX19^{Pep} (PEX19₁₄₋₃₃) based on their crystal structure. These data contains the interacting segments of sPEX3, the residues involved in this segment, the residues of PEX19, that interact with those of sPEX3 and the type of interaction, as well as the portion of this interaction in the complex structure (PBD: 3MK4)^[28,136]

2.2.1.3 PEX19

The *PEX19* gene is located in chromosome 1 and comprises 8.3 kbp, from which the eight exons are transcribed in human. PEX19 translation starts at the first exon and results in a 32.8 kDa- protein consisting of 299 amino acids^[121]. Functionally, PEX19 recognizes the peroxisomal membrane proteins (PMPs) such as PEX2, PEX11, PEX13, PEX16, PMP22, PMP34, PMP70 and PEX26 through a putative peroxisomal membrane targeting signal (mPTS)^[34]. In addition, a splice variant of PEX19 lacking aa 273-299 (an unfolded chain sub-sequential to alpha-4) is able to bind several proteins, PEX3 (involved in PMP import), ALDP, ALDRP and PMP70 (involved in transport of VLCFA-CoA)^[72].

PEX19 is a highly hydrophilic and very soluble cytosolic protein, that can be purified to a concentration of over 100 mg/mL^[73]. This matches a low negative GRAVY index based on a Kyte Doolittle Hydrophobicity Plot^[124]. According to this plot, the estimated

hydropathy index of PEX19 corresponds to -0,612^[124]. Regarding the secondary structural organisation of PEX19 CD analysis indicates a highly flexible N-Terminal segment (aa 1-156) and a rigid C-terminal segment (aa 156-299)^[73]. In accordance with this, the solved crystal structure of PEX19 comprises only the rigid C-terminal segment of PEX19 (residue 161-283) (PDB: 2WL8)^[136] which is composed of four alpha helices (alpha-1-4) (see Figure 2.5)^[58]. Regarding its topology, alpha-2,-3 and-4 form a bundle of three antiparallel helices, which is perpendicular to alpha-1. The core of this helical bundle has a hydrophobic arrangement and is unexposed to solvent access, while alpha-2 has a polar surface. In contrast, alpha-1 possess a hydrophobic surface that is highly exposed to solvent^[49,58]. Moreover, human and yeast PEX19 contains a CAAX motif (C: Cys, A: Aliphatic amino acids X: Thr, Ser, Gln Ala, Met) at the C-terminus, which is prone to post-translational farnesylation^[74]. Farnesyl is an isoprenoid which is attached to proteins covalently. Removal of this motif affects the PEX19-PMP binding, whereas it is dispensable for function in yeast^[75]. PEX19 binds most of the PMPs harvesting a putative signal sequence called mPTS that can vary in length and sequence^[34]. Furthermore, the mPTS sequence may locate to different regions of the PMPs, contrary to PTS1 and PTS2 in matrix protein import^[25]. As a TA protein PEX26 is one of the PMPs which contains its mPTS at the C-terminus presenting the amino acid sequence from 270 to 305. This sequence includes basic amino acid residues which are important for subcellular localisation of PEX26. Reduction of positive charges in this sequence through replacement of lysins with serine resulted in a decreased peroxisomal localisation^[64]. In addition, PEX26 is mislocalised to mitochondria in case of siRNA knockdown of PEX19^[62].

2.2.2 Tail-anchored membrane protein import into the ER

Yeast TA protein import into the ER encompasses distinct pathways including, a main pathway, GET (Guided Entry of Tail-anchored proteins) and an alternative ones, SRP (Signal Recognition Particle) depending on co- or post translational import of TA proteins^[76-77]. However, the HSP40/HSP70 complex serves as another alternative for the luminal short polypeptides or for TA proteins with less effective targeting sequences, which are not recognized or captured by the SRP. Therefore, these kind of proteins or peptides are recognized by cytosolic HSP70 post-translationally and translocated through SEC61 at the ER membrane^[78].

The GET pathway comprises three steps of TA import into the ER membrane as following: TMS capture, TA release and transfer to the membrane receptor, respectively. In yeast, the TMS of TA proteins is captured by SGT2 (small glutamine-rich tetratricopeptide repeat-containing protein) post-translationally^[52]. Thereafter, the TA-GET3 complex is recruited to the ER membrane receptor complex consisting of GET1 and GET2, where the TA protein is inserted into the ER membrane after docking of GET3 to the GET1-GET2 complex. TA proteins and GET3 complex formation requires the presence of ATP for release of the TA protein from the pre-targeting complex^[52, 79-80].

In mammals, the TMS of TA proteins is recognized and captured post-translationally by BAG6, one of the subunits of the pre-targeting complex in the TRC (Transmembrane Recognition Complex) pathway and the TA protein is transferred from the pre-targeting complex to a GET3 homolog TRC40. Furthermore, the release of the TRC40-TA-protein complex from the pre-targeting complex requires ATP hydrolysis. The recruitment of the TRC40-TA-protein complex to the ER membrane is facilitated by a membrane receptor, GET1 homolog protein, WRB (tryptophan-rich basic protein)^[81].

The SRP pathway facilitates the membrane protein import into the ER membrane universally in all organisms, whereas post-translational SRP associations with two TA proteins of ER such as proteins synaptobrevin 2 (SYB2) and Sec61 β were also reported^[82]. The process of SRP-dependent TA import comprises the recognition of hydrophobic sequences by SRP co-translationally for the prevention of TA aggregation and recruitment of them together with the ribosome to ER membrane^[82].

Accordingly, the hydrophobic sequence of TA is recognized during the exit from ribosomes by SRP protein. This is followed by the recruitment of the whole SRP-TA-ribosome complex to the ER membrane, where the SRP docks the SRP receptor and transfers the TA-ribosome complex to a receptor channel complex SEC61. The release of the TA protein into the ER membrane is facilitated by SEC61 complex^[82].

2.2.3 Tail-anchored membrane protein into mitochondria

Two of the critical parameters regarding the targeting of TA proteins to subcellular compartments are the range of positive-charge and hydrophobicity of their TMS ^[87]. Mitochondrial TA proteins demonstrate a lower TMS hydrophobicity and charge in comparison to peroxisomal ones, which plays an important role directing them to the

mitochondria^[84]. However, the mitochondrial TA protein targeting remains still poorly understood regarding TA protein targeting signals and receptors as well as machinery involved in this targeting^[84]. On the one hand, mitochondria don't contain an SRP-like (Signal Recognition Particle) mechanism as in the ER. On the other hand, they employ an alternative pathway for several TA proteins like FIS1 and MFF, which are required in peroxisomes as well^[31]. The import of FIS1 in mitochondria is independent of the TOM70 and requires HSP70 in mammalian cells. However, in yeast, PEX19 is able to import Fis1 and Gem1 into mitochondria^[32]. Accordingly, PEX19 is not completely selective as a peroxisome specific cytosolic receptor and is required for TA protein import to mitochondria as well.

2.3 Mass spectrometry analysis

Mass spectrometry is a powerful method that has continuously expanded its scope of application during the last decades. These advances in mass spectrometry especially in the field of biomolecules and proteomics, enables much more information than just their mass information. In general, the ionisation process determines the attainable information from mass spectrometry-based methods and comprises two approaches; matrix-assisted laser desorption (MALDI) or electrospray ionisation (ESI). MALDI-based methods are not suitable regarding the analysis of intact features of proteins, however, they provide information mostly for protein identification in proteomic studies using the peptide mass fingerprint (PMF) method or for the identification of species in bacteriology, as well as in the establishment of biomarkers^[85-86]. In contrast, ESI-based methods cover, beside all MALDI-based approaches, a broad range of methods to determine the stoichiometry of subunits in protein complexes (native MS) or the identification of intra- and intermolecular interactions of proteins or protein complexes (XL-MS), as well as for the investigation of subunit exchanges in protein complexes. Application of these two methods require three main parameters which should be considered before analysis. These parameters are pressure, flow rate of samples in capillaries and the mass range of samples. Pressure is mainly important in the analysis of multimeric protein complexes due to the necessity to use higher pressure in the transfer region between source and analyser compared to monomeric complexes. Regarding the flow rate of the samples, a developed small-scale ES instrument, the ES-nanoflow, enables samples to be loaded into capillaries with 1-2 $\mu\text{L}/\text{min}$. The mass range of these instruments can change in scales from 4000, 8000 to 20000 m/z , which

corresponds to mass limits of 100 kDa, 400 kDa and 2400 kDa for the proteins. In addition, the required sample amounts and concentration in these methods are in range of 5-10 μ L of a 1-20 μ M protein solution^[88].

2.3.1 Native mass spectrometry

Native mass spectrometry (native-MS) elucidates the stoichiometric characteristics of protein assemblies and protein-protein interactions using native-like conditions. Unlike PMF and XL-MS, native-MS requires an intact and native-like, quaternary state of proteins or protein complexes. Therefore it employs a different setup of instruments and buffer conditions compared to PMF and XL-MS^[89]. In order to preserve native-like states of proteins, thus non-covalent interactions, a specific medium is required, which reduces a the non-volatile residuals on proteins. NH_4OAc -Buffer is a volatile substance under low pressure and currently used for native-MS analysis to ensure that proteins keep their native-folded state at the ionisation step. After protein purification and buffer exchange, a typical workflow of a native MS analysis comprises steps including data acquisition using quadrupole orthogonal time of flight mass spectrometer (q-ToF) and data processing using *MassLynx*, as well as deconvolution using tools such as *Massign* or *UniDec*^[90-91]. For the data acquisition, the samples are applied to the instrument with 1-2 μ L/min sample flow. Then ionisation step begins, in which sprayed sample droplets evaporate and are gradually reduced in size. This process occurs according to the Rayleigh limit, which describes a function of surface tension and charge repulsion in the droplets^[92] (see Figure 2.6, A). Accordingly, during evaporation droplets gradually reach a limit of charge repulsion and surface tension which results in droplet fission until they finally produce stable and multiple charged molecule ions. After exclusion of buffer components and impurities, the stable ions enter into the quadrupole, in which they are further selected by defined values of radio frequency and direct current ensuring a stable mass/charge (m/z) ratio. The selected stable ions can reach the collision cell of the instrument. Since native-MS elucidates assembly of protein complexes, the pressure is increased in the collision cell through a defined flowrate of an inert gas (such as argon), in order to produce detectable monomeric protein ions by collision induced dissociation (CID) (see Figure 2.6, B). In CID the ionised proteins were accelerated into a cell in which they collide with the inert gas, argon^[93]. The collision with argon results in fragmentation of proteins or protein complexes to peptides or monomers, respectively. Regarding the protein complexes,

a model proposed that the fragmentation by collision caused a partially unfolding of a monomer and thus locally uncovering of proteins, which resulted in charge migration to the uncovered surface of proteins. Following this, the new charge arrangement of protein monomer led to further unfolding of the protein and charge migration, which ended up with splitting of monomers from the complex. Since the exposed surface of both protein monomers are symmetric, the charge migration gave rise to any mass difference regarding the monomer and complex masses^[94].

During the detection step, these monomer ions as well as complex ions are accelerated resulting in TOF differences due to their mass (see Figure 2.6, B). Accordingly, they reach TOF detectors with different time intervals and reveal their m/z ratios and their stoichiometry in protein complexes on the ES spectra. Of note, intensity ratios of analytes on ES spectra are not quantitative due to their changing ionization efficiency, which cannot be regulated.

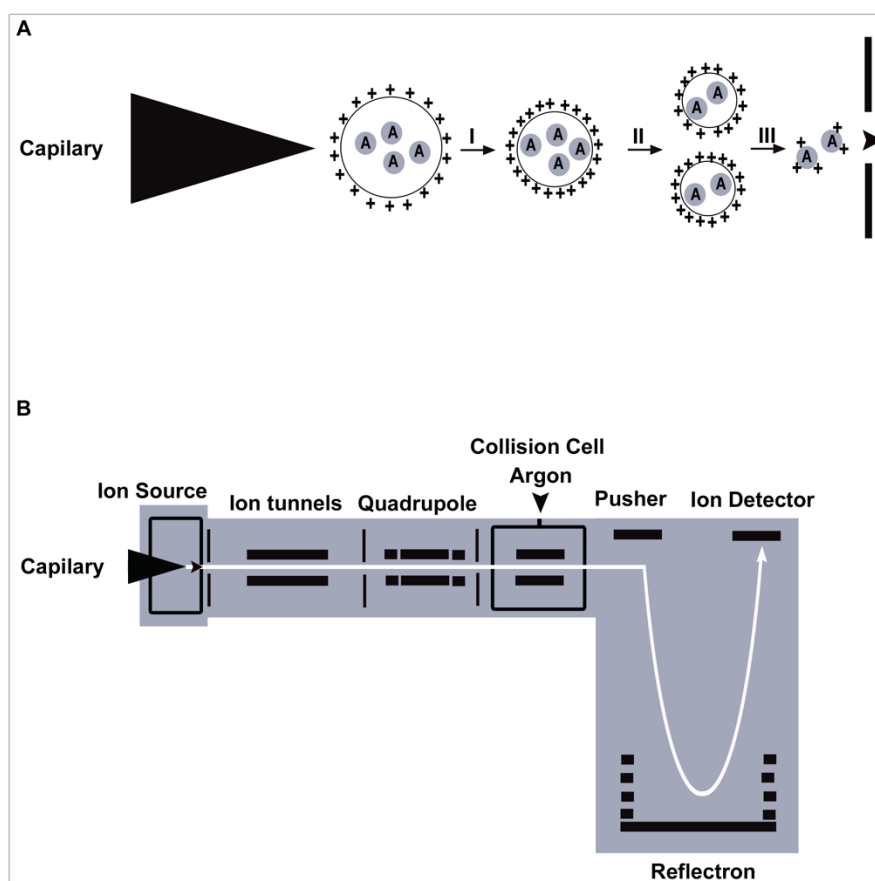


Figure 2.6: A schematic diagram of ESI and a q-TOF mass spectrometer.

[A] Ion formation in electrospray ionisation (ESI) interface. The sprayed sample droplets evaporate and gradually shrink until they reach the Rayleigh limit^[92]. At this limit, the surface tension is not sustainable with the charge repulsion anymore, which results in a Coulombic explosion (I) of the droplets. This produces smaller droplets, that are ripped apart through the same process repeatedly (II). The fission of the droplet occurs until they produce singly or

multiply charged analyte molecules (A) (III). **[B]** The charged analytes enter into the ion tunnel and then the quadrupole where they are selected to ensure a stable mass/charge (m/z) ratio. The selected ions reach the collision cell of the instrument, in which argon is introduced with a defined flowrate for collision induced dissociation (CID)^[93]. For the detection, the ions are accelerated (pusher) resulting in TOF differences (Reflectron) due to their mass. Finally, they reach TOF detectors (Ion detector) with different time intervals, which reveal their spectra based on their m/z ratios. Figure adapted from reference [143]

2.3.2 Protein cross-linking coupled with mass spectrometry

Protein cross-linking coupled with mass spectrometry (XL-MS) is a powerful tool, that consists of a combination of LC-MS and cross-linking chemistry. This combination enables the characterization of protein-protein complexes regarding their intra/intermolecular interacting segments or even solvation of the three-dimensional structures of proteins or protein complexes.

After protein purification, a standard workflow of a XL-MS analysis to uncover the stoichiometry and interactions of proteins or protein complexes, comprises the following steps: Cross-linking of proteins, tryptic digestion and data collection through LC-MS as well as data processing using platforms such as *pLink*^[95].

Cross-linking of the proteins is performed using appropriate cross-linkers according to information that should be attained. Since XL-MS elucidates the structural characterization or stoichiometry and the interaction of proteins or protein complexes, it employs cross-linkers that provide distance information through diverse reactive groups and spacer-lengths dependent on the used crosslinkers and on the residues to cross-link. Such kind of cross-linkers connect the reactive groups of proteins intra- or intermolecularly with a defined spacer-length or zero-length. However, the length of these bonds between two cross-linked residues is flexible and is given as an average value by producers for spacer containing cross-linkers. These parameters are further elucidated in computational modelling studies in order to refine predictions as well as to restrain the possible structural models for membrane proteins and for other proteins that are not amenable to crystallisation and thus structural analysis. The frequently used cross-linkers in XL-MS analysis comprise homo- or heterobifunctional ones such as BS³ or EDC, respectively. BS³ as a homobifunctional one and belongs to the amine-reactive cross-linker group, hence it connects selectively the primary amines of lysines on target proteins with a spacer length of 11.4 Å. Moreover, BS³ cross-links occur in a range of 24 Å and their lengths vary between 5.58 and 11.42 Å^[96]. In contrast, EDC is a carbodiimide, i.e. a carboxyl-to-amine crosslinker, thus it non-selectively connects the carboxyl group of an amino acid (Asp and Glu or C-terminal carboxyl) with the

primary amine group of other ones (Lys, N-terminal amine) forming an amid bond. Since EDC doesn't contain any spacer, it is a zero-length crosslinker. Therefore, the parameter, flexible spacer-lengths, can be excluded in structural studies, which thereby makes EDC more accurate^[97].

According to standard work-flow, cross-linked proteins are subjected to digestion using trypsin. Trypsin is a serine endopeptidase, which contains a serine as a nucleophilic amino acid in its acid-base-nucleophile triad. Trypsin cleaves peptide bonds C-terminal to lysine and arginine residues. The tryptic digestion of cross-linked proteins is followed by data collection of the proteolytic peptides employing LC-MS coupling. Basically, LC-MS is a two-dimensional method which enables the separation of the proteins in the first dimension according to their retention through specific interactions (such as hydrophobic, commonly used in LC-MS), between analytes in the mobile phase and the stationary phase. However, before this step a SEC step might be required, to enrich less abundant cross-linked peptides. In the second dimension, the separated analytes are measured by mass spectrometry which employs diverse mass analysers including TOF or q-TOF. In a last step the data are processed using the *pLink* platform^[95].

3. Aims of the work

Class I peroxisomal membrane proteins (PMPs) are synthesized in the cytosol and inserted into the peroxisomal membrane post-translationally. PEX19 is the cytosolic chaperone-like receptor protein for the *class I* PMPs and stabilises them already at the stage of translation harvesting them through their putative mPTS targeting signal^[34]. Subsequently, the cargo loaded PEX19 docks to its receptor PEX3 on the peroxisomal membrane, where the insertion of the *class I* PMPs takes place. In this assembly, the cargo loaded PEX19 and PEX3 form a hydrophobic pocket on peroxisomal membrane, in which the TA protein is located^[28]. In addition, the hydrophobicity in this pocket which is built through the adjacent hydrophobic residues of PEX3 and PEX19 as well as by the peroxisomal membrane promote the membrane insertion through an unusual membrane intercalation without ATP requirement.

PEX26 is one of the *class I* PMPs and a TA protein, which is inserted into the peroxisome membrane in this manner. In addition, PEX26 is highly hydrophobic and requires PEX19 stabilisation to prevent its aggregation.

Based on the information mentioned above, the main focus of this work was to understand the characteristics of the PEX19-PEX26 complex regarding the following questions:

- I. What are the molecular characteristics of the PEX19-PEX26 complex?
- II. Is PEX19 able to stabilise PEX26 and form a stable recombinant complex?
- III. Are the recombinant PEX3, PEX19 and PEX26 able to form a stable ternary complex?
- IV. Which segments of PEX19 and PEX26 do participate in this complex formation?
- V. Is the recombinant PEX19-PEX26 complex able to complement the PEX26-deficient fibroblasts?
- VI. Is PEX19-PEX26 complex able to insert PEX26 into LUV membrane?
- VII. Does the insertion of PEX26 into LUV membrane occur spontaneously or in a PEX3-dependent manner?
- VIII. Does the insertion of PEX26 into LUV membrane occur despite the lack of the N-terminal TMS of PEX3?

4. Materials and methods

4.1 Buffers, reagents and solutions

All Chemicals used for the preparation of buffers, reagents and solutions were purchased from Roth (Karlsruhe, Germany), Thermo Scientific (Karlsruhe, Germany) or Sigma Aldrich (München, Germany). All enzymes and reagents used for cloning procedures and PCR were provided by Thermo Scientific (Karlsruhe, Germany). Oligonucleotides were synthesized and provided by Biomers (Ulm, Germany).

4.2 Molecular biology

4.2.1 Plasmids

The plasmids used in this work are listed in Table 4.1. Detailed plasmid cards of pNT61, pFS150, pFS151, pFS154 and pSS01 can be found in the Appendix 9.1-9.5 The DNA and amino acid sequences of nPEX3, PEX19 and PEX26 are listed also in Appendix 9.6-9.10. The vectors used in this work are kindly provided by Friederike Schmidt (pFS150, pFS151 and pFS154), Nora Treiber (pNT61), Jan Dieckmann (pJD10), Elisabeth Becker (pEB22.11). pcDNA.3.1.zeo was purchased from Invitrogen (Thermo Scientific, Waltham, USA).

Table 4.1: Plasmid used in protein overproduction and immunofluorescence analysis

Label	Tags and cDNAs	R	Vector
pNT61	Trx-His ₆ -Thr-TEV-[PEX3 ₂₆₋₃₇₃]	Amp	pET32a
pFS150	His ₆ -TEV-[PEX19 ₁₋₂₉₉]	Amp	pDuet
pFS151	His ₆ -TEV-[PEX19 ₁₋₂₉₉ -PEX3 ₂₆₋₃₇₃]	Amp	pDuet
pFS154	His ₆ -TEV-[PEX19 ₁₋₂₉₉ -PEX26 ₁₋₃₀₅]	Amp	pDuet
pSS01	His ₆ -TEV-[PEX19 ₁₋₂₉₉ -PEX26 ₁₋₃₀₅ -PEX3 ₂₆₋₃₇₃]	Amp	pDuet
pcDNA.3.1.zeo	Empty Vector	Amp	-
pJD10	myc-PEX26	Amp	pcDNA.3.1.zeo
pEB22.11	pEGFP-PTS1	Amp	pEGFP-C1

4.2.2 Cloning and transformation

The cloning of the vector pSS01 was carried out as in the following steps:

The cDNA of nPEX3 (PEX3₂₆₋₃₇₃) including its *T7*-promotor and *Lac*-operon from pFS151 was amplified using the polymerase chain reaction with the following primers^[98], FP: 5'-ATCCTTAATTAAGGAGTACACGGCCGCATAATC-3' (Tm: 54°C),

RP: 5'-CTAGCTCAGCTAGTCATTTCTCCAGTTGCTGAGG -3' (Tm: 55°C). The components and the program for PCR reaction are listed in Table 4.2 and 4.3 respectively.

Table 4.2: PCR reaction used for the cloning of pSS01

Component	Volume (in 50 μ L)
Forward Primer (20 μ M)	0.5
Reverse Primer (20 μ M)	0.5
dNTP-Mix (10 μ M)	1
DNA-Template (20 ng/ μ L)	1
Pfu-Buffer-MgSO ₄ (10X)	5
Pfu DNA Polymerase (0.05 U/ μ L)	2.5
H ₂ O	39.5

Table 4.3: Thermocycling conditions used for the cloning of pSS01

Step	Time	Temperature ($^{\circ}$ C)	Cycles
Denaturation	3 min	95	1
Denaturation	30 s	95	35
Annealing	30 s	50	
Elongation	2 min/bp	72	
Elongation	15 min	72	1
Hold	-	4	-

Next, the amplicon was analysed with agarose gel electrophoresis. For agarose gel electrophoresis, 1 μ L of 6x DNA loading dye was mixed with 5 μ L of the amplicon and loaded onto a 0.8% (w/v) agarose gel. The gel was produced by 0.8% agarose in 0.5x TBE buffer. 3 μ L of MIDORI^{Green} (NIPPON Genetics, Düren, Germany) was added 50 mL of agarose gel solution and the gel was cast into a gel chamber. Gels were run for 1 hour at 100 V before DNA was visualized under UV light. The purification of the correct amplicons from agarose gel was carried out with the *QIAquick PCR Purification Kit* (Qiagen, Hilden, Germany) according to the manufacturer's instructions. After their purification, the vector pFS154 and the amplicon are digested with restriction endonucleases *PacI* and *BlnI* prior to ligation as in the Table 4.4. After ligation using *T4-DNA-Ligase* (Table 4.5), the produced new plasmid (pSS01) was electro transfected into DH5 α (*E. coli*) cells and then, the plasmid-containing cells are selected using Amp100 resistance.

Table 4.4: Reaction setup of the restriction for pSS01

Component	Volume (in 50 μ L)
G Buffer (10X)	5
DNA	4
<i>Bpl</i>	2
<i>PacI</i>	4
H ₂ O	35

Table 4.5: Reaction setup of the ligation for pSS01

Component	Volume (in 20 μ L)
Vector DNA (20 ng/ μ L)	5
Insert DNA (20 ng/ μ L)	2.5
T4-DNA-Ligase Buffer	2
T4-DNA-Ligase	1
H ₂ O	9.5

The purification of the vectors was carried out with the *Wizard® Plus Minipreps DNA Purification System* (Promega, Madison, USA) from into *DH5 α* (*E. coli*, Table 4.7) cells according to the manufacturer's instructions. New plasmid constructs are sequenced based on the dideoxy method of Sanger using fluorescence labeled ddNTPs as terminator nucleotides^[99]

For the electro transfection of vectors pSS01, pNT61, pFS150, pFS151 and pFS154 an electro-competent, ampicillin- and chloramphenicol-resistant *E. coli* strain; *Rosetta2* was used (Table 4.7). LOBSTR-BL21(DE3)-RIL (*E. coli*, Table 4.7) cells are used in optimization of expression conditions as an option for expression strain. Accordingly, 50 μ L competent cells and 1 ng of plasmid are mixed and their electroporation was carried out using cooled 2 mm electroporation cuvettes at 2500 volt applying 2 constant pulses, 5 milliseconds each. Thereafter, 400 μ L of pre-warmed SOC medium was added and mixed as soon as possible and then incubated for 1 hour at 37°C. Next, 30 and 300 μ L of the culture were plated onto two agar plates each including both antibiotics Amp100 and Cam25. After incubation for 18 hours at 37°C, one of the colonies are used to inoculate 20 mL of LB medium prior to recombinant protein overproduction or for the preliminary expression tests.

Table 4.6: Solutions and mediums used in cloning step or transformation of *Rosetta2* cells

Name	Content
Amp100	Ampicillin: 100 mg/mL in H ₂ O
Cam25	Chloramphenicol: 25 mg/mL in EtOH
IPTG Solution	1M IPTG in in H ₂ O
SOC Medium	10 mM NaCl, 2.5 mM KCl, 10 mM MgCl ₂ , 10 mM MgSO ₄ , 20 mM Glucose, 2% (w/v) Peptone, 0.5% (w/v) yeast extract
LB-Medium	1% NaCl, 1% Peptone, 0.5% yeast extract, pH 7.0

Table 4.7: Host cells and cell lines used in protein overproduction and immunofluorescence analysis

Name	Strain
DH5 α	F ⁻ ϕ 80/ <i>lacZ</i> Δ M15 Δ (<i>lacZYA-argF</i>) U169 <i>recA1 endA1 hsdR17</i> (r _K ⁻ , m _K ⁺) <i>phoA supE44 λ⁻ thi-1 gyrA96 relA1</i>
Rosetta2 (DE3)	F- ompT hsdS _B (r _B -m _B -) gal dcm (DE3) pRARE2 (CAM ^R)
LOBSTR-BL21(DE3)-RIL	F- ompT hsdS _B (r _B -m _B -) gal dcm (DE3) pRARE2 (CAM ^R)

4.3 Protein analysis

All Chemicals and materials such as columns, labelling reagents and used for the protein analysis were provided by GE-Healthcare (Frankfurt am Main, Germany), Thermo Scientific (Karslsruhe, Germany) or Sigma Aldrich (München, Germany).

4.3.1 Protein overproduction and purification

For the protein over production, 2 L of LB medium including Amp100 and Cam25 was inoculated with 20 mL of the overnight cultures of transformed *Rosetta2* cells and incubated for 4 to 5 hours at 37°C. Thereafter, cultures were induced with 1 mL of IPTG (1 mM), after they were grown to an OD₆₀₀ = 0.5 to 0.6. Induced cultures were incubated at appropriate temperatures, depending on the stability of the proteins (16°C for pSS01, pFS154 and 18°C for pNT61, pFS150 and pFS151), for further 18 hours. After a centrifugation step (28000 g, 45 min, 4°C), harvested cell pellets were stored at -80°C for the purification steps.

Immobilized metal affinity chromatography (IMAC) is a widely-used method for protein purification, especially for recombinant proteins fused to a polyhistidine tag. The stationary phase of this chromatography method consists of an agarose or silica matrix. The chelating ligand such as iminodiacetic acid (IDA), nitrilotriacetic acid (NTA), carboxymethylated-aspartic acid (CM-Asp), 8-hydroxyquinoline, ortho-phosphoserine, and N,N,N'-tris (carboxymethyl) ethylenediamine, is attached to this stationary phase

through a spacer consisting of a hydrophilic chain^[100]. The spacers are principally designed to prevent unspecific interaction between matrix and spacer with proteins. The central divalent metal ions such as Ni²⁺, Cu²⁺ and Zn²⁺ are fixed in the ligand through metal coordination bonds. The IMAC technique is based on the interaction between fixed central metal ions and the polyhistidine tag (*His*₆) fused the recombinant proteins. Depending on the target molecules, the metal ions that are used with these chelating groups can be classified into three groups. Hard metal ions are preferred for the target molecules containing phosphorus, aliphatic nitrogen and oxygen and soft metal ions for sulphur containing targets. The third group comprising Ni²⁺, Cu²⁺ and Zn²⁺, is classified between the both group and prefer to bind targets that contain aromatic nitrogens, oxygens, and sulphur groups. Ni²⁺ is commonly used metal ion which binds to the aromatic nitrogens of the *His*₆-tag fused to proteins, which is weaker than the coordination bonds between oxygen groups of the chelating ligand, NTA.

Prior to IMAC protein purification, harvested cell pellets were resuspended in lysis buffer (HISAPN-Lys, Table 4.8) and incubated for 2 hours at 4°C. After 30 seconds (pulse 1 s, pause 9 s) ultrasonication treatment using 20% intensity, the disrupted cell lysates were centrifuged (28000 g for 1 h, at 4°C). The supernatants filtered using syringe filters (0.45 µm pore size) were loaded onto 1 mL *HisTrap*TMHP columns within 1 h, at 4°C. Prior to elution the loaded columns were washed with at least 5 mL of equilibration buffer (HISAPN-S-Eq, Table 4.8). Elution of the proteins were carried out with AKTA Purifier FPLC system (GE Healthcare, München, Germany) using elution buffer (HISBPN-S-EI). 1 mL of eluted protein was directed to TEV cleavage using a 1:100 (v/v) dilution of TEV-protease (0.5 mg/ mL, Table 4.8) in a dialysis (membrane, (SpectrumTM Spectra/Por MWCO: 6-8,000) against 500-fold dialysis buffer (HISA₀PN-S, Table 4.8) overnight. Prior to gel filtration, the cleaved proteins were loaded onto *HisSpinTrap*TM columns, that was previously equilibrated with HISAPNS-Eq buffer and spun down (800 g, 1 min, 4°C). For preparative and analytical SEC purification, the flow through fractions from former step were loaded onto *Superdex*TM200 *HiLoad*TM 16/60 and *Superdex*TM200 *increase* 3.2/300 columns respectively using HISA₀PNS-SEC buffer (Table 4.8)

Table 4.8: Buffers and solutions used in protein overproduction and purification

Name	Content
HISA	20 mM NaH ₂ PO ₄ , 300 mM NaCl, 10 mM Imidazol, pH 8.0
HISB	20 mM NaH ₂ PO ₄ , 300 mM NaCl, 500 mM Imidazol, pH 8.0
HISAPN	50 mM NaH ₂ PO ₄ , 500 mM NaCl, 25 mM Imidazol, pH 7.0
HISAPNS	HISAPN +200 mM Sorbitol, pH 7.0
HISAPNS-Eq	HISAPN-S + 5mM β-MEtOH, 1mM PMSF, PI 1:100
HISA ₀ PNS	50 mM NaH ₂ PO ₄ , 500 mM NaCl, 200 mM Sorbitol, pH 7.0
HISAPN-Lsy	HISAPN + 5mM β-MEtOH, 1mM PMSF, PI 1:100, DNaseI 1:100, RNaseA: 1:100, 2 mg/mL Lysozyme, 10 mM MgCl ₂
HISA ₀ PNS-SEC	HISA ₀ PNS + 5mM β-MEtOH, 1mM PMSF, PI 1:100
HISA ₀ PN-S-Dia	HISA ₀ PN-S + 5mM β-MEtOH
HISBPNS	50 mM NaH ₂ PO ₄ , 500 mM NaCl, 500mM Imidazol, 200 mM Sorbitol, pH 7.0
HISBPNS-EI	HISBPNS + 5mM β-MEtOH, 1mM PMSF, PI 1:100
RNase A	10 mg/mL RNase: 10 mM TRIS, 15 mM NaCl, pH 7.5
DNase I	1 mg/mL DNase I: 20 mM TRIS, 1 mM MgCl ₂ , 50% (w/v) Glycerol, pH 7.5
PMSF Solution	100mM PMSF in 2-Propanol
PI	Protease inhibitor cocktail: 23 mM AEBSF, 100 mM EDTA 2 mM Bestatin, 0.3 mM Pepstatin A, 0.3 mM E-64
TEV-protease	Purified, 0.5 mg/ mL in 50 mM TRIS, 1 mM EDTA, 5 mM DTT, 50% Glycerol

4.3.2 Bicinchoninic acid protein assay

Bicinchoninic acid protein assay (BCA) is a widely-used method for the determination of unknown protein concentrations through a BCA solution in samples. This solution is a highly alkaline (pH 11.25) mixture of bicinchoninic acid, sodium carbonate, sodium bicarbonate, sodium tartrate, and copper (II) sulphate. Accordingly, the determination of protein concentrations is carried out in two steps. Firstly, Cu²⁺-ions in the solution are reduced to Cu⁺ through the peptide bonds of the proteins. This reduction occurs proportionally to the peptide bonds presents in the solution of protein samples. Whereas in the second step, the free Cu⁺-ions are chelated by two bicinchoninic acid molecules forming a purple coloured complex^[101]. This complex absorbs 562 nm wavelength light proportionally to the unknown protein concentration. The final determination of the unknown protein concentrations is carried out using standard solutions of BSA and an appropriate spectrophotometer.

The protein assay of the samples was carried out with the *Pierce™ BCA Protein Assay Kit* (Thermo Scientific, Waltham, USA) according to the manufacturer's instructions. Accordingly, the protein samples were diluted tenfold using H₂O, preparing two duplicates each. A tenfold dilution of the same buffer was used as a blank. After adding 950 µL of BCA reagent to 50 µL of the protein samples as well as to the blank, the samples were incubated for 30 minutes at 37°C. After cooling the samples for 10 minutes to room temperature, the absorbance of the samples was measured using a spectrophotometer at 562 nm. The measured absorbances were used further calculations of the protein concentrations in the samples using a calibration curve. The calibration curve is obtained by measurement of the absorption of a set of standard BSA samples at 562 nm. These standards are made at various concentrations within a range, that includes unknown protein samples.

4.3.4 Sodium dodecyl sulphate polyacrylamide gel electrophoresis

Sodium dodecyl sulphate–polyacrylamide gel electrophoresis (SDS-PAGE) separates denatured proteins according to their size in a charge-independent manner. In order to shield their own charge, the proteins are treated with an anionic detergent, sodium dodecyl sulphate (SDS) containing buffer prior to their separation on the SDS-PA gel. This requires the linearization of the proteins through disruption of their tertiary and secondary structures for an efficient SDS uptake. In addition to SDS, this buffer includes 2-mercaptoethanol as a reducing reagent in order to disrupt the tertiary structure of proteins. The secondary structures of the proteins are disrupted by heat treatment during sample preparation for SDS-PAGE. The sample preparation is carried out by adding Laemmli buffer (4X) (Table 4.9) to the protein samples^[102]. Then, the mixtures are heated up to 80°C for 5 min. After cooling down to room temperature, the samples were loaded on a 12% SDS-PA gel, that was prepared as described in Table 4.10. After loading the samples, the electrophoresis was carried out at 20 mA for the stacking step and 40 mA for the separation step in SDS running buffer for 1 h. After electrophoresis, the SDS-PA gel was stained with Coomassie Staining Solution for 20 min at RT and destained using Coomassie Destaining Solution for 1h at RT (Table 4.9).

Table 4.9: Buffers and solutions used in SDS-PAGE analysis

Name	Content
APS	10% Ammoniumpersulfat in H ₂ O
Stacking Gel Buffer	1.5 M TRIS, pH 6.8
Separating Gel Buffer	1.5 M TRIS, pH 8.8
SDS-Running Buffer	25 mM TRIS, 192 mM Glycin, 0.1% SDS (w/v)
Laemmli Buffer (4X)	250 mM TRIS, 8% (w/v) SDS, 4% (v/v) Glycerin, 20% (v/v) 2-mercaptoethanol, 0.04% (w/v) BPP, pH 6.8
Coomassie Staining Solution	0.25% Coomassie BB R250, 30% EtOH, 10% (v/v) Acetic Acid
Coomassie Destaining Solution	30% (v/v) EtOH, 10% (v/v) Acetic Acid
Transfer Buffer:	20 mM TRIS, 150 mM Glycin, 0.05% SDS (w/v), 20% MeOH (v/v)

Table 4.10: Polyacrylamid gels used in SDS-PAGE analysis

Resolving gel solution (2 gels)	12%	Stacking gel solution (2 gels)	5%
30% Acrylamid : bisacrylamid (37.5:1)	3.2 mL	30% Acrylamid : bisacrylamid (37.5:1)	500 µL
Resolving gel buffer (1.5 M TRIS, pH 8.8)	2.0 mL	Stacking gel buffer (1.5 M TRIS, pH 6.8)	375 µL
H ₂ O	2.6 mL	H ₂ O	2.1 mL
SDS 10%	80 µL	SDS 10%	30 µL
TEMED	3.2 µL	TEMED	3 µL
10% APS	80 µL	10% APS	30 µL

4.3.5 Western blot analysis

The Western blot technique comprises three steps in which the separated proteins are transferred, recognized and detected. Firstly, the transfer of the proteins is carried out through electrophoresis of the proteins onto a specific membrane such as nitrocellulose or PVDF depending on protein size and using an appropriate buffer. An optimal transfer buffer provides an efficient transfer of the proteins from SDS-PA gel to the membrane and their immobilization with a low conductivity. In the second step the transferred proteins are recognized and consequently immuno-conjugated by specific primary and secondary antibodies^[103]. The primary antibodies are generated through introduction of immunogen molecules (peptides or proteins) to a host organism, which can be mono- or polyclonal. However, the secondary antibodies are generated to recognize the Fc-Domain of the primary antibodies and are often conjugated to HRP^[107]. The HRP carrying proteins are treated with a substrate that

consist of luminol which releases visible light of 425 nm wavelength, and with an enhancer which prevents the rapid decay of this chemoluminescence. The final detection of the proteins is carried out through a film consisting of silver halide layers, that turn into metallic silver if they are exposed to light.

Separated proteins of an SDS-PAGE gel were directed to Semi-Dry blotting using a PVDF membrane. Prior to blotting, the PVDF membrane was treated with MeOH for 5 s and then soaked in transfer buffer. All Whatman papers and the SDS-PAGE gel were soaked in the same transfer buffer as well. Blotting settings were 0.8 mA/cm² of membrane for 1 h, at RT. After blocking with appropriate blocking solutions (PEX19 and PEX26 in B-PBS-T and PEX3 in B-PBS-Tx, Table 4.11), the membrane was incubated with appropriate primary and secondary antibodies (PEX19 and PEX26 in A-PBS-T and PEX3 in A-PBS-STx) as given in the Table 4.12.

Table 4.11: Buffers and solutions used in western blot analysis

Name	Content
PBS:	10 mM Na ₂ HPO ₄ , 1.8 mM KH ₂ PO ₄ , 140 mM NaCl, 2.7 mM KCl pH 7.4
B-PBS-T	PBS+ 0.1% (v/v) Tween20 + 10% Milk powder
B-PBS-STx	PBS + 0.1% (v/v) Triton-X100, 0.02% SDS, 10% Milk powder
A-PBS-T	PBS+ 0.1% (v/v) Tween + 5% Milk powder
A-PBS-STx	PBS + 0.1% (v/v) Triton-X100, 0.02% SDS, 5% Milk powder
W-PBS-T	PBS+ 0.1% (v/v) Tween
W-PBS-STx	PBS + 0.1% (v/v) Triton-X100, 0.02% SDS
Stripping Buffer	Stacking Gel Buffer + 100 mM β-MEtoH , 2% SDS

Washing steps (3 times for 5 mins) were carried out after each antibody-incubation using the proper washing solutions at room temperature (for PEX19 and PEX26, W-PBS-T and for PEX3, W-PBS-STx). The ECL detection was carried out with *Pierce*[™] *ECL Western Blotting Substrate* (Thermo Scientific, Waltham, USA) according to the manufacturer's instructions.

Table 4.12: Primary and secondary antibodies used in western blot analysis

Name	Source	Dilution
α -PEX3 ^[128] , primary	Rabbit	1:10000
α -PEX19 ^[28] , primary	Rabbit	1:5000
α -PEX26 ^[23] , primary	Rabbit	1:3000
α -Rabbit IgG-HRP (Horse radish peroxidase), secondary, (Sigma Aldrich, München)	Goat	1:15000

4.3.6 Native mass spectrometry

The possibility to employ native mass spectrometry (native-MS) was kindly provided by Prof. Dr. Bettina Warscheid the Department of Biochemistry and Functional Proteomics, University of Freiburg, Germany. Native-MS spectra of purified nPEX3, nPEX3-PEX19 and PEX19-PEX26 were acquired by two different systems, a *Q-TOF Ultima* and a *Synapt G1* using the appropriate settings (see Appendix Table 9.1). Prior to acquisition, the purified proteins were directed to buffer exchange using *ZebaSpin* columns equilibrated with native-MS spraying buffer (50-200 mM ammonium acetate pH 6.5-8.0).

For acquisition, 3 to 10 μ L of sample were applied into the systems using a gold-coated capillary, which ensured a stable sample flow (1-2 μ L/min). After the parameters peak-shape and signal stability were optimized, the collision energy was changed to narrow the peak-width and to reduce the noise for an optimal acquisition of native-MS spectra. After optimization, the acquisition was carried out in a manner to obtain spectra including the monomeric as well as the complexed proteins. Furthermore, in order to validate complex formation of two monomeric proteins, the CID technique was employed^[93].

In the evaluation step, the raw acquisition files from *Waters* devices were processed using *MassLynx* software. For the manual annotation, the peak series with Gaussian distribution characteristics were chosen and added to mass options that would be considered as an option in the automatic validation step. Automatic validation was carried out by examining the chosen peaks if they share reasonable Gaussian distribution assigned to common mass. After annotation of all spectra manually, the masses and corresponding charges were exported for deconvolution using the tools *Massign* and *UniDec* for further validation of the manual annotations^[90-91]. The manual annotation data was also plotted to spectra using python-scripts. These evaluations

were performed by Julian Bender and Dr. Friedel Drepper at the Department of Biochemistry and Functional Proteomics, University of Freiburg, Germany.

In order to optimize the peak shapes for deconvolution, the data from the manual annotation was fitted to optimal peak shapes automatically using *peak width* tool. This peak fitting process is based on a condition that implements the appropriate ratios of Gaussian to Lorentzian character in the peaks. After fitting peak shapes, *UniDec* processed the manual annotation data using default parameters. The Native charge offset range was restricted to ± 10 , in order to eliminate extremely high or low charge states in complex samples. The further evaluation of the returned plots was carried out restricting the mass and charge range to the values covering the observed peak series and fitting then to the experimental data. Finally, the results were plotted to zero-charge spectra and exported as images^[91].

Massign is an algorithm developed for the processing native-MS data^[90]. In general, it returns the smoothed mass spectrum data exported from *MassLynx*. Furthermore, *Massign* allows an automatic as well as semiautomatic data processing. In general, the data imported from *MassLynx* in *Massign* are firstly smoothed in order to reduce noise as well as linearized transforming the data to a linear x-axis. Next, the background was subtracted in order to find mass series, which could be assigned to an automatically or semi-automatically adjusted *m/z* range and selecting assigned Gaussian peak envelopes including at least three peaks. Accordingly, *Massign* returns a list of masses with corresponding charge states, which is overlaid with the manual mass list resulted from *MassLynx* in order to visualize which parts of the spectra are not covered. After all components were simulated, this component spectra were simulated using a Levenberg-Marquardt algorithm, in which the tolerance parameters were optimized to minimize the deviation of the sum of simulations from the manual assignment. This data is used to assign masses to the components of the protein complexes.

4.3.7 Protein cross-linking of nPEX3 and PEX19-PEX26

The crosslinker BS³ contains an NHS ester at each end of a 11.4 Å long spacer arm that consists of 8 carbon^[108]. NHS esters form highly selective amid bonds with primary amine groups on the side chains of lysines. Cross-linking of PEX19-PEX26 and nPEX3-PEX19-PEX26 samples was carried out using the homobifunctional cross-linker BS³. The cross-linking, reaction was prepared as shown in Table 4.13.

Accordingly, BS³ was dissolved in HISA₀PNS buffer prior to the reaction in order to prevent hydrolysis of the NHS-esters. A 25 µL cross-linking reaction was composed of a 35-fold excess of BS³ and a 5 to 50 µM final concentration of protein in HISA₀PNS. Another reaction without the cross-linker BS³ was used as negative control.

The reaction mix was incubated (750 rpm 1 hat 4°C) in a thermoshaker. In order to quench unreacted BS³ in the samples, 1 M of Tris-HCl pH 7 was added to a final concentration of 50mM TRIS and incubated further for 15min (750 rpm 1 hat 4°C). Optimal cross-linking conditions were determined by testing cross-linker concentrations around a crosslinker: proteins molar ratio of 35:1. The optimal cross-linking reaction is described as higher-mass products on SDS-PAGE gels but no smear or disappearing of distinct protein bands^[104]. The cross-linked proteins were either analyzed directly on SDS-PAGE for the 'in-gel digestion' or precipitated in 100% cold acetone (-18°C) for the 'in-solution digestion'.

Table 4.13: Cross-linking of purified nPEX3 and PEX19-PEX26

Component	Volume (in 25 µL)
BS ³ (240 µM)	0.5 µL
Protein sample (6.9 µM)	20 µL
H ₂ O	4.5 µL
Tris (1 M)	1,25 µL (+ 25 µL reaction)

4.3.8 Protein digestion for mass spectrometry

For in-gel digestion of the samples, separated protein bands were excised from the gel and destained by treating 10 mM ammonium bicarbonate at RT for 10 min. Then the PAGE-gel slices were washed using 5 mM ammonium bicarbonate and 50% ethanol at room temperature for 10 min. The reduction of proteins was carried out in 10 mM DTT, 10 mM ammonium bicarbonate at 56°C for 30 min, which was followed by the alkylation of proteins in 50 mM iodoacetamide and 10 mM ammonium bicarbonate at RT (in dark) for 30 min. Then the PAGE-gel slices were treated with 10 mM ammonium bicarbonate and following this with 100% EtOH at RT for 10 min respectively. After desiccation of gel slices, proteins were treated with 0.03 mg/mL trypsin in a total volume including 10 mM ammonium bicarbonate at 37°C overnight. Subsequently, the peptides were extracted from the gel slices treating them with 50 µL of 0.05% (v/v)

trifluoroacetic acid (TFA) and 50% acetonitrile solution by sonication at 4°C for 10 min. Evaporated peptides were stored at -80 for proteomic analysis by LC-MS.

For in-solution digestion, after cross-linking the proteins were precipitated using 5-fold volumes cold acetone (-20°C) for 18h at -20°C. Next, The samples were centrifuged (15000 g, 10 min, 4°C) and the precipitated proteins were resuspended in 10 µL 20 mM ammonium bicarbonate including 60% MeOH using ultrasonication three times for 5 min. Prior to trypsin digestion, the reduction of proteins was carried out with 5 mM TCEP to the same solution and incubating for 30 min at 65°C. Then, the reduced proteins were alkylated with 5 mM of iodoacetamide at RT for 30 min in darkroom. Alkylation was stopped adding 20 mM DTT to the reactions. The digestion of samples was carried out with 0.015 mg/mL trypsin adding total volume with 20 mM ammonium bicarbonate to 25 µL for 18 h at 37°C. Evaporated peptides were stored at -80 for proteomic analysis by LC-MS system.

4.3.9 Mass spectrometry analysis of nPEX3 and PEX19-PEX26

After native-MS and cross-linking steps, the fraction of samples containing the proteolytic peptides of nPEX3, PEX19 and PEX26 from both experiments were subjected to proteomic analysis. Accordingly, the peptides were resuspended in 15 µl 0.1% TFA and treated by sonication for 2 min. TFA addition to a mobile phase at a concentration of 0.1% gives rise to proper peak shapes on most columns in LC analysis. Next, the samples were centrifugated (16000 g 2 min 4°C) in order to separate precipitated impurities. Then the supernatant was transferred onto a *RSLCnano HPLC system* (Thermo Scientific, Waltham, USA), which employed a *PepMapTM 0.3/5* pre-column at a flow-rate of 30 µl/min for the pre-enrichment of the samples and to the analytical column *Acclaim PepMapTM (75 µm/500 mm)* at a flow-rate of 0.25µl/min. The separation of the peptides was carried out using the gradient as described in Appendix Table 9.2. Finally, the separated peptides were directly subjected to mass spectrometry analysis using a *Q ExactiveTM Plus System* (Thermo Scientific, Waltham, USA) or an *OrbitrapTM XL System* (Thermo Scientific, Waltham, USA) using the parameters described in Appendix Table 9.3.

4.4 Cell culture experiments

All chemicals and reagents used in the buffer and media preparation (Table 4.14) for cell culture were purchased from Roth (Karlsruhe, Germany), Thermo Scientific

(Karlsruhe, Germany) or Sigma Aldrich (München, Germany). Cells were cultured in Dulbecco's modified Eagle's medium (DMEM) supplemented with 10% (v/v) fetal calf serum (FCS), 2 mM glutamine and 0.1 mM (50 mg/mL) gentamicin. Cells were incubated at 37°C in the presence of 8.5% CO₂. All other experiments including transformation, immunostaining and immunofluorescence steps were carried out at room temperature.

Table 4.14: Buffer and media used in cell cultivations

Name	Content
Electroporation Buffer	250 mM Saccharose, 1 mM MgCl ₂ , in D-PBS
Dulbecco's Modified Eagle Medium-Complete (DMEM)	10% (v/v) FCS, 2 mM Glutamin, 50 µg/ml Gentamicin in DMEM (high glucose)
Hank's Balanced Salt Solution (HBBS)	400 mg/l KCl, 60 mg/l KH ₂ PO ₄ , 350 mg/l NaHCO ₃ , 8 g/l NaCl, 48 mg/l Na ₂ HPO ₄ , 1 g/l D-Glucose, 10 mg/l Phenol-red
Dulbecco's phosphate-buffered saline (DPB-S)	2 g/l KCl, 2 g/l KH ₂ PO ₄ , 80 g/l NaCl, 21,716 g/l Na ₂ HPO ₄
Trypsin- EDTA	0,5 g/l Trypsin, 0,2 g/l EDTA in PBS

4.4.1 Transformation of PEX26-deficient human fibroblasts

PEX26-deficient human fibroblasts, PBD059 used in complementation experiments, were provided by A. B. Moser and H. W. Moser (Kennedy Institute, Baltimore, USA). Transformation of human fibroblasts with purified the PEX19-PEX26 complex (also labelled ones (L-PEX19-PEX26) were carried out using the *NeonTM Capillary Electroporation System* (Thermo Scientific, Waltham, USA)^[105].

One day prior to the transformation, the number of required cells were calculated based on six set of samples, including 4 different experimental groups; negative (pcDNA3.1.zeo) and positive control (pJD10) as well as duplicates of PEX19-PEX26 and labelled PEX19-PEX26 samples. The required PBD059 cell number was 4×10^5 cells for two rounds of electroporation of each sample. According to this, the required cell amount corresponded to twelve 75 cm² culture flasks with an 80-90% cell density on the day of transformation. The required cells were incubated at 37°C in the presence of 8.5% CO₂ in a complete DMEM medium containing 10% FCS, 2 mM glutamine and 50 mg/mL gentamicin.

For the transformation, the cells in twelve 75 cm² culture flasks are washed twice with HBBS and trypsinized using 3 ml of Trypsin- EDTA solution. After dissociation of the cells from the flasks, they are resuspended in 10 ml of complete DMEM and pooled.

Determination of the cell counts were carried out using a *Neubauer* hemocytometer. Then, the volume of the cell suspension including the required total number of cells (6×10^5) was centrifuged (200 g, 5 min, RT). The pellet was washed twice with HBBS and centrifuged again (200 g, 5 min, RT). The final pellet was resuspended in 120 μ L of Dulbecco's PBS containing 250 mM sucrose and 1 mM $MgCl_2$ and divided into six samples. Prior to transformation, purified plasmids were added to these samples as in the following Table 4.15. Based on this All twelve transformations were carried out in 10 μ L capillary tips applying 1050 V for 30 ms.

Table 4.15: Experimental groups used in complementation of PEX26-deficient human fibroblasts (PBD059)

Sample	Content
Control (-)	20 μ L (PBD059) + 1 μ L pcDNA3.1.zeo (66 ng) + 1 μ L pEB22.11 (66 ng)
Control (+)	20 μ L (PBD059) + 1 μ L pJD10 (66 ng) + 1 μ L pEB22.11 (66 ng)
PEX19-PEX26 (2X)	20 μ L (PBD059) + 2 μ L PEX19-PEX26 (4 μ M)
L-PEX19-PEX26 (2X)	2 μ L (PBD059) + 2 μ L L-PEX19-PEX26 (4 μ M)

Next, the transformed cells were transferred into a six-well-plate which included pre-warmed complete DMEM and three cover slips in each well and incubated at 37°C in the presence of 8.5% CO_2 for 14 h.

4.4.2 Immunostaining of fibroblasts

After 14 hours of incubation on the cells on coverslips, they were washed with DPB-S and treated with 3% formaldehyde in DPB-S at RT for 30 min, for the fixation of the cells on coverslips. Next, they were washed again three times with DPB-S and subjected to permeabilization using 0.5% Triton-X100 in DPB-S at RT for 5 min. For the immunostaining of the cells, the primary antibodies were diluted in 30 μ L of DPB-S as in the following table and pipetted on a sterile parafilm. Incubation of cells with the primary antibodies was carried out at RT for 30 min. After incubation, the cover slips were washed five times with DPB-S and incubated with the secondary antibodies (Table 4.16). Then, the dishes were washed 5 times with DPB-S and placed on microscope slides using 15 μ L of Mowiol-DABCO solution for fluorescence microscopy analysis^[106]

Table 4.16: Antibodies used for western blot and immunofluorescence analysis

Name	Source	Dilution
α -PEX14 ^[129] , primary	Rabbit	1:400
α -AFP, primary (QBiogene/MP Biomedicals, Illkirch, France)	Mouse	1:100
α -MouseAlexa-Fluor-488, secondary (Molecular Probes/Invitrogen, Darmstadt, Germany)	Donkey	1:300
α -Rabbit-Alexa-fluor-594, secondary (Molecular Probes/Invitrogen, Darmstadt, Germany)	Donkey	1:200

4.4.3 Immunofluorescence microscopy analysis

Final assessment of the stained cells was carried out using a *Zeiss Axiovert 200M* fluorescence microscope equipped with a *Plan-Apochromat 63x/1.4* oil objective. *AxioVision 4.8* software was used for taking and processing of representative images.

4.5 LUV Integration

The lipids used for LUV preparation were purchased from Avanti Polar Lipids (Alabaster, USA)

4.5.1 Protein labelling of nPEX3^T and PEX19-PEX26

The labelling of purified nPEX3^T (Thx-His₆-Thr-TEV-nPEX3) and PEX19-PEX26 samples was carried out using a maleimide-derivative of *Alexa Fluor® 488-C₅* (Thermo Scientific, Waltham, USA) which conjugates selectively reduced thiol groups of cysteines. Maleimides don't react with histidine and methionine. The labelling reaction proceeds as a Michael-type Addition by a thiolate-catalysed thiol addition to an N-substituted *Alexa Fluor® 488-C₅-maleimide (Alexa488)*.

For the labelling, 1 mL of 5 μ M of purified proteins in HISA₀PNS (Table 4.8) buffer were treated with 0.5 μ L of TCEP (stock solution, 50 mM) for 30 min on ice, in order to reduce the disulphide bridges. Next, 0.5 μ L of *Alexa488* (stock solution, 10 mM) was diluted to 10 μ L using HISA₀PNS buffer prior to reaction start. This solution added to the reaction mixture stepwise within 1 h (1 μ L every 5 min) on ice to prevent protein aggregation. Afterwards the mixture was incubated in a dark room overnight, at 4°C. In order to remove unbound *Alexa488*, the mixture was transferred into a dialysis membrane (Spectrum™ Spectra/Por MWCO: 6-8,000) and dialyzed against 1000 mL of dialysis buffer (HISA₀PN-S-Dia: HISA₀PNS + 5mM β -MEtOH, 1mM PMSF, PI 1:100)

overnight. To assess the degree of labelling (DOL) of the proteins, absorption spectra of the samples was acquired over a 200-800 nm wavelength range using a *Nanodrop 2000* (Thermo Scientific, Karlsruhe, Germany). According to this spectrum, the A_{495} and A_{280} correspond to the absorption maximums of measured proteins at 495 and 280 nm. Based on this, the DOL was calculated using the extinction coefficient, ϵ_{dye} of *Alexa488*: $71000 \text{ cm}^{-1} \text{ M}^{-1}$ and extinction coefficients, $\epsilon_{280}(\text{Protein})$ of nPEX3^T and PEX19-PEX26: 52707 and $31111 \text{ cm}^{-1} \text{ M}^{-1}$ respectively. Absorbance at 280 nm was corrected by a correction factor (CF) defined as $\text{CF}_{280} = A_{280}(\text{freedye}) / A_{495}(\text{freedye})$. The CF_{280} value for *Alexa488* corresponds to 0.11. The DOL was calculated according to following equation^[112].

$$\text{DOL} = \frac{\epsilon_{280}(\text{Protein}) \times A_{495}}{(A_{280} - \text{CF}_{280} \times A_{495}) \times \epsilon_{\text{dye}}}$$

4.5.2 Preparation of large unilamellar vesicles (LUVs)

In order to mimic the peroxisomal membrane, we prepared LUVs using the extrusion method to produce LUVs with average diameter of 400 MWCO. The lipids and their compositions for LUV preparations were as following: Egg PC: 65.8%, Egg PE: 28.2% and Ni-DGS: 6% (Table 4.16). Prior to the experiments, individual lipid stock solutions (Egg PC and Egg PE: 10 mg/mL, Ni-DGS: 5mg/mL) preserved in chloroform were mixed to give the above-mentioned molar ratio corresponding to 1 mg of total lipid. The resulting solution was evaporated for 2 hours under vacuum to remove the chloroform. 2 mg of the dried lipid-mix was dissolved in 400 μL of LUVA₀- S (Table 4.17) mixing gently until a homogenic and cloudy solution was achieved. Next, the mixture was transferred to a cryo-vial and incubated in pre-warmed to 40°C in a water bath for 3 min. Then the mixture was flash-frozen in liquid nitrogen. The frozen mixture was thawed for 3 minutes at 40°C and then briefly vortexed. This freeze & thaw step was repeated six times. The resulting mixture (~400 μL) was extruded using an extruder (*Avestin*, Ottawa, Canada). In this step, the mixture was passed through a membrane with 400 nm MWCO (polycarbonate membrane Diameter: 19 mm, *Avestin*, Ottawa, Canada) 31 times using two *Hamilton* syringes (1 mL) according to the manufacturer's instructions. The extruded suspension was stored on ice during the experiments. In order to confirm the size distribution of LUVs, we used dynamic light scattering.

Table 4.16: Lipids used for LUV preparation

Name	Content
EggPC	L- α -phosphatidylcholine (Chicken)
EggPE	L- α -phosphatidylethanolamine (Chicken)
Ni-DGS	2-dioleoyl-sn-glycero-3-[(N-(5-amino-1-carboxypentyl) iminodiacetic acid) succinyl] (nickel salt)

Table 4.17: Buffers used in LUV preparation and integration assay

Name	Content
LUVA ₀ -S	50 mM NaH ₂ PO ₄ , 500 mM NaCl, 10% Sucrose, pH 7.0
LUVA-S ₀	50 mM NaH ₂ PO ₄ , 500 mM NaCl, 25 mM Imidazol, pH 7.0
LUVB-S ₀	50 mM NaH ₂ PO ₄ , 500 mM NaCl, 500 mM Imidazol, pH 7.0

4.5.3 Dynamic light scattering analysis of LUVs

Dynamic light scattering is a powerful technology that provides a rapid analysis of homogeneity of protein and nucleic acid, as well as particles like LUV containing solutions. Basically, DLS analyses the diffusion behaviours of macromolecules in solutions. A typical DLS measurement encompasses the analysis of light-scatter from a sample, that is exposed to a monochromatic light. Accordingly, the intensity of light is analysed in a time dependent manner that provides information about the molecular mass and the hydrodynamic radii of macromolecules. The Hydrodynamic radius, described as the Stokes radius, also corresponds to the size parameters obtained from SEC^[110-111]. DLS analysis of the LUVs was carried out using the *DLS-Zetasizer* (Malvern, Kassel, Germany) according to the manufacturer's instructions. For DLS, A 50 μ L of the LUVs was filled in a 1 cm quartz cuvette and measured performing three sets of twenty acquisition in LUVA₀-S buffer using manual settings. The obtained results provided information about size distribution of the LUVs that had been previously extruded using a 400 MWCO filter.

4.5.4 LUV-protein integration assay

The prepared LUV suspension (400 μ L) was divided into 11 separate tubes (35 μ L each) corresponding to one control tube (A, Table 4.18, step (I)) and five incubation tubes with two replicates of each (B-F, Table 4.18, step (I)). Blocking of the LUVs was performed using 100 μ L of 4% BSA in LUVA-S₀ (Table 4.17) for 1 h, on ice (Table 4.18, step (II)). Next, the blocked LUV were centrifuged (16000 g, 10 min, 4°C). Next, 1 mL

of each supernatant was removed and discarded. The all following washing and centrifugation steps of the samples were carried out three times for each sample. Next, the samples were washed using 1 mL of LUVA-S₀ (Table 4.17). The LUVA-S₀ buffer doesn't contain any sucrose in comparison to the buffer, that was used during LUV preparation, however, this buffer contains 25 mM of imidazole to prevent unspecific interactions of proteins with Ni-DGS-lipids. As following, the LUVs was pelleted by centrifugation (16000 g, 10 min, 4°C) and 1 mL of each supernatant was removed carefully and discarded. In the following step, 50 µL of the appropriate labelled proteins (as described in Table 4.18) were added to the appropriate tubes (Table 4.18, step (IV)) except for the fractions of A, which was considered as negative control. For each incubation step, 5 µM of the appropriate protein was incubated with the liposomes. After gently mixing, the tubes were incubated for 1h on ice. Since the proteins contained a fluorescent label (*Alexa488*), the samples were prevented from light. After incubation, the samples B, D, E and F were washed by adding 1 mL LUVA-S₀, while the samples B were washed with 1 mL of LUVB-S₀, to eluate unbound nPEX3^T. This eluted sample B was considered as a kind of control to examine the nPEX3^T and LUV interaction. The LUVs were pelleted again by centrifugation (16000 g, 10 min, 4°C). In the final steps of samples E and F, the LUVs were incubated with labelled PEX19-PEX26 (5 µM in 50µL) (Table 4.18, step (V)) for 1 h on ice. Washing steps of these samples were carried out using 1 mL of LUVA-S₀ buffer for the samples E and 1 mL of LUVB-S₀ for the samples of F. Here we considered the sample F as negative control for the binding of PEX26 to the liposomal membrane. After centrifugation (16000 g, 10 min, 4°C) all samples were subjected to flow cytometry (FC, Table 4.18) analysis.

Table 4.18: LUV-protein integration assay

	(I)	(II)	(III)	(IV)	(V)	(VI)	(VII)
A	BSA/LUVA-S ₀	LUVA-S ₀	-	-	-	-	FC
B	BSA/LUVA-S ₀	LUVA-S ₀	nPEX3L	LUVA-S ₀	-	-	FC
C	BSA/LUVA-S ₀	LUVA-S ₀	PEX3L	LUVB-S ₀	-	-	FC
D	BSA/LUVA-S ₀	LUVA-S ₀	PEX19/26L	LUVA-S ₀	-	-	FC
E	BSA/LUVA-S ₀	LUVA-S ₀	PEX3	LUVA-S ₀	PEX19/26L	LUVA-S ₀	FC
F	BSA/LUVA-S ₀	LUVA-S ₀	PEX3	LUVA-S ₀	PEX19/26L	LUVB-S ₀	FC

Treatment of Ni-NTA-LUVs in 6 different experimental groups including the steps I: blocking with BSA, II: three times washing of blocked liposomes using LUVA-S₀, III: Incubation (except A) with appropriate proteins including nPEX3^T (labelled nPEX3^T for B and C), nPEX3^T

(unlabelled, for E and F) and PEX19-PEX26 (labelled PEX19-PEX26 for D), **IV**: Three times washing using appropriate buffers, LUVA-S₀ (B, D, E and F) and LUVB-S₀(C), **V**: Incubation with PEX19-PEX26 (labelled PEX19-PEX26 for E and F). **VI**: Three times washing using appropriate buffers: LUVA-S₀ (E) and LUVB-S₀(F), **VII**: Flow cytometry (FC) analysis of all experimental groups

4.5.5 Flow cytometry-based LUV-protein integration assay

Flow cytometry is powerful a technology that provides rapid analysis of single cells or particles, like LUVs or GUVs regarding different parameters like, relative size, shape, number and fluorescence^[109]. Accordingly, depending on the experimental setup, particles or cells are analysed using laser light scattering or single or multiple fluorescence light parameters. The light scatter facilitates two different measurements as forward and side scatter. The forward scatter (FSC) provides information about the relative size of cells or particles through light scattering with a small-angle, while the side scatter (SSC) reveals information on the internal complexity or granularity of them using an angle of 90°^[113]. The fluorescence analysis employed in flow cytometry determines the fluorescence intensity in different populations. The fluorescence signals of the analyte can originate from fluorescent proteins like GFP, fluorescently coupled proteins or LUVs as well as of DNA binding dyes. Based on the fluorophores used in the measurements, flow cytometry can use single or multiple fluorescent channels including FITC (490/525 nm) and PE (496/578 nm).

Flow cytometry analysis of our samples was carried out with a *CytoFLEX* flow cytometer (Beckman Coulter, California, USA) according to the manufacturer's instructions. Since we labelled our proteins with *Alexa488* (495/515 nm), the measurements of the 11 samples were carried out using the FITC (490/525 nm) channel to acquire the signal intensity of 1000 events (LUVs) in total. The acquisition of the 1000 events (LUVs) was carried out using slow flow rate (10 µL/min) in 300 sec.

4.5.6 Carbonate extraction of nPEX3^T and PEX26

Carbonate extraction is employed in the analysis of membrane-protein interactions especially in order to distinguish between integral and peripheral membrane proteins^[114]. Peripheral membrane proteins are able to dissociate from their specific organelle membrane by increasing the ionic strength through treatment with high salt concentrations or by using chelating agents like EDTA, as well as using high concentration of denaturing agents like of urea, NaOH or Guanidine Hydrochloride.

Integral membrane proteins are amphipathic and released from membrane only through disruption of the lipid bilayer using detergents like Triton-X100 or SDS.

In order to analyse a possible integration of proteins into the LUVs after incubation and flow cytometry steps, the LUVs were subjected to treatment with 1% Triton-X100 and 1 M Na₂CO₃. Each sample was diluted to 90 µL and then divided into three fractions of 30 µL. The three fractions were treated separately with 60 µL of LUVA-S₀, 60 µL of 1% Triton-X100 and 60 µL of 1 M Na₂CO₃ and named as T (Total), TX (Triton-X100) and CO (Na₂CO₃) respectively. After 30 min incubation on ice each sample was centrifuged (100000 g for 1 h, at 4°C). Then, each sample was separated into supernatant and pellet. The supernatant fractions (~90 µL) were treated with 4-fold SDS sample buffer, while 30 µL of 1-fold SDS sample buffer was added to the pellet fraction. All samples were heated to 80°C and frozen at -20°C. The detection of each protein was carried out using western-blot analysis using the antibodies against PEX3 and PEX26.

5. Results

PEX26 is a TA protein and member of *class I* PMPs, which is inserted into the peroxisome membrane in a PEX19-dependent manner. In addition, PEX26 is highly hydrophobic and requires PEX19 for stabilisation to prevent its aggregation *in vivo*. In this work, we aimed to purify the complex of PEX19-PEX26 and analyse it concerning its stoichiometry using SEC and native MS analysis. In addition, we wanted to characterize interacting segments of the protein complex using the XL-MS technique. Regarding its functionality, we subjected this complex to a complementation assay using PEX26-deficient fibroblasts. Moreover, this complex should be used to integrate PEX26 into LUVs utilizing PEX3 as a docking protein.

5.1. Optimizing the purification conditions of the PEX19-PEX26 complex

As PEX26 is highly hydrophobic and requires PEX19 for stabilisation we assumed that the co-expression of full length *His₆-PEX19* with *PEX26* and co-purification of both proteins could result in a functional native-like complex, in which the flexible N-terminal half of PEX19 and the TMS of PEX26 would be mutually stabilized. Obtaining a native like complex of PEX19 and PEX26 would enable us to further investigate structural characteristics and functions of this complex. Therefore, we expressed *PEX26* bicistronically with *PEX19* using conditions, that were optimized in the following steps. After overexpression of *PEX19-PEX26*, the purification of the proteins was performed using IMAC in all optimization steps. In order to find optimal conditions for the complex of PEX19 and PEX26, we decided to use the expression and purification conditions from a former study on PEX3 and PEX19 as a basis for our expression vector pFS154 (see Section 4.2.1)^[28]. In that study, *Rosetta2* was used as a host strain, LB medium as cultivation medium (Induction 1 mM IPTG), and HISA-B buffers for purification and further analysis of PEX3 and PEX19 interactions. The expression vector pFS154 is based on a two-promotor system of the vector pETduet, that consists of two separate multiple cloning sites (MCS), which are preceded by own T7 promoters/lac operators and ribosome binding sites (*rbs*). MCS-I included the ORF of *PEX19* which is fused to sequences encoding an N-terminal polyhistidine tag (*His₆*) and TEV cleavage sequence respectively, while MCS-II contained the ORF of full-length *PEX26* (see Appendix 9.4). We expressed our vector in LB medium at 18°C, induced with 1 mM IPTG using the same conditions as described for PEX3^[28] (see Figure 5.1, A: BI: before induction, AI: after induction). *His₆-PEX19-PEX26* was purified by

*HisSpintrap*TM columns as described in Section 4.3.1. The two bands (see Figure 5.1, A.: 737-I and 737-II) that appeared approximately at the expected sizes corresponding to 35 and 40 kDa, respectively were excised, subjected to tryptic *in gel* digestion to extract proteins and submitted to mass spectrometric identification. Mass spectrometry analysis confirmed the identity of *His*₆-PEX19 and PEX26. The observed top scores were 166 and 165 for *His*₆-PEX19 and PEX26 respectively (protein scores greater than 70 are significant, $p < 0.05$) (see Figure 5.1, B and C). The sequence coverage of the proteins was 48.8% for *His*₆-PEX19 and 43.3% for PEX26.

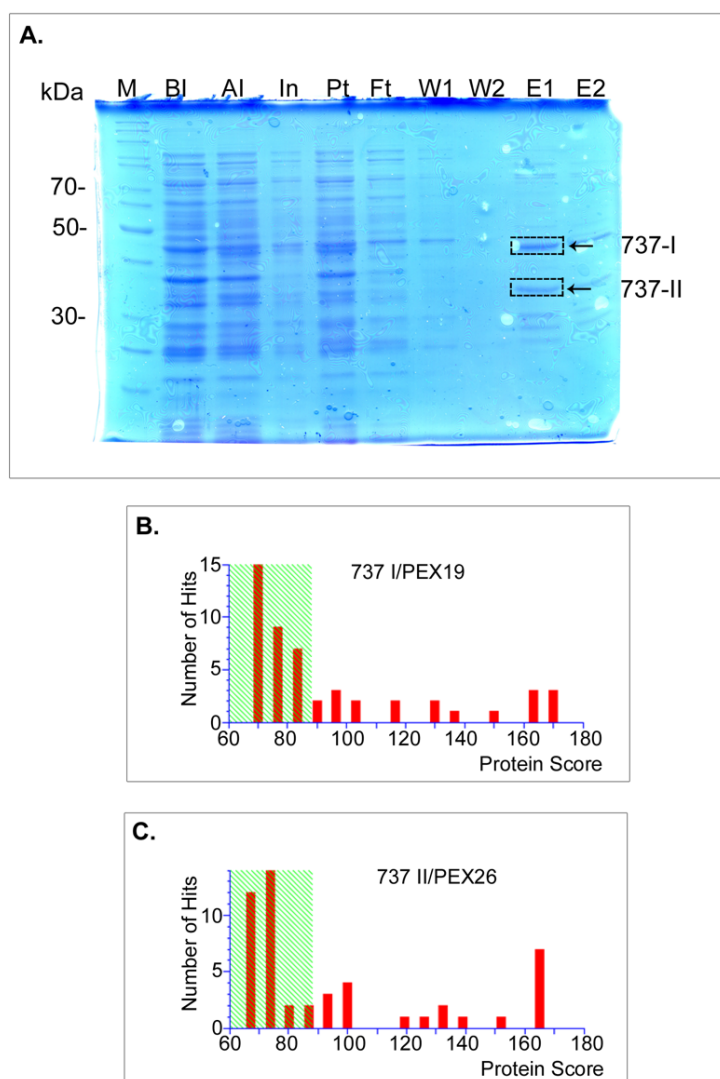


Figure 5.1: The preliminary expression and purification conditions of *His*₆-PEX19-PEX26 used as a basis for the optimization step.

[A] SDS-PAGE analysis of purified *His*₆-PEX19-PEX26. A 12% SDS-PA gel was loaded with the protein samples treated with 4-fold sample buffer and stained with Coomassie Brilliant Blue R-250 after electrophoresis. The portions of loaded samples depend on the working volumes of each experimental steps as following; 0.01% for the lanes of before induction (BI) and after induction (AI), 0.03% for the lanes of Input (In), pellet (Pt) and flow through (Ft), 1.7% for the lanes of the washing steps (W1-W2) and elution steps (E1-2). Lane M indicates molecular weight size marker (Thermo Scientific). The two excised gel bands: 737-I and 737-II were

subjected to tryptic digestion and mass spectrometry analysis. **[B]** Mass spectrometry analysis of 737-I has confirmed the identity of His₆-PEX19 with top score of 166 and 48.8% sequence coverage. **[C]** Mass spectrometry analysis of 737-II has confirmed the identity of PEX26 with a top score of 165 and 43.3% sequence coverage. (protein scores greater than 70 are significant, $p < 0.05$) Theoretical molecular mass of the proteins: PEX19: 32.8 kDa and PEX26: 33.9 kDa.

In order to optimize the expression strain for cDNAs, we tested two different *E. coli* strains; *Rosetta2* and *LOBSTR-BL21-RIL* (see Figure 5.2: Lane I and V). A *BL21 (DE3)* derivative, *Rosetta2* host strain was developed to optimize the expression of eukaryotic proteins to cover the rarely used codons; AUA, AGG, AGA, CUA, CCC, GGA and CGG in *E. coli* [115]. These are contained on a compatible plasmid, pRARE, which also exhibited chloramphenicol (34 µg/mL) resistance to *Rosetta2* cells [127]. *LOBSTR-BL21-RIL* is also a *BL21* derivative and was developed to enhance purity of histidine tagged proteins reducing the expressions of the contaminant *E. coli* proteins ArnA and SlyD. This strain also includes extra copies of the rare tRNA genes; *argU*, *IleY* and *leuW* and conferred chloramphenicol resistance gene [130]. After retransformation of both strains with pFS154 (His₆-PEX19-PEX26), the expression was performed using 1mM IPTG for induction overnight at 18°C. Since we didn't observe an improvement on the expression levels using *LOBSTR-BL21-RIL*, we decided to use the *Rosetta2* host strain for further optimization (see Figure 5.2: Lane I and V)

For protein expression media, we tested *lysogeny broth* (LB) which is the most widely used medium for the growth of bacteria and *terrific broth* (TB) which is developed to improve yields in recombinant protein production in *E. coli*. The aim of this step was to obtain an equal production amount of both, PEX19 and PEX26 following the assumption of a binary complex of PEX19 and PEX26. Accordingly, since we could purify almost the same amount of PEX19-PEX26 using the two different media, we decided to stick to LB for further optimization (see Figure 5.2: Lane II and V). In order to optimize the temperature conditions, we tested pFS154 transformed *Rosetta2* cells growing at 12°C or 16°C overnight. Concerning the ratio of produced PEX19 and PEX26, both gave almost the same results, however, the expression at 16°C resulted in a higher amount of proteins. Thus, we decided to use 16°C as preferred temperature for protein production (see Figure 5.2: Lane III and V).

For further optimization, we tested our vector pFS154 using three different concentration of IPTG. Thus, we induced pFS154 transformed *Rosetta2* cells in LB medium at 16°C, adding 0,1 µM, 0,5 µM and 1 µM of IPTG to the cultures overnight.

Since the amount of proteins increased proportionally with increasing IPTG concentrations from 0,1 μM to 1 μM , we decided to use 1 μM IPTG for induction.

After optimizing the expression parameters comprising expression strain, media, temperature and IPTG induction concentration, we continued with the optimization of purification parameters, including buffer condition as buffer substance, ionic strength, pH and osmolytes.

Since we wanted to analyse the interactions of the proteins with each other as complex and their functionality regarding the complementation of PEX26-deficient fibroblasts (PBD059) and LUV integration experiments, we required an appropriate buffer which provides native-like conditions for all experiments. Therefore, we firstly calculated the theoretical *pI* of nPEX3 (PEX3₂₆₋₃₇₃), PEX19 and PEX26, with pH 6.28, 4.26, 5.94, respectively^[124]. Concerning this, we considered potential buffer substances regarding their buffering range, $\text{pK} \pm 1$ depending on *pI* of the proteins. Thus, phosphate ($\text{H}_2\text{PO}_4^-/\text{HPO}_4^{2-}$, pK_2 : 7.20) and HEPES (pK_2 : 7.48) were two potential buffering systems to use as basis for other buffer components like, salt, protein stabilizing osmolytes and reducing agents. In order to figure out the best ionic strength for the proteins, we tested, $\text{KH}_2\text{PO}_4/\text{KOAc}$, and $\text{NaH}_2\text{PO}_4/\text{NaCl}$ (see Figure 5.2: Lane IV and V). Since potassium precipitated with SDS in the steps of SDS-PAGE analysis, we withdrew from using a potassium containing buffer system, with the presumption that this would interfere with further analysis steps negatively. Thus, we decided to use a $\text{NaH}_2\text{PO}_4/\text{NaCl}$ system for further experiments.

Additionally, we tested the purification of the proteins employing higher a concentration of imidazole and NaCl-based on our purification buffer system NaH_2PO_4 (50 mM, pH 7.0). We concluded that the higher NaCl (500 mM) and imidazole (500 mM) containing buffers gave rise to better purification results (see Figure 5.2: Lane I-II and V).

Osmolytes like betaine, proline, sucrose, glycerol and sorbitol support correct protein folding stabilizing the native folded state of proteins. In order to prolong the stability of a native folded state of proteins during our further analysis, we tested the addition of glycerol or sorbitol (10% and 200 mM, respectively) based on the optimized purification buffer. Finally, we concluded that phosphate buffer (50 mM NaH_2PO_4 , pH:7.0) including 500 mM NaCl and 200 mM sorbitol was the most convenient one for our further analysis of the PEX19-PEX26 complex (see Figure 5.2: Lane I-II and V).

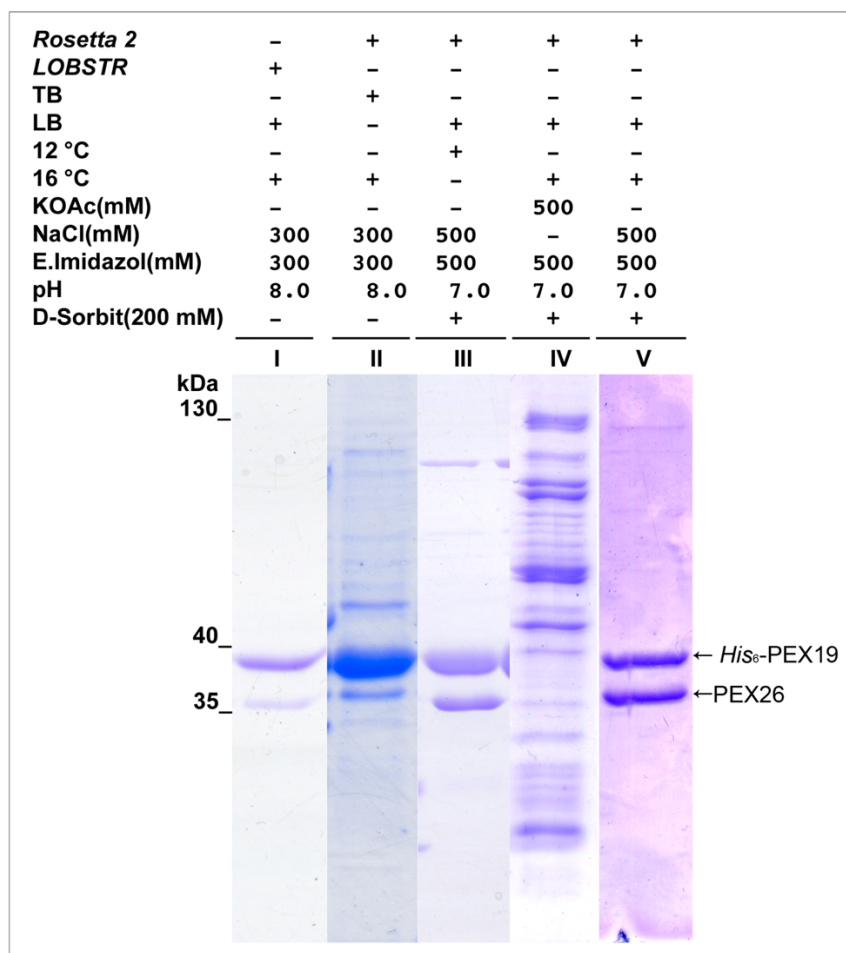


Figure 5.2: Optimisation of expression and purification conditions for the *His*₆-PEX19-PEX26. SDS-PAGE analysis of all optimization steps of *His*₆-PEX19-PEX26 purification. For each step, a 12% SDS-PA gel was loaded with the protein samples treated with 4-fold sample buffer and stained with Coomassie Brilliant Blue R-250 after electrophoresis. The portion of loaded samples depend on the working volumes of purification step and corresponds to 1.7% of the total expression mass. Theoretical molecular mass of the proteins: PEX19: 32.8 kDa and PEX26 :33.9 kDa.

5.2. Purification of the recombinant PEX19-PEX26 complex

In order to analyse the PEX19-PEX26 complex regarding its interactions and functionality, we purified PEX19-PEX26 as a complex. This approach was based on the knowledge that PEX26 is a very hydrophobic TA protein, which is stabilised by its native receptor protein PEX19 already at the stage of translation, *in vivo*. In addition to this, PEX19 possesses a very flexible N-half, that could not to be crystallised for further structural analysis^[73]. According to the IMAC chromatogram, the fractions of eluted proteins were analysed using SDS-PAGE (see Figure 5.3: A and D). Two gel bands approximately running at the expected range between 35 and 40 kDa (see Figure 5.3: D, Lane A2-A3). Prior to further analysis of the complex, purified proteins were treated with TEV protease to cleave the N-terminally fused *His*₆-tag from PEX19 through

dialysis against HISA₀PN-S buffer at 4°C overnight (see Figure 5.3: D, Lane T). After TEV cleavage and dialysis, the proteins are subjected to another purification using IMAC spin columns, *HisSpintrap*TM to separate uncut PEX19 and cleaved His₆-tag residues from the PEX19-PEX26 complex. The following SDS-PAGE analysis confirmed that the His₆-PEX19-PEX26 complex had been successfully cleaved (see Figure 8, D, Lane In). In the final purification step the cleaved complex was further purified using *preparative* size exclusion chromatography (SEC). The *preparative* SEC separates proteins from high molecular aggregates and other contaminant proteins employing a *Superdex*TM200 *HiLoad*TM 16/60 (*GE Healthcare*) column depending on their size and retention time. Accordingly, the 14th to 19th fraction (see Figure 5.3: B) were pooled for further analysis using analytical SEC (see Figure 5.3: C) to estimate the stoichiometry of the complex. In addition, this allowed to acquire more reliable information on possible high molecular aggregates, which would be dissolved to monomers on SDS-PAGE gels. Accordingly, analytical SEC indicated a peak series with the elution volumes of a: 1.14, b: 1.24, c: 1.31, d: 1.42 mL that correspond to 419, 241, 169, 98 kDa and could be assigned to aggregated PEX26 (a and b), to the PEX19-PEX26 complex (c) as well as to unbound PEX19 (d), respectively (see Figure 5.3: C and D, Lanes: a-d). The assigned total molecular mass of the complex corresponded to 169 kDa whereas the calculated theoretical molecular mass of PEX19 and PEX26 as well as that for the PEX19-PEX26 complex were 32.80, 33.89 and 66.69 kDa, respectively. Additionally, no monomeric PEX26 could be observed, but its aggregates in various sizes corresponding to 419 kDa and 241 kDa were seen. Thus, we conclude that PEX19 and PEX26 form a stable heteromeric complex with an assigned mass of 169 kDa. Verification of both proteins was performed employing western blot analysis with PEX19 and PEX26 antibodies (Figure 5.4: A and B, respectively). For the SEC comparison, the purification of full-length PEX19 was performed using same conditions as in the purification steps of PEX19-PEX26 based on the vector pFS150 (see Appendix 9.2)

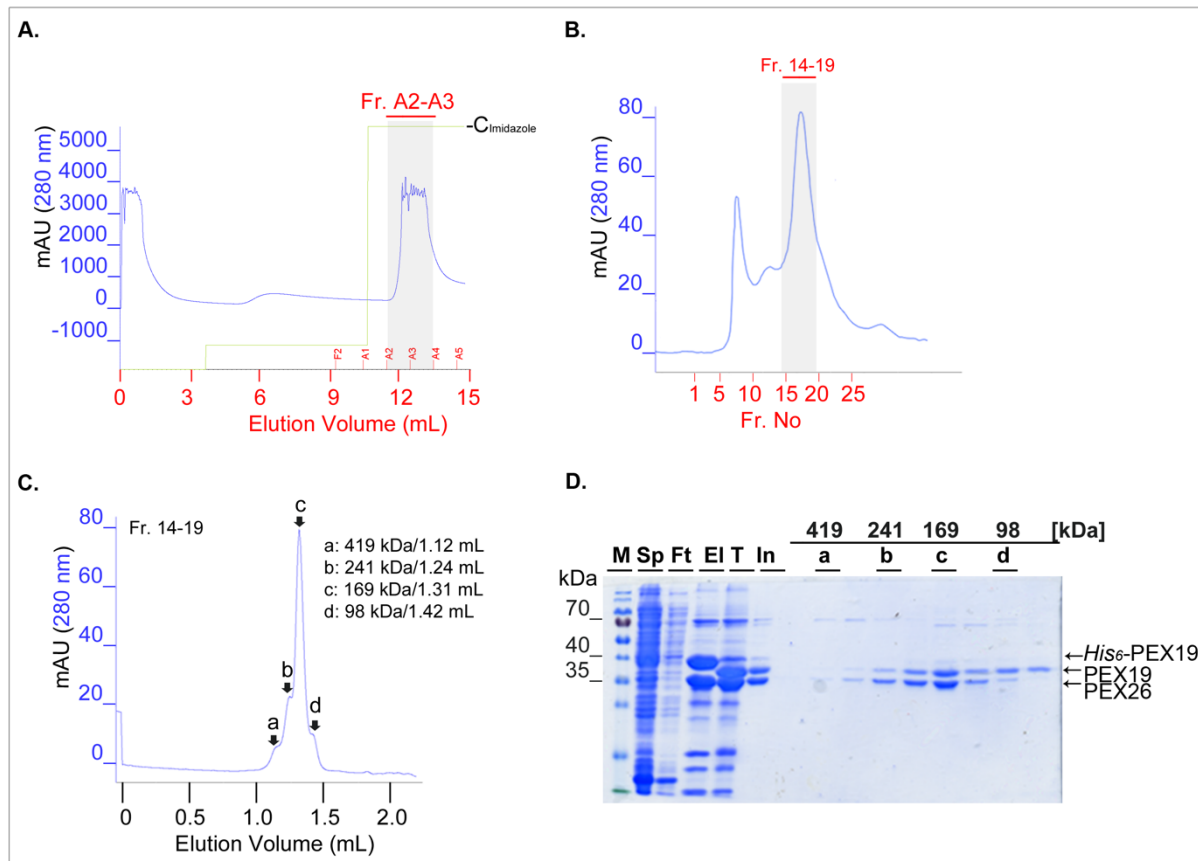


Figure 5.3: The recombinant PEX19 forms a complex with PEX26 *in vitro*.

[A] IMAC elution chromatogram of PEX19-PEX26. The fractions A2 and A3 are pooled prior to TEV cleavage. **[B]** After TEV cleavage and second IMAC purification using *HisSpintrap*TM, the fraction of PEX19-PEX26 (In) was separated using a *Superdex*TM200 *HiLoad*TM 16/60 (*GE Healthcare*) column and fractions 14 to 19 were pooled prior to analytical SEC. **[C]** Analytical size exclusion chromatogram of SEC fractions 14-19 (Fr.14-19) of PEX19-PEX26. Pooled fractions were analysed using a *Superdex*TM200 *increase* 3.2/300 (*GE Healthcare*). The fractions after analytical SEC analysis comprising the volumes from 1.10 to 1.50 mL. The Assigned peaks with corresponding fractions; a: 419, b: 241, c: 169, d: 98 kDa. **[D]** SDS-PAGE analysis of the IMAC and SEC fractions. A 12% SDS-PA gel was loaded with the protein samples treated with 4-fold sample buffer and stained with Coomassie Brilliant Blue R-250 after electrophoresis. The portions of loaded samples depend on the working volumes of each experimental steps as following; 0.03% for the lanes of supernatant (Sp) and flow through (Ft), 0.5% for the lanes of elution (A₂-A₃), TEV-cleavage (T) and input (In) and 0,3% for the lanes of SEC fractions. Lane M indicates molecular weight size marker (Thermo Scientific). Theoretical molecular mass of the proteins: His₆-PEX19: 35.27 kDa PEX19: 32.8 kDa PEX26: 33.9 kDa

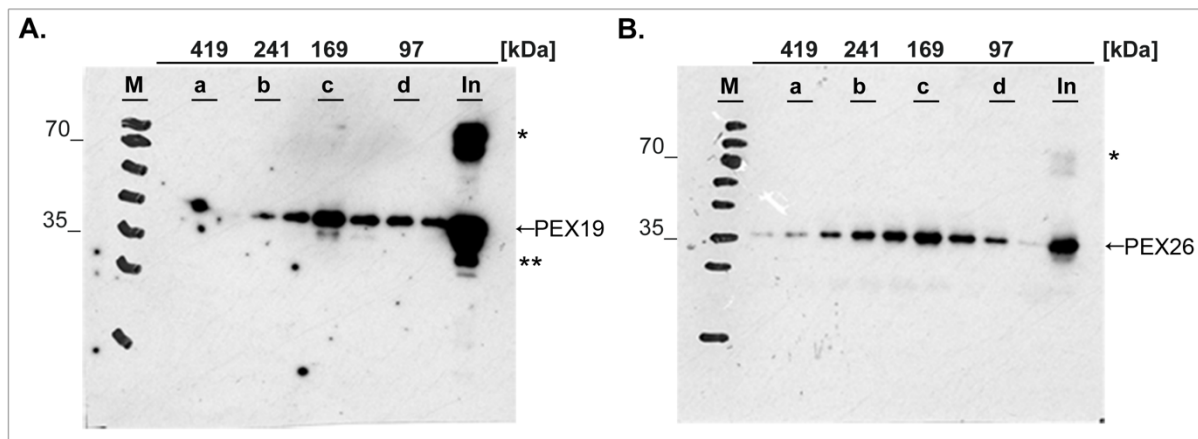


Figure 5.4: Western Blot analysis of purified PEX19 and PEX26

[A] Western blot analysis of the fractions after analytical SEC analysis (see Figure 8, B for the SDS-PAGE analysis of the samples) comprising the volumes 1.14 to 1.43 mL using antibodies against PEX19 and **[B]** using antibodies against PEX26. The fractions a-d correspond to the maximum of each peaks. (*) indicates the high molecular aggregates of PEX19-PEX26 complex, which was supposed to be formed during sample preparation or electrophoresis. (**) indicates degraded bands of PEX19. Lane M indicates molecular weight size marker (Thermo Scientific). Theoretical molecular mass of the proteins PEX19: 32.8 kDa and PEX26: 33.9 kDa

5.3. Ternary complex of co-expressed *nPEX3*, *PEX19* and *PEX26*

An *in vitro* ternary complex formation between *nPEX3*, *PEX19* and *PEX26* was already reported^[117]. In order to analyse whether recombinantly produced *nPEX3* binds to the *PEX19*-*PEX26* binary complex forming a ternary complex *in vitro*, we constructed a vector; pSS1 (see Section 4.2.1), which comprises the three cistrons of *PEX19*, *PEX26* and *nPEX3*, respectively. The co-expression is based on pETduet-vector, that consists of two separate MCS. MCS-I included the ORF of *PEX19* which is N-terminally fused to a *His*₆-tag and TEV cleavage sequence respectively, while MCS-II contained only the ORF of full-length *PEX26*. Based on this vector, we cloned the ORF of *nPEX3* including its own T7 promoter and *lac* operon into the MCS-II subsequent to the ORF of *PEX26*. In addition, former studies reported that the overproduction of full length *PEX3* including the transmembrane segment (TMS) resulted in insoluble aggregates, that's why we excluded the sequence for the first 25 amino acids i.e. the TMS of *PEX3*₍₂₆₋₃₇₃₎ (*nPEX3*) from our expression vector (see Appendix 9.5)^[28]. Transfection of this plasmid vector (pSS1: *His*₆-*PEX19*-*PEX26*-*nPEX3*) was performed using the *E. coli* *Rosetta2* cells. The first purification step was performed using IMAC (see Figure 5.5). According to the IMAC chromatogram, the eluted fractions (see Figure 5.5: A, Fractions: A2-A4) were analysed using SDS-PAGE. Three gel bands at approximately the expected masses between 35 and 40 kDa were observed and represent a ternary

complex which was formed through interactions of nPEX3, PEX19 and PEX26 *in vitro* (see Figure 5.5: Lane A3-A4). The fractions A3-A4 showing nPEX3, PEX19-PEX26 were pooled (fraction In). (see Figure 5.6: B, Fraction In). Prior to further analysis of the complex, purified proteins are treated with TEV protease to cleavage N-terminally fused *His*₆-tag from PEX19 through dialysis against HISA₀PN-S buffer at 4 °C overnight (see Figure 5.6: Lane T). After TEV cleavage and dialysis, the proteins were subjected to another purification using a *HisSpin*TM column to separate uncut PEX19 and the *His*₆-tag residues from PEX19-PEX26-nPEX3 complex (see Figure 5.6: Lane Ft). SDS-PAGE analysis confirmed the cleavage. See the small PEX19 shift on the gel in comparison to uncut PEX19 (Figure 5.5: Lane In and T). In the final step the purified proteins were further analysed using analytical SEC. Accordingly, three peaks appeared in the SEC chromatogram with elution volumes of a:1.13 mL b: 1.28 mL c: 1.34 mL that correspond to 436 kDa, 206.9 kDa and 152.1 kDa. The following SDS-PAGE analysis including peak fractions with elution volumes from 1.09 mL to 1.45 mL showed that fraction b represents the three protein bands of PEX19, PEX3 and PEX26 respectively, whereas the intensities of the PEX19 and PEX3 bands were higher in fractions b to c. In contrast, the PEX26 band disappeared in later fractions after b. Verification of all three proteins was performed employing western blot analysis with PEX3, PEX19 and PEX26 antibodies (Figure 5.6: A and B, respectively).

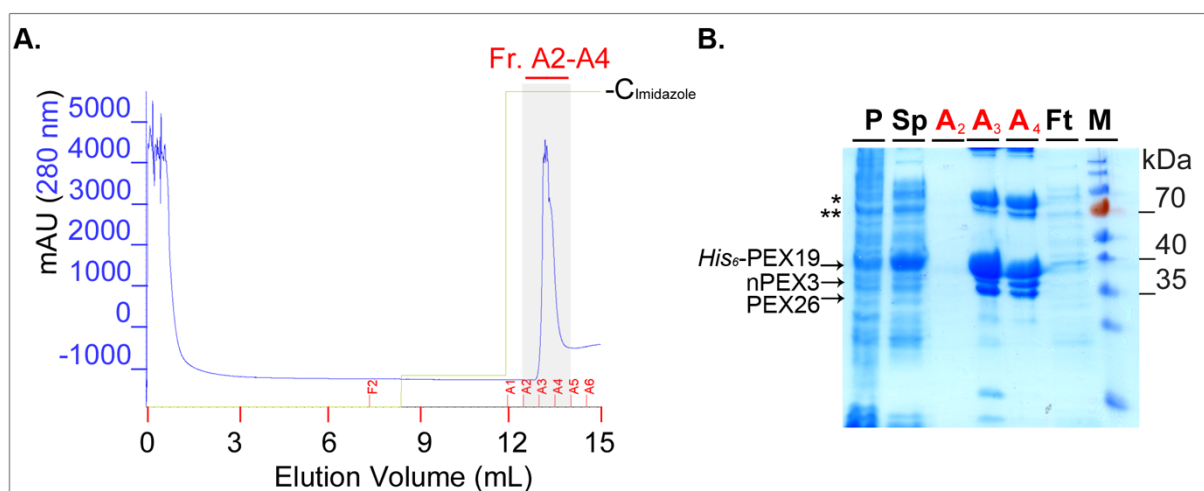


Figure 5.5: Co- expression and -purification of the recombinant His₆-PEX19-PEX26-nPEX3. [A] IMAC elution chromatogram of co-expressed *His*₆-PEX19-PEX26-nPEX3 [B] SDS-PAGE analysis of IMAC fractions. A 12% SDS-PA gel was loaded with the protein samples treated with 4-fold sample buffer and stained with Coomassie Brilliant Blue R-250 after electrophoresis. The portions of loaded samples depend on the working volumes of each experimental steps as following; 0.03% for the lanes of supernatant (Sp) and flow through (Ft), 1.0% for the lanes of elution, A₂, A₃ and A₄. * and ** indicates the high molecular aggregates of the proteins, which are supposed to be formed during heat treatment or electrophoresis.

Lane M indicates molecular weight size marker (Thermo Scientific). Theoretical molecular mass of the proteins His₆-PEX19: 35.27 kDa, PEX19: 32.8 kDa, PEX26: 33.9 kDa and nPEX3: 39.6 kDa

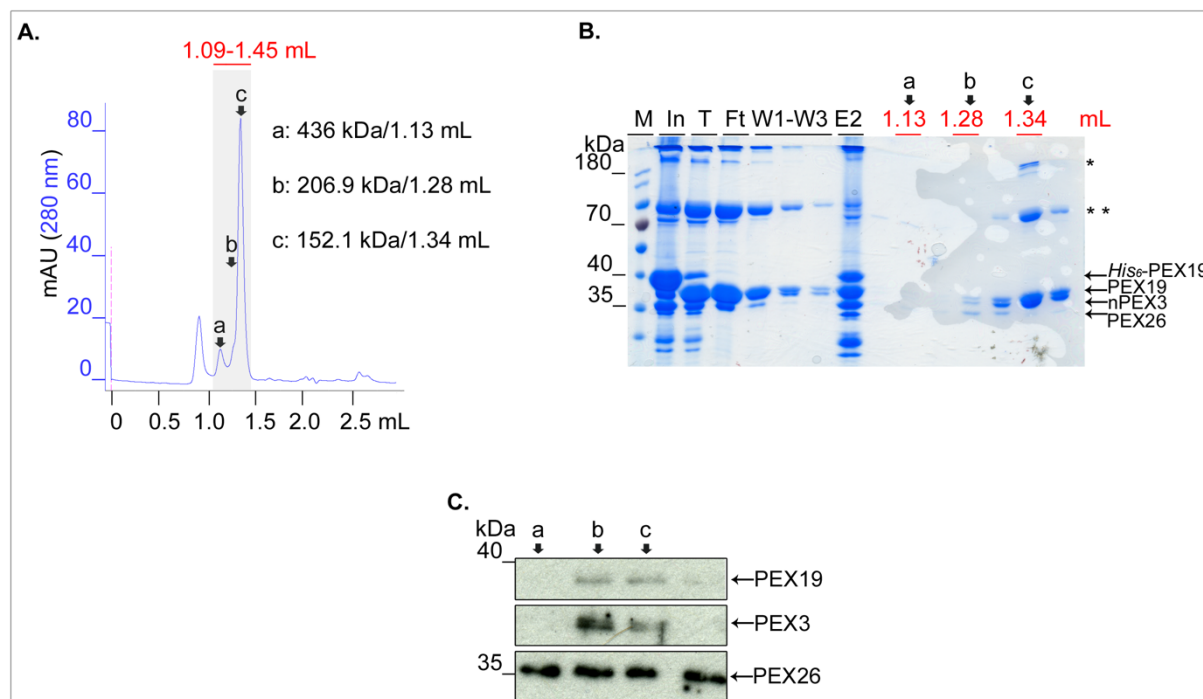


Figure 5.6: SEC Analysis of the recombinant complex of nPEX3 and PEX19-PEX26

[A] After IMAC purification, the pooled fractions of A3-A4 (see Figure 5.5: A and B) including nPEX3, PEX19-PEX26 (In: Input) were subjected to analytical SEC and analysed using a *Superdex™200 increase 3.2/300* (GE Healthcare). Assigned peaks correspond to a: 436 kDa, b: 206.9 kDa, c: 152.1 kDa. **[B]** SDS-PAGE analysis of purification and analytical SEC fractions. A 12% SDS-PA gel was loaded with the protein samples treated with 4-fold sample buffer and stained with Coomassie Brilliant Blue R-250 after electrophoresis. The portions of loaded samples depend on the working volumes of each experimental steps as following; 0.5% for Input (In, the pooled fractions A3-A4 after IMAC), TEV cleavage (T), flow through (Ft) after TEV cleavage, washing steps (W1-W3) and second elution (E2), as well as 0.3% for the SEC fractions. The fractions after analytical SEC analysis comprised the volumes from 1.09 mL to 1.45 mL. **[C]** Western blot analysis of the fractions after analytical SEC analysis comprising the fractions a, b and c using antibodies against PEX19, PEX3 and PEX26. * and ** indicate high molecular aggregates of the proteins, which are supposed to be formed during heat treatment or electrophoresis. Lane M indicates molecular weight size marker (Thermo Scientific). Theoretical molecular mass of the proteins His₆-PEX19: 35.27 kDa, PEX19: 32.8 kDa, PEX26: 33.9 kDa, nPEX3: 39.6 kDa

5.4. Ternary complex of purified nPEX3 and PEX19-PEX26

In order to analyse the PEX3-PEX19-PEX26 ternary complex formation, we purified nPEX3^T (Thx-His₆-Thr-TEV-nPEX3) and the complex of His₆-PEX19-PEX26 separately for further investigation through SEC and native-MS. Former observations indicated that the overproduction of full length PEX3 including the transmembrane segment (TMS) resulted in insoluble aggregates^[28]. In addition, the use of detergents

in the purification steps of PEX3 led to protein aggregation^[118]. Therefore, we refrained from using detergents in all steps to archive a native-like state of proteins.

The expression of nPEX3^T is based on the vector pNT61 (see Section 4.2.1). The MCS includes the ORF of nPEX3 which is N-terminally fused to tags, *Thioredoxin*, *His₆* as well as *Thrombin* and *TEV* cleavage sequences respectively. Transfection of this plasmid vector was performed using the *E. coli* expression strain *Rosetta2* (DE3). Subsequently, we purified nPEX3^T using the same purification conditions as for the purification of PEX19-PEX26 to avoid a buffer change latter, that might have compromised the stability of PEX26. After overexpression, homogenization and centrifugation, the supernatant was loaded on a *HisTrapHpTM* column. The elution of nPEX3^T was performed using HISBPN-S elution buffer. According to the IMAC chromatogram fractions A2-A5 of eluted nPEX3^T were further analysed using SDS-PAGE (see Figure 5.7: A and B, A2-A5). An intensive protein band appeared approximately at the expected mass of about 55 kDa on the SDS gel. The eluted fractions A3 and A4 representing nPEX3^T were pooled prior to further analysis.

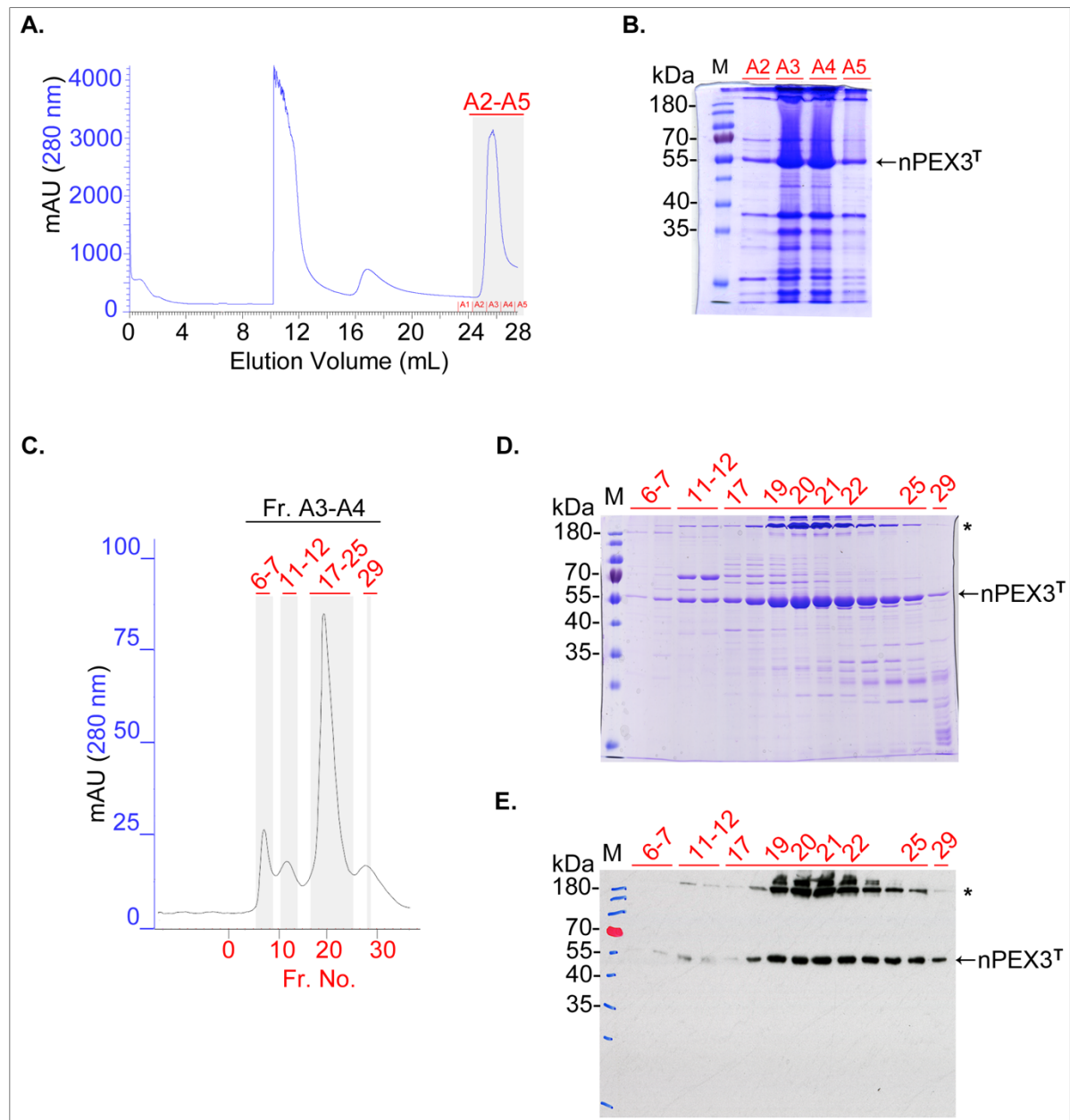


Figure 5.7: IMAC purification of the nPEX3^T for ternary complex formation

[A] IMAC elution chromatogram of nPEX3^T **[B]** SDS-PAGE analysis of IMAC fractions. A 12% SDS-PAGE gel was loaded with the protein samples treated with 4-fold sample buffer and stained with Coomassie Brilliant Blue R-250 after electrophoresis. The portions of loaded samples depend on the working volumes of each experimental steps and correspond to 1.0% for all fractions of elution; A₂, A₃, A₄ and A₅. Lane M indicates molecular weight size marker (Thermo Scientific). Theoretical molecular mass of nPEX3^T: 57.3 kDa **[C]** Preparative SEC separation of purified nPEX3^T after IMAC purification. **[D]** SDS-PAGE analysis of SEC fractions. The SDS-PAGE analysis of the fractions comprised the fractions; 6-7, 11-12, 17-25 and 29. The portions of loaded samples depend on the working volumes of each experimental steps and correspond to 0.5% for all fractions of elution. **[E]** their western blot analysis of the fractions using antibodies against PEX3. * and ** indicate high molecular aggregates of the proteins, which are supposed to be formed during heat treatment or electrophoresis. Lane M indicates molecular weight size marker (Thermo Scientific). Theoretical molecular mass of nPEX3^T: 57.3 kDa

Prior to further analysis, the pooled fractions (A3-A4) of nPEX3^T were separated on a *SuperdexTM200 HiLoadTM 16/60 (GE Healthcare)* column (see Figure 5.8: A). The SEC fractions 6-7, 11-12, 17-25 and 29 were analysed by SDS-PAGE and Western Blot analysis (see Figure 5.8: A, B and C). Accordingly, purified nPEX3 showed very intensive bands above 55 kDa in all fractions. Additionally, the same fractions showed higher bands at above 170 kDa, indicating oligomer formation of nPEX3 with various sizes on SDS-PAGE (see Figure 5.8: B and C). We concluded that nPEX3 eluates as a monomer at 50 kDa from the gel filtration column, however its heat treatment in SDS-PAGE sample buffer resulted in formation of nPEX3 (PEX3₂₆₋₃₇₃) oligomers (see Figure 5.8: A, (*)). Furthermore, an aliquot of the pooled fractions 19-22 was subjected to TEV cleavage and further SEC analysis (see Figure 5.9: A and B: Lane T). SDS-PAGE analysis confirmed the cleavage through a shift on the gel in comparison to uncut nPEX3^T (see Figure 5.8: Lane EI and T). In the final step the purified proteins were further analysed using analytical SEC. Accordingly, three main peaks appeared in SEC chromatogram with the elution volumes of a: 0.94 mL, b: 1.56 mL and 1.69 mL. Following SDS-PAGE analysis including peak fractions of elution volumes from 0.90 to 1.0 mL and from 1.50 to 1.64 mL showed that fraction a resembled aggregate of nPEX3 assigned to 1.1 MDa, whereas b resembled the monomeric nPEX3 with the assigned mass of 50 kDa. The third peak represented TEV protease, which was used in the cleavage step. Since we planned to investigate the ternary complex using native-MS, we additionally purified PEX19-PEX26 as described in Section 5.2. Fraction d was analysed using SEC (see Figure 5.8: C and D).

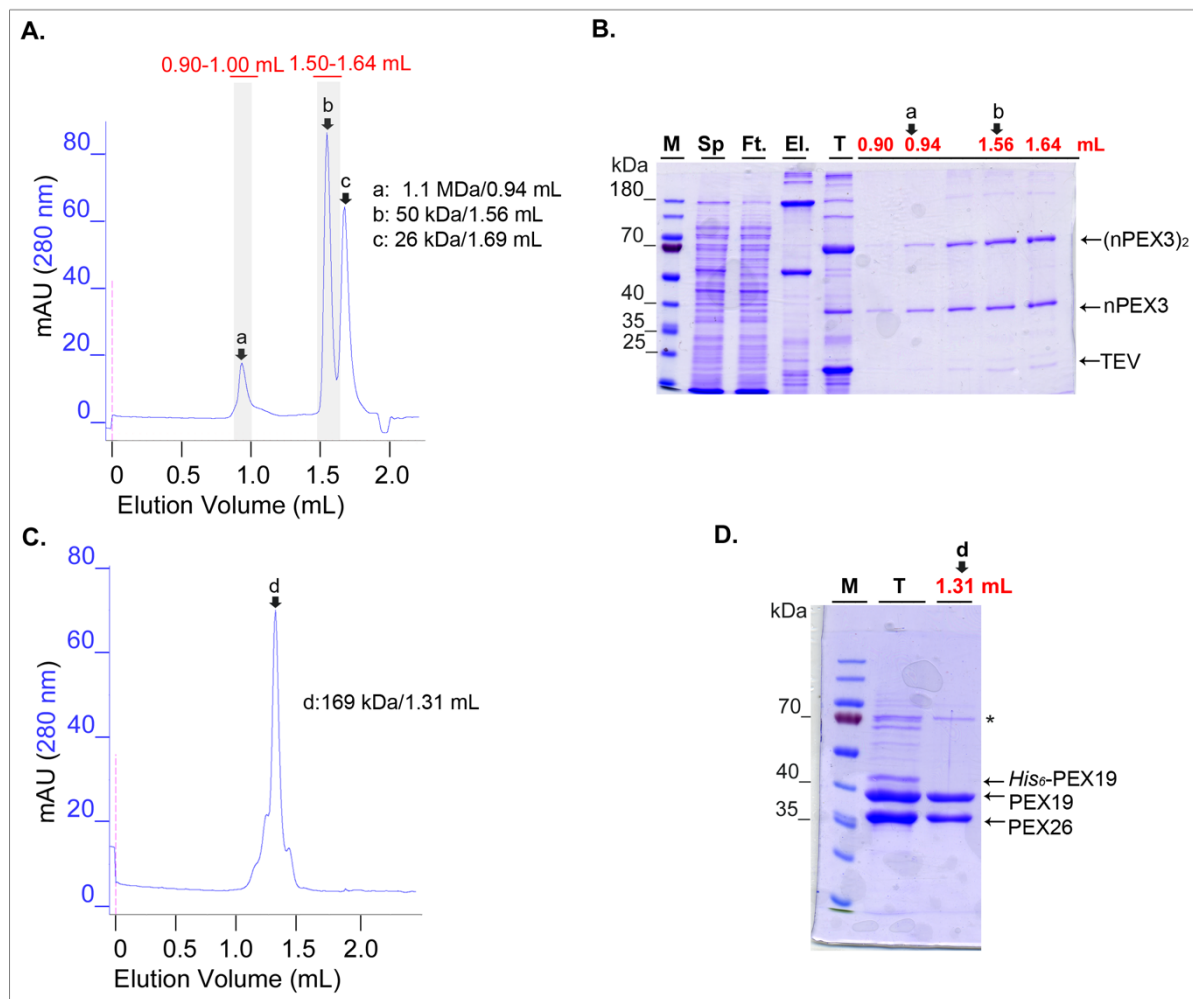
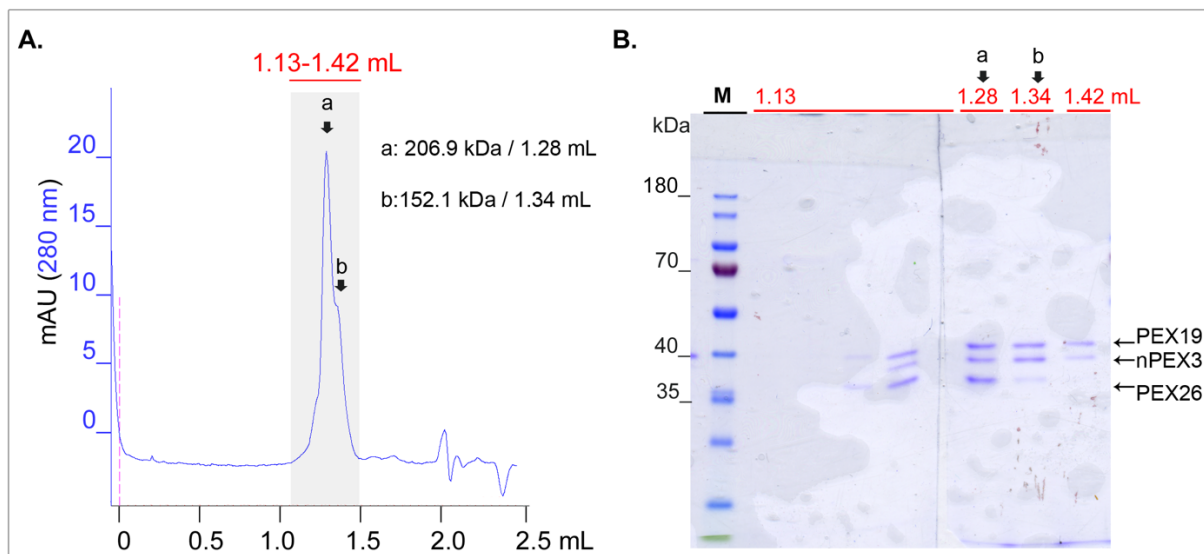


Figure 5.8: Purification and SEC analysis of the nPEX3 and PEX19-PEX26 for ternary complex formation. [A] SEC analysis of cleaved nPEX3^T which originates from pooled fractions of 19-22 (see Figure 5.7: C and D). Analytical SEC using a *SuperdexTM200 increase 3.2/300* column (*GE Healthcare*) shows the assigned peaks correspond to a: 1.1 MDa, b: 50 kDa, c: 26.2 kDa. [B] SDS-PAGE analysis of the IMAC, TEV cleavage and SEC fractions of nPEX3^T. A 12% SDS-PA gel was loaded with the protein samples treated with 4-fold sample buffer and stained with Coomassie Brilliant Blue R-250 after electrophoresis. The portions of loaded samples depend on the working volumes of each experimental steps as following; 0.03% for the lanes of supernatant (Sp) and flow through (Ft), 0.5% for elution (El, IMAC) and TEV-cleavage (T), as well as 0,3% for the lanes of SEC fractions comprising the volumes from 0.90 to 1.0 mL and 1.50 to 1.64 mL. [C-D] Analytical size exclusion chromatogram of purified PEX19-PEX26 (same as in section 5.2). Pooled fractions were analysed using a *SuperdexTM200 increase 3.2/300* (*GE Healthcare*) prior to ternary complex formation. The Assigned peak d corresponds to 169 kDa. * indicates high molecular aggregates of one of the proteins, which are supposed to be formed during heat treatment or electrophoresis. Lane M indicates molecular weight size marker (Thermo Scientific). Theoretical molecular mass of the proteins His₆-PEX19: 35.27 kDa, PEX19: 32.8 kDa PEX26: 33.9 kDa, nPEX3^T: 57.3 kDa, nPEX3: 39.6 kDa.

Prior to the native-MS experiments, we investigated whether recombinant nPEX3 binds to the purified PEX19-PEX26 binary complex. Therefore, we mixed nPEX3 and PEX26 in a 1:1 molar ratio and subjected them to an analytical SEC (see Figure 5.9:

C). A main peak appeared in the SEC chromatogram in the range of the elution volumes from 1.13 to 1.42 mL. The following SDS-PAGE analysis of peak fractions with elution volumes from 1.13 to 1.42 mL showed that fraction a represented three protein bands, PEX19, PEX3 and PEX26, respectively (see Figure 5.9: D). Whereas the intensity of PEX19 and PEX3 bands increased at 1.34 mL, the PEX26 band disappeared after 1.28 mL indicating an equilibrium for the ternary complex formation as following:

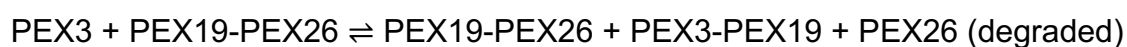


5.5. Native MS analysis of the recombinant PEX19-PEX26 complex

After the co-expression of *His*₆-PEX19 with PEX26 and following purification, SDS-PAGE analysis revealed that *His*₆-PEX19 co-elutes with PEX26, indicating a complex formation. In order to confirm this and to reveal the stoichiometry of the complex, we analysed pooled fractions of purified proteins employing SEC. The SDS-PAGE analysis of SEC fractions, which included the both proteins, indicated a complex of 169 kDa (see Figure 5.3: C, fractions, c: 1.31 mL, 169 kDa). Supporting this, a former study reported 95.2 kDa for PEX19 based on a SEC analysis of monomeric PEX19^[28]. In addition, our SEC analysis of purified PEX19 showed that monomeric PEX19 was assigned to 98 kDa (see Figure 5.3: C, fractions, d: 1.42 mL, 98 kDa), while the assigned size of PEX26 in this complex formation was calculated 71 kDa. Furthermore, the monomeric nPEX3 was assigned to 50 kDa on a SEC chromatogram (see Figure 5.8: A, fractions, b: 1.56 mL, 50 kDa) conforming with the assigned size of PEX19 (98 kDa) referring to PEX3-PEX19 (152.1 kDa) complex. Additionally, the size of PEX3-

PEX19-PEX26 complex on the SEC chromatogram was assigned to 206.9 kDa (see Figure 5.9: A, fractions, a: 1.28 mL 206.9 kDa). Whereas, the sum of the assigned monomeric sizes of the proteins including PEX3: 50 kDa, PEX19: 98 kDa and PEX26: 71 kDa is equal to 219 kDa, which indicates a 12 kDa size difference.

Additionally, we showed in a former analysis that co-expression of *PEX19*, *PEX26* and *PEX3* resulted in two different complex formations as PEX3-PEX19 (152.1 kDa) and PEX3-PEX19-PEX26 (206.9 kDa) (see Figure 5.6: A, fractions: b and c). Based on this, we suggested following equilibrium, in which PEX3 weakens the interaction between PEX19 and PEX26 resulting in a complex formation between PEX3 and PEX19 rather than a ternary complex of all three proteins;



In order to test our thesis, we analysed the purified proteins further employing native-MS with appropriate settings (see Appendix, Table 9.1). Native-MS elucidates proteins or protein complexes in native-like quaternary state, which is ensured using a NH_4OAc -buffer at the ionisation steps, but not in the mobile phase or during detection^[119]. Prior to acquisition, the acquisition buffer conditions were optimized using various ammonium acetate buffers with concentrations between 50 mM and 200 mM and pH values between 6.5 and 8.0. After optimization of the peak shape and signal stability by varying the buffer conditions, we decided to use 200 mM ammonium acetate pH 6.5 in the next step of acquisition. The purified proteins were directed to a buffer exchange using *Zeba Spin* columns equilibrated with native-MS spraying buffer (200 mM ammonium acetate pH 6.5). During acquisition, the collision energy was changed to narrow the peak-width for an optimal acquisition of native-MS spectra. Additionally, the collision energy is used to fragment the purified proteins during the acquisition (CID, collision induced dissociation)^[93]. Therefore, this approach is very helpful for the verification through the recovery of monomeric proteins in the acquisition of complexing proteins. We performed our independent experiments using 40 to 80 V collision energies for the acquisition of the spectra of purified proteins and complexes. Additionally, the data referring to the verification of complex formation were acquired using collision energies in the range from 70 to 350 V.

Accordingly, we performed three acquisitions for PEX3, the PEX19-PEX26 complex and for mixing both in a 1:1 molar ratio. Comparative native mass spectra of all three-acquisitions showed peak series between 2000 and 5000 m/z region (see Figure 5.10). Therefore, the nPEX3 spectrum indicated a dominant peak series around 3000 m/z

region, that corresponded to 39.6 kDa for monomeric nPEX3 (see Figure 5.10: A: top row, theoretical mass of monomeric nPEX3: 39.39 kDa). Furthermore, we observed an additional peak series at higher, 4000 to 5000 m/z scales in another identical and independent experiment. These were assigned to 79.1 kDa for homodimeric nPEX3, a species which had already been reported in a former study^[28]. The obtained native MS spectrum for purified PEX19-PEX26 revealed peak series around 3000 m/z and around 4000 m/z which could be assigned to 33.2 kDa for monomeric PEX19 and 66.9 kDa for a PEX19-PEX26 heterodimer, respectively (see Figure 5.10: A: Middle row, theoretical mass for: PEX19: 32.9, PEX26: 33.9, PEX19-PEX26: 66.9 kDa). The difference of the assigned PEX19 mass from the theoretical one indicates an unknown adduct of about 300 Da. Monomeric PEX26 could not be identified in this spectrum.

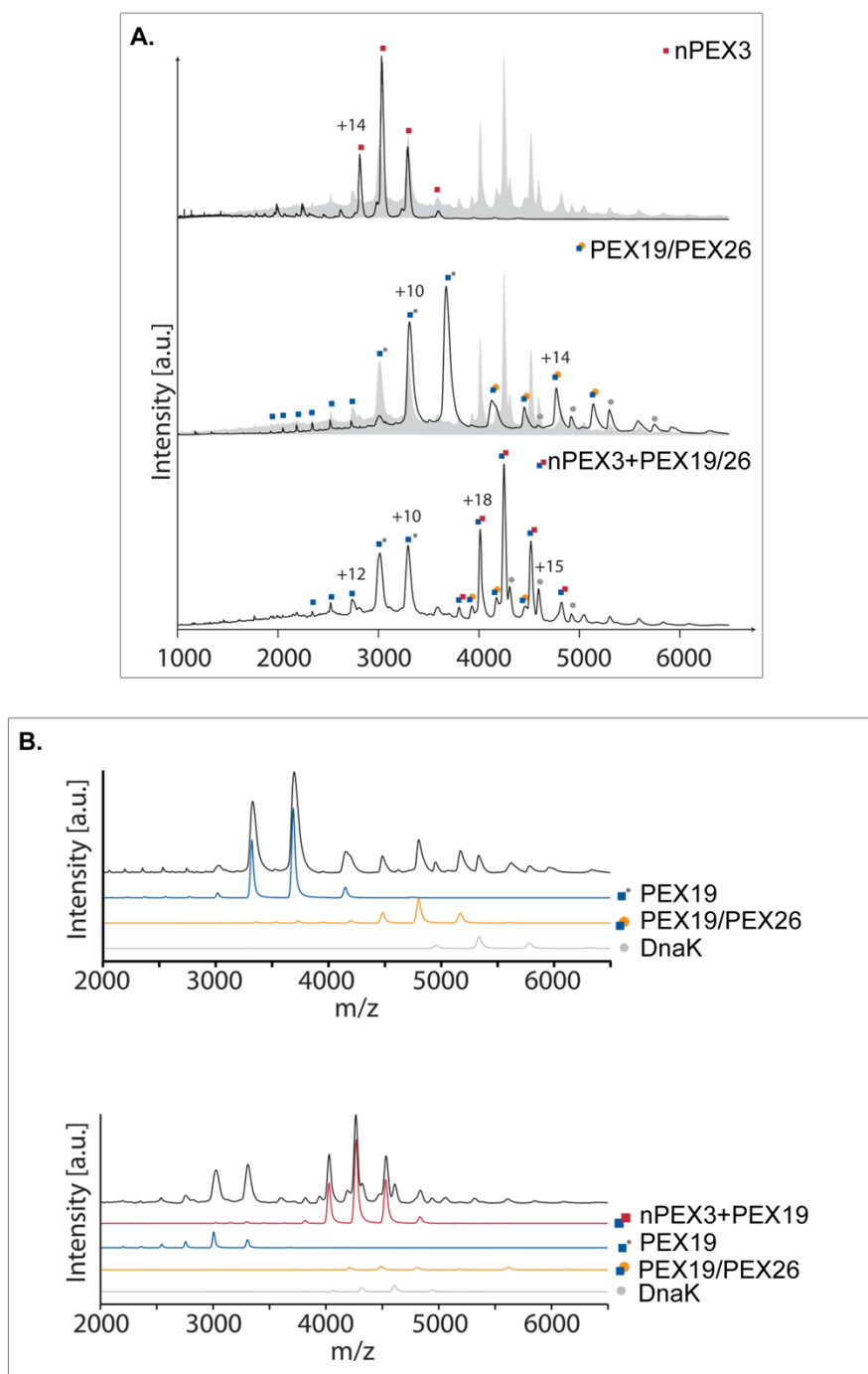


Figure 5.10: Native-MS confirms *in vitro* complex formation of the recombinant PEX19 and PEX26. [A] Manual annotation of samples including nPEX3 (top row), PEX19-PEX26 (middle row) and nPEX3-PEX19-PEX26 (bottom row). Top row: Spectrum of nPEX3 is gained employing a *Synapt G1* mass spectrometer at both 40 V trap and transfer collision energy. The peak series (~3000 m/z) labelled with red squares corresponds to 39.6 kDa and refers to monomeric nPEX3. Middle row: Spectrum of heterodimeric PEX19-PEX26 gained at 50 V collisional energy employing a *Q-TOF Ultima* mass spectrometer. The peak series labelled with a blue square (*) (2000-3500 m/z) corresponds to 33.2 kDa (PEX19) and (*) indicates an unknown adduct of PEX19 about 300 Da. The blue/orange squares (4000-5000 m/z) correspond to 66.9 kDa (PEX19-PEX26 heterodimeric) complex. Bottom row: The spectrum is gained directly after mixing both samples from the top and middle row in a stoichiometry of 1:1 at 110 V collision energy employing a *Q-TOF Ultima* mass spectrometer. As in middle row, the peak series labelled with blue[*] squares (2000-3500 m/z) correspond to 33.2 kDa (PEX19) and the ones with blue/orange squares (4000-5000 m/z) correspond to 67.1

kDa (PEX19-PEX26 heterodimeric complex). Additionally, the peak series (4000-5000 m/z) indicate a 72.5 kDa PEX3/PEX19 complex. **[B]** Top: Charge state deconvolution of the spectrums using *Massign*. Relative intensity of the main peaks (extracted from middle row,^[A]) show monomeric PEX19 and heterodimeric PEX19-PEX26, before adding PEX3 to the PEX19-PEX26 complex. Bottom: Relative intensity of the main peaks (extracted from lower row,^[A]) of monomeric PEX19, heterodimeric PEX19-PEX26 and heterodimeric nPEX3-PEX19 after adding nPEX3 to the PEX19/PEX26 complex. Theoretical molecular mass of the proteins: PEX19: 32.8 kDa PEX26: 33.9 kDa, nPEX3: 39.6 kDa. These evaluations were provided by Julian Bender and Dr. Friedel Drepper at the Department of Biochemistry and Functional Proteomics, University of Freiburg, Germany.

Regarding the acquisition of PEX19-PEX26 in the presence or absence of nPEX3, we observed that the intensity of the PEX19-PEX26 peak was reduced from 21% to 2.7% after adding nPEX3 in a 1:1 molar ratio (see Figure 5.11: A). Furthermore, after mixing of the proteins, the spectrum revealed a very dominant peak series between 4000-5000 m/z region assigned to a 72.5 kDa nPEX3-PEX19 complex (see Figure 5.11: B). Supporting this, a former study reported a stable binary complex PEX19-PEX3 with a K_d -value of 10 nM, calculated after ITC analysis^[28]. Excess of PEX19 was also observed in the same range as in the spectra of PEX19-PEX26 at around 3000 m/z corresponding to 33.2 kDa. Based on this comparative native-MS analysis of the purified PEX19-PEX26 binary complex and its interaction with monomeric nPEX3, we conclude that purified PEX19-PEX26 forms a stable native-like binary complex, in which PEX26 is present stabilized by PEX19.

Since we analysed our samples acquiring the spectrums employing the *CID* method, we could recover monomeric nPEX3 and PEX19 originating from their heterodimeric complexes. In contrast, monomeric PEX26 was neither detectable on the native-MS simulation spectrum nor in the spectrum using the *CID* technique. Based on this, we conclude that monomeric PEX26 is highly instable as monomer in alignment with our former observations regarding the insolubility of PEX26.

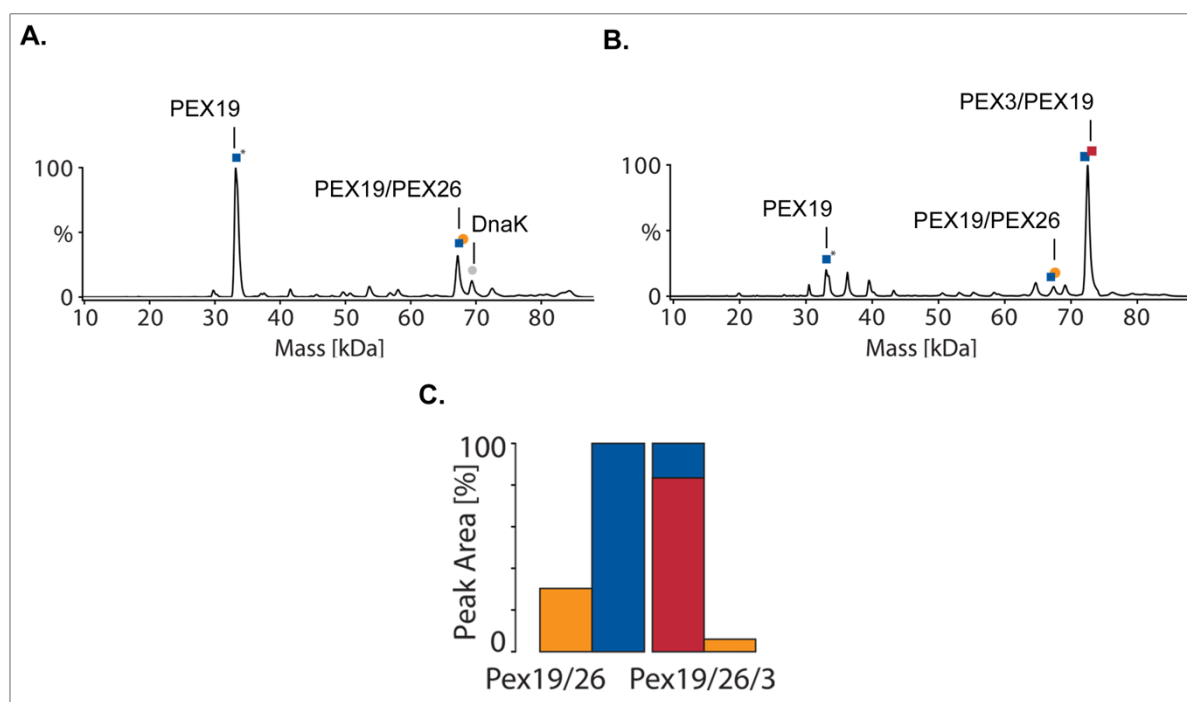


Figure 5.11: Zero-Charge state deconvolution of PEX19-PEX26 using *UniDec* in the absence and presence of nPEX3. Quantification of the contribution of the different species to the native-MS spectra observed for PEX19-PEX26 and nPEX3 (see Figure 5.10: A, middle and bottom row). **[A]** Zero-charge mass spectra for PEX19-26 in absence and **[B]** in presence of nPEX3. The peaks are labelled as following; blue (*) square: PEX19 with an unknown adduct about 300 Da, the blue square and orange circle: PEX19-PEX26, red and blue square: PEX3-PEX19 and grey square: DnaK. **[C]** Quantification and comparison of areas under the curve for the species identified for PEX19-PEX26 (orange) without and with nPEX3 (red). Areas were normalized to the sum of areas for PEX19 and the nPEX3-PEX19 heterodimer. The relative peak area for PEX19-PEX26 was 21% in the absence of nPEX3 and decreased to 2.77% in its presence. Theoretical molecular mass of the proteins PEX19: 32.8 kDa, PEX26: 33.9 kDa, nPEX3: 39.6 kDa. These evaluations were provided by Julian Bender and Dr. Friedel Drepper at the Department of Biochemistry and Functional Proteomics, University of Freiburg, Germany.

In a next step we analysed the simulated sample (see Figure 5.10: A, bottom row) by high-resolution mass spectrometry after tryptic digestion to identify the most abundant proteins in the samples, which is based on intensity-based absolute quantification (iBAQ) using *MaxQuant*^[120]. Relative iBAQ analysis of nPEX3 shows 52.66% abundance based on PEX19-normalisation, while sequence coverage of nPEX3 indicates 95.1%, due to the 25-amino-acid-truncation of nPEX3 (Table 5.1). The estimated iBAQ value for PEX26 was 91.55% based on PEX19-normalisation (100%), the sequence coverage refers to 100% for both PEX19 and PEX26. Furthermore, we observed another peak in the spectrum of PEX19-PEX26, that could be identified as *DnaK*. This protein, that originates from *E. coli*, was also the fourth most abundant protein in the samples. *DnaK* belongs to the cation channel-forming heat shock protein-70 (hsp70) family and functions as chaperon in stress induced metabolic reactions by

protein misfolding^[131]. Therefore, we suggest that the over-production of our proteins in *E. coli* cell induced the concentration of DnaK, resulting in the higher abundance (15.26%, rel iBAQ) in our samples. The rest of the more abundant proteins included in our samples were identified as the kinase GyrB (0.67%, rel iBAQ), the chaperone RpsA (0.39%, rel iBAQ), an oxidoreductase YagS (0.37%, rel iBAQ), a DNA binding protein RpoD (0.27%, rel iBAQ) and another kinase ManX (0.15%, rel iBAQ), which are probably originated from our *E. coli* expression strain *Rosetta2*^[121]. Additionally, NinE (0.46%, rel iBAQ) originates from an *Enterobacteria phage* that uses *E. coli* as a host, natively^[121]. Accordingly, we conclude that the relative higher abundance of DnaK might originate from the interaction with the purified misfolded proteins in our samples, which would be formed in response to stress during the overexpression steps. Therefore, we suppose that DnaK has no specific effect on the complex formation of PEX19-PEX26. Considering the rest of the abundant proteins, we assume that these proteins are contaminant proteins originated from *E. coli*, which have unspecific interaction with our purified proteins.

Table 5.1: Most abundant proteins included in the nPEX3-PEX19-PEX26 samples as in Figure 5.10: A, bottom row.

Rank	Protein Names	Unique Sequence Coverage [%]	Native-MS Mass[kDa]	MW [kDa]	Rel. iBAQ [%]
1	PEX19	100	32.8	32.9	100.00
2	PEX26	100		34.0	91.55
3	PEX3 ₂₆₋₃₇₃	95.1	39.6	39.4	52.66
4	DnaK	99.4	69.1	69.1	15.26
5	GyrB	80.1		90.0	0.67
6	NinE	12.5		6.5	0.46
7	RpsA	62.8		61.2	0.39
8	YagS	11.6		33.9	0.37
9	RpoD	40.9		70.3	0.27
10	ManX	59.8		35.1	0.15

In addition to native-MS, the samples including nPEX3-PEX19-PEX26 (see Figure 5.10: A, bottom row) were analyzed using *High Resolution Mass Spectrometry* to measure protein abundance. Intensity-based absolute quantification (iBAQ) of proteins were performed using *MaxQuant*. iBAQ values were normalized depending on the intensities of PEX19 (Rel. iBAQ[%]). The sequence coverage of nPEX3 correspond only to 95.1%, due to its truncation at N-terminus (PEX3₂₆₋₃₇₃). Theoretical molecular mass of the proteins PEX19: 32.8 kDa, PEX26: 33.9 kDa, nPEX3: 39.6 kDa. These evaluations were provided by Julian Bender and Dr. Friedel Drepper at the Department of Biochemistry and Functional Proteomics, University of Freiburg, Germany.

5.6. XL-MS analysis of the PEX19-PEX26 complex

Combination of two powerful approaches, chemical cross-linking and mass spectrometry enables building a linkage map of peptides interacting in protein complexes. Furthermore, linkage maps of proteins or protein complexes can also restrict possible number of candidates from structural predictions depending on their tertiary or quaternary structural information.

The homobifunctional cross-linker BS³ cross-links proteins selectively through two primary amine groups of lysine sidechains, which should have proximity range of 24 Å^[96]. This also corresponds to the constant length of the BS³ spacer arm that reveals 3D-proximity of cross-linked peptides in protein complexes. To define interacting segments of the PEX19-PEX26 binary complex and those of PEX19-PEX26 with nPEX3 (PEX3₂₆₋₃₇₃) as well regarding their proximity, we cross-linked them using BS³. Subsequently cross-linked proteins are subjected to tryptic digestion followed by LC-MS analysis. Further Identification of the cross-linked peptides was performed using the *pLink* algorithm^[122].

In order to find an optimal cross-linker concentration, we titrated the samples containing the purified PEX19-PEX26 and PEX19-PEX26 and nPEX3 with varying final concentrations of BS³. The range of concentrations was 0.06 mM to 4.8 mM for the samples containing the purified PEX19-PEX26 and 0.2 to 7.9 mM for the samples containing the purified PEX19-PEX26 and nPEX3. SDS-PAGE analysis of both titrations showed, that the higher concentrations of cross-linker resulted in the appearance of shifted bands (see Figure 5.12: A: lane 2.4 mM and B: 4.8 mM). However, the optimal BS³ concentration was 1.2 mM for the samples containing the purified PEX19-PEX26 and 0.5 mM for the samples containing the purified PEX19-PEX26 and nPEX3 respectively. Following this, we excised these appearing protein bands (see Figure 5.12: A: a, b and c, B: d) from SDS-PAGE gels and subjected them to *in-gel* digestion and preceding LC-MS analysis. Additionally, we performed two independent identical experiments with the optimized concentrations of BS³, 1.2 mM and 0.5 mM for PEX19-PEX26 and PEX19-PEX26-nPEX3, respectively. However, we didn't analyse these two experiments via SDS-PAGE, instead we performed *in-solution* digestion of cross-linked proteins directly after cross-linking reactions and analysed them further with LC-MS. In general, the SDS-PAGE analysis of cross-linked proteins confirms the cross-linking through a shift on SDS-PA gel in comparison to control fractions (see Figure 5.12: A and B). However, in most of the cross-linking

experiments, the fractions of cross-linked proteins are very low, thus, they are invisible on the SDS-PAGE gel. In addition, the extraction of the cross-linked proteins from SDS-PAGE gels prior to LC-MS analysis result in very less yields in comparison to *in-solution* approach. Our *In-gel* experiments showed PEX19-PEX26 cross-links with corresponding frequencies; K60: 7, K130: 4, K138: 3 and K245: 5, while *in-solution* experiments resulted in six cross-links with the frequencies of G1: 3, K33: 1 K60: 3, K90: 1, K130: 2, and K245: 4 (Table 5.2). The identified cross-links of nPEX3 and PEX19 are between the residues PEX19-G1 and PEX3-K189 and -K208 according to *in-gel* analysis. The corresponding frequencies are; K189: 2 and K208: 1 (Table 5.3).

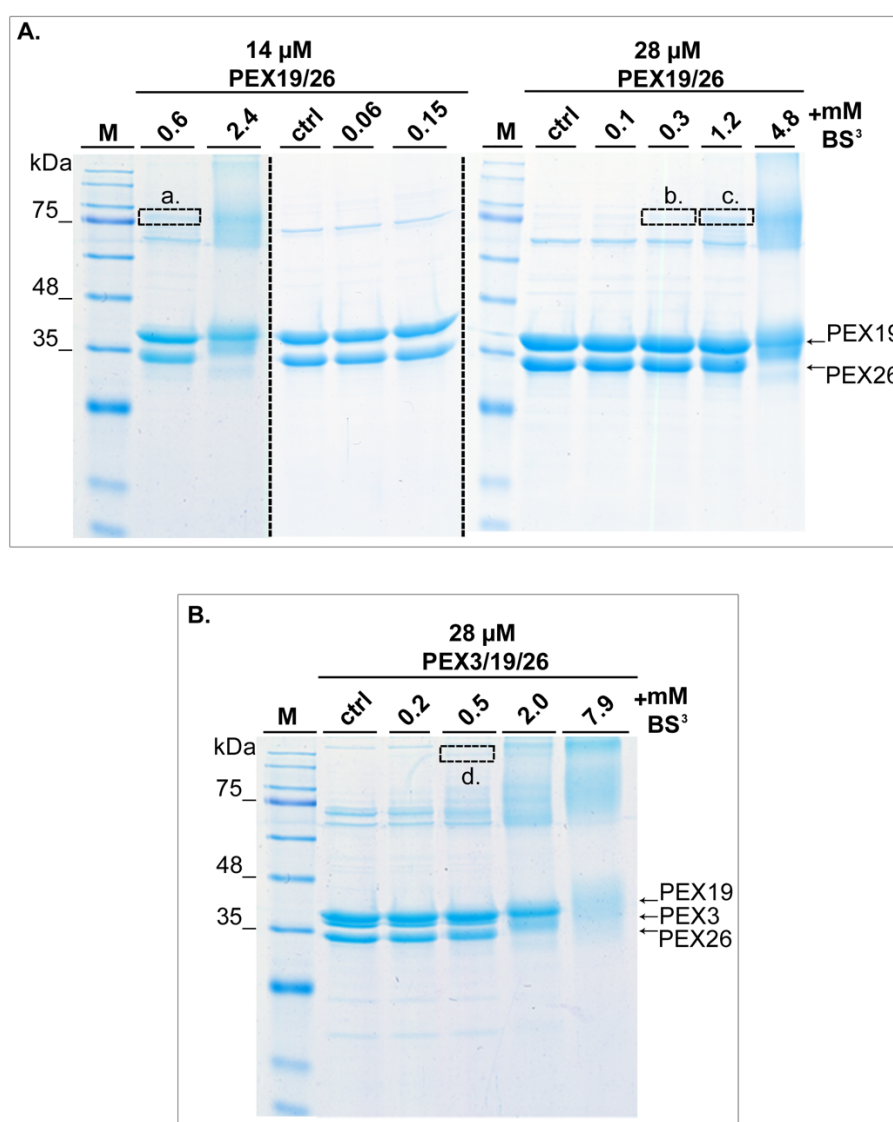


Figure 5.12: SDS-PAGE analysis of BS³ titration with PEX19-PEX26 and PEX19-PEX26 + nPEX3. [A] The SDS-PAGE analysis of cross-linker titration using various concentration of BS³ (0.06 to 4.8 μM) and PEX19-PEX26. 14 μM of the PEX19-PEX26 complex were treated with 0.06 to 2.4 μM BS³ (left). In addition, 28 μM of the PEX19-PEX26 complex were treated

with 0.1 to 4.8 μM BS³ (right). Control reactions comprises treatments of the samples with the same conditions as in the cross-linking reactions without BS³. **[B]** The SDS-PAGE analysis of cross-linker titration using various concentration of BS³ (0.2 to 7.9 μM) with 28 μM of nPEX3-PEX19-PEX26. Dashed rectangles show digested bands after cross-linking with BS³ through *in gel* method. 12% SDS-PA gels were loaded with the protein samples treated with 4-fold sample buffer and stained with Coomassie Brilliant Blue R-250 after electrophoresis. The portions of loaded samples depend on the working volumes of SEC corresponds to 0.1% for all fractions. Lane M indicates molecular weight size marker (Thermo Scientific). Theoretical molecular mass of the proteins PEX19: 32.8 kDa PEX26: 33.9 kDa, nPEX3: 39.6 kDa.

Table 5.2: Cross-linked peptides of the PEX19 and PEX26 based on LC-MS analysis of *in-gel* and *in-solution* experiments

Position/Peptide (PEX19)	Position/Peptide (PEX26)	Freq.
1 / GMAAAEEGCSVGAEADRELEELLESALDDFDK	292 / KAAF ^R SR	3
34 / AKPSPAPPSTTTAPDASGPQK	292 / KAAF ^R SR	1
61 / SPGDTAKDALFASQEK	292 / KAAF ^R SR	10
90 / FFQELFDSELASQATAEFEKAM ^K	292 / KAAF ^R SR	1
131 / VGSDMTSQQEFTSCLKETLSGLAK	292 / KAAF ^R SR	6
139 / ETL ^S GLAKNATDLQNSSMSEEELTK	292 / KAAF ^R SR	3
246 / ICEQFEAETPTDSETTQ ^K AR	292 / KAAF ^R SR	9

The cross-linked peptides of PEX19 and PEX26 were identified using *pLink*. All cross-links are illustrated with corresponding frequencies from three independent experiments comprising two *in-solution* and one *in-gel* (see Figure 5.12: A) experiments. The cross-linked residues are shown in red. These evaluations were provided by Julian Bender and Dr. Friedel Drepper at the Department of Biochemistry and Functional Proteomics, University of Freiburg, Germany.

Table 5.3: Cross-linked peptides of the nPEX3 and PEX19 based on LC-MS analysis of *in-gel* and *in-solution* experiments

Position/Peptide (PEX19)	Position/Peptide (PEX3)	Freq.
1 / GMAAAEEGCSVGAEADR	189 / QAVQ ^K VLGSVSLK	2
1 / GMAAAEEGCSVGAEADR	208 / HSLSLLDLEQ ^K KLK	1

The cross-linked peptides of nPEX3 and PEX19 were identified using *pLink*. All cross-links are illustrated with corresponding frequencies from *in-gel* (see Figure 5.12: B) experiments. The cross-linked residues are shown in red.

Regarding the samples containing the PEX19-PEX26 binary complex, we observed in total seven peptides (G1, K34, K60, K90, K130, K138 and K245) of PEX19 from all three experiments, that are cross-linked to only one peptide of PEX26 including the lysine at position 292 (Table 5.2). All cross-linked residue pairs should be within close proximity each other i.e. within the radius 24 Å in order to be accessible from the cross-linker BS³ in the binary complex of PEX19-PEX26. K292 is located at one of the

predicted PEX19 binding site (BSII) in PEX26, which is also close to BSI, that includes the TMS of PEX26. The six of seven PEX19 peptides were located to the flexible N-half (see Figure 5.13: alpha A-E), that consists of five amphipathic segments^[55], while one of those to the rigid core of PEX19 (see Figure 5.13: Alpha1-4)^[58, 62].

Accordingly, the first cross-links of PEX19 occurred at N-terminus with the side chains of glycine, which is a residual amino acid after cleavage of *His*₆ from full length PEX19 and is not natively included in its sequence. The second cross-link of PEX19 occurred with a side chain of lysine on the alpha-a segment of PEX19. The third cross-link of PEX19 occurred with a side chain of lysine in the disordered segment of PEX19 between alpha a and very near of b, while the fourth one directly on the segment alpha b. The fifth cross-link of PEX19 occurred with a side chain of lysine on the alpha-d segment of PEX19, whereas the sixth cross-link of PEX19 occurred with a side chain of lysine in the disordered segment of PEX19 between very near of alpha d and e.

Furthermore, the identified PMP binding pocket of PEX19 comprises a hydrophobic cavity, which is formed through participation of all four structurally clarified alpha-helices (alpha-1-4).

In addition, we found two more cross-linking between the PEX19 residue G1 with two PEX3-residues; K189 and K208 (Table 5.3). These two residues are part of alpha-4 and alpha-5 of PEX3 (see Figure 5.13) and locate on the cytosolic apex in tertiary structure of PEX3. Moreover, the clarified sPEX3 (40-373) and PEX19 (14-33) complex structure includes only 14-33 residues of PEX19. Accordingly, we suggest that these two cross-links are strongly reasonable. Therefore, the missing PEX19 N-terminus (first 13 amino acids) in this complex structure must be closely located to alpha-4 and alpha-5 of PEX3 in native structure.

Based on our analysis, our findings indicate a strong participation of either PEX19's N-half or its rigid core to PEX26 binding i.e. stabilization. The participating segments include especially three alpha-helical segments; alpha-B, alpha-D (within flexible N-half) and alpha-4 (within rigid core) and also three unfolded regions within PEX19-N-half, which have close proximity to PEX26's tail anchor within the range of 24 Å (see Figure 5.13). Additionally, PEX26 contains four lysines within PEX19-BSI and BSII (K253, K254, K282 and K292). Two of these lysines (K253 and K254) are part of the TMS of PEX26, while the other two in PEX19-BSII of PEX26. Since cross-links of PEX26 only occurred on lysine (K292) in the second PEX19 binding site (BSII), we conclude that the three remaining lysines in these regions are not accessible to our

cross-linker BS³ or protected through hydrophobic pocket of PEX19. However, the former suggestion is limited in some extent, based on the fact that the residue pairs, which are located within the radius 24 Å, are able to form cross-links through BS³

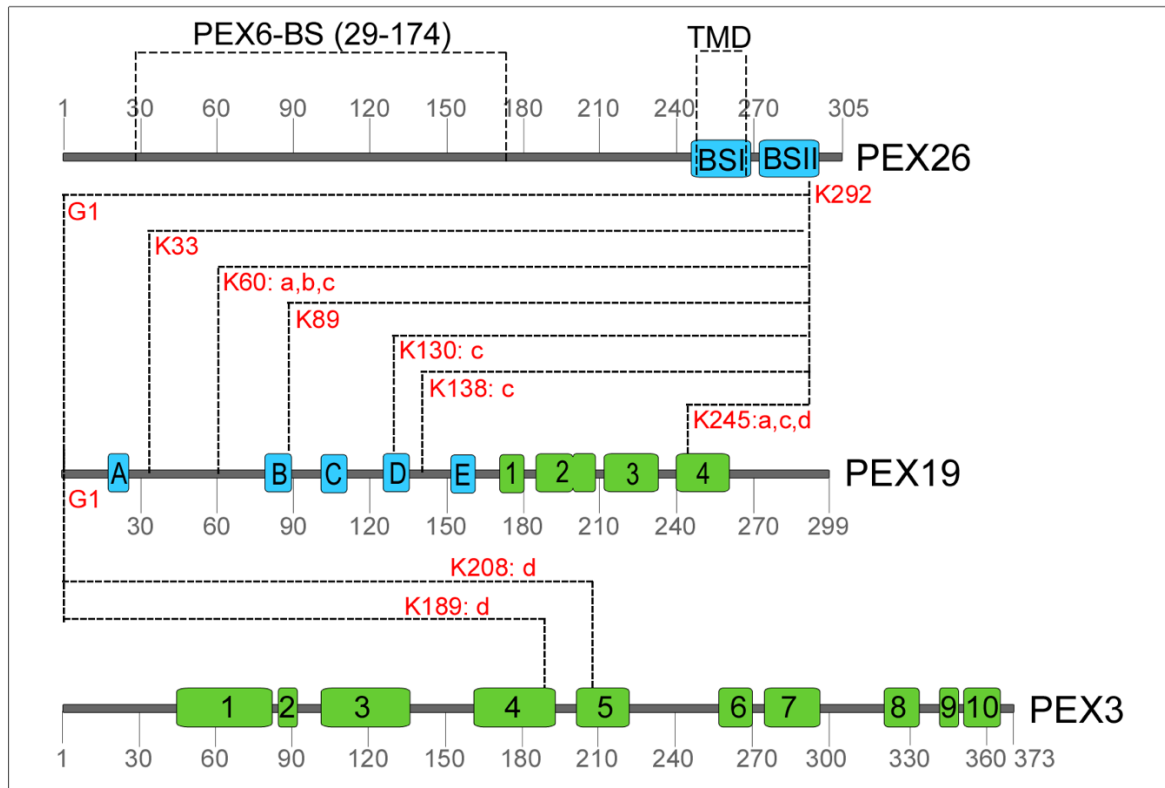


Figure 5.13: Identified cross-links between the PEX3, PEX19 and PEX26. Schematic presentation of full length PEX26, PEX19 and PEX3 including putative secondary structure alpha helices and elements (in blue) and alpha helices included in the crystal structure (in green). PEX26 is shown with two predicted membrane targeting signals (PEX19 Binding Site I-II) and its predicted transmembrane domain (TMS) as well as PEX6 binding site (PEX6-BS). Cross-linked peptides via lysines between PEX19 and PEX26 are shown with dashed lines. Accordingly, totally seven peptides of PEX19 at **G1**, **K33**, **K60**, **K89**, **K130**, **K138** and **K245** formed intermolecular cross-links with one PEX26 peptide at **K292**. These data were obtained from three independent experiments, a cross-linking experiment using samples cut out from the gel (*in-gel*) and two *in-solution* experiments. The letters a, b, c and d illustrate the excised bands from the SDS-PAGE analysis used to identify the cross-links through in-gel experiment (see Figure 5.12). These evaluations were provided by Julian Bender and Dr. Friedel Drepper at the Department of Biochemistry and Functional Proteomics, University of Freiburg, Germany.

5.7. Complementation of PEX26-deficient fibroblasts

A CHO mutant PEX26-deficient cell line ZP167 isn't able to form functional peroxisomes but has peroxisomal remnants, instead. ZP167 cells co-expressing Flag-PEX26 with PEX6-HA indicate a co-localisation of Flag-PEX26 and PEX6-HA, however this was barely observed with PEX1-HA^[46]. PEX1 and PEX6 form a hexameric complex, that regulates recycling of PEX5 to the cytosol^[132]. Furthermore, co-immunoprecipitation analysis of GST-tagged PEX26 with PEX1 and PEX6 showed

that PEX26 binds PEX6 directly, while the PEX26 interaction to PEX1 occurs in a PEX6-dependent manner. Additionally, steady state levels of PEX5 were severely reduced in all three, PEX1-, PEX6- and PEX26-deficient (CG8) cells^[47]. In addition, PEX26 expression in ZP167 cells showed the same phenotype as wild-type CHO cells. The transfection of a *PEX26* plasmid was able to re-establish the export complex of PEX1 and PEX6 and recover EGFP-PTS1 import^[46]. Therefore, we decided to test the purified recombinant PEX19-PEX26 complex in PEX26-deficient fibroblasts (PBD059) for its functionality. The cell line, PBD059 is assigned to CG8 and shows the most severe defect in matrix protein import caused by a homozygous frame shift mutation at T77^[23].

In order to show that our binary complex is able to complement the PBD059 cells, we transformed them with purified 4 μ M of PEX19-PEX26 using the *Neon Electroporator*. Additionally, we performed a transformation of the same line with an empty mammalian vector, pcDNA.3.1.zeo as negative control (Control (-)). Furthermore, a myc-PEX26 expressing construct (cloned in pCND3.1.zeo) was used for transformation of PBD059 cells as positive control group (Control (+)).

Since we wanted to invest the functionality of PEX19-PEX26 complex in another experiment using LUVs, we already had labelled a fraction of the purified complex with *Alexa488* (DOL: 20%). Therefore, we were interested to test this labelled complex using PBD059 cells fibroblasts, as well.

In order to analyse protein import into peroxisomes we additionally co-transfected the cells with a construct that codes for the green fluorescence protein EGFP carrying a PTS1 targeting sequence (EGFP-SKL) in each experimental group.

To show the cellular localisation of peroxisomes and to analyse the import of the marker protein EGFP-SKL, immunofluorescence staining of all four experimental groups were performed using primary antibodies, against PEX14 as peroxisomal membrane marker and anti-EGFP antibodies to enhance the intrinsic GFP signal in the cells. The secondary antibodies were labelled with the fluorophores *Alexa488* (green) and *Alexa594* (red), respectively. Thus, in this import assay, the transformation describes the fibroblasts that demonstrated green signal originating from EGFP-SKL either in cytosol or peroxisomes, whereas the complementation encompassed the fibroblast that showed red and green signal in peroxisomes.

After immunostaining, matrix protein import in transfected cells was assessed by fluorescence microscopy based on two independent identical experiments. The

quantification of transformation rates calculated based on 500 fibroblasts from each experimental group, while the complementation rates based on the transformed cells. The statistical quantification as well as significance of each group were calculated using *Prism* based on *mean squared deviation* and represented on bar plot.

Therefore, transformation rates of all experimental groups differ between 15 and 17%. The representative images of all experimental groups are shown in Figure 5.14: A and their quantification in Figure 5.14: B. Accordingly, the negative control group fibroblast transfected with the empty vector, pCDNA.3.1.zeo, illustrated red puncta indicating the peroxisomal marker protein PEX14 (see Figure 5.14: A and B) in peroxisomal remnants. In contrast, the same cell showed a dispersion of green signal originating from EGFP-SKL in the cytosol, thus almost no co-localisation (0.34%) of both signals. Based on this, no complementation of PTS1-SKL and PEX14 had occurred in these fibroblasts. (see Figure 5.14: A; 1st Row and B). By contrast, the positive control group (Control (+)) showed colocalisation of PEX14 (red) and EGFP-SKL (green) signals on the overlay in the same cell. This indicated a successful EGFP-SKL import into peroxisomes in 32% of transformed cells (see Figure 5.14: A; 2nd Row and B). Furthermore, the fibroblasts transfected with purified PEX19-PEX26 have demonstrated co-localisation of PEX14(red) and EGFP-SKL (green) in 53% of transformed cells. Supporting this, the fibroblasts transfected with the labelled PEX19-PEX26 (L-PEX19-PEX26) (DOL: 20%) showed in 38% of transformed fibroblast (Figure 5.14: A; 3rd and 4th Row). In conclusion, the transformation of PBD059 fibroblast with purified recombinant PEX19-PEX26 as well as L-PEX19-PEX26 resulted in even higher complementation rates in comparison to positive control group. This indicated a complementation of PBD059 cells fibroblasts which is proven by a successful EGFP-SKL import.

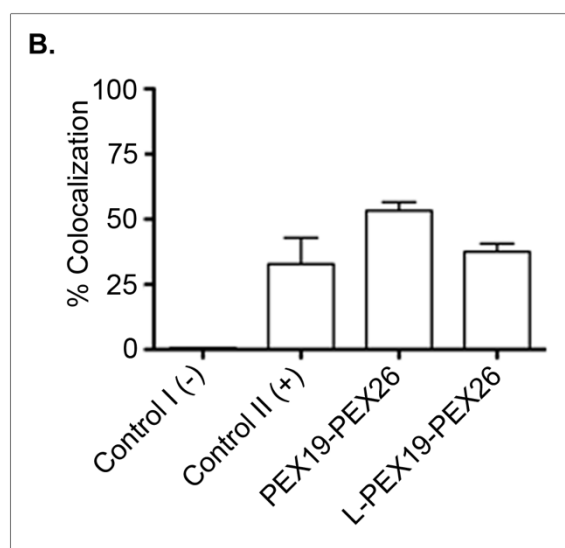
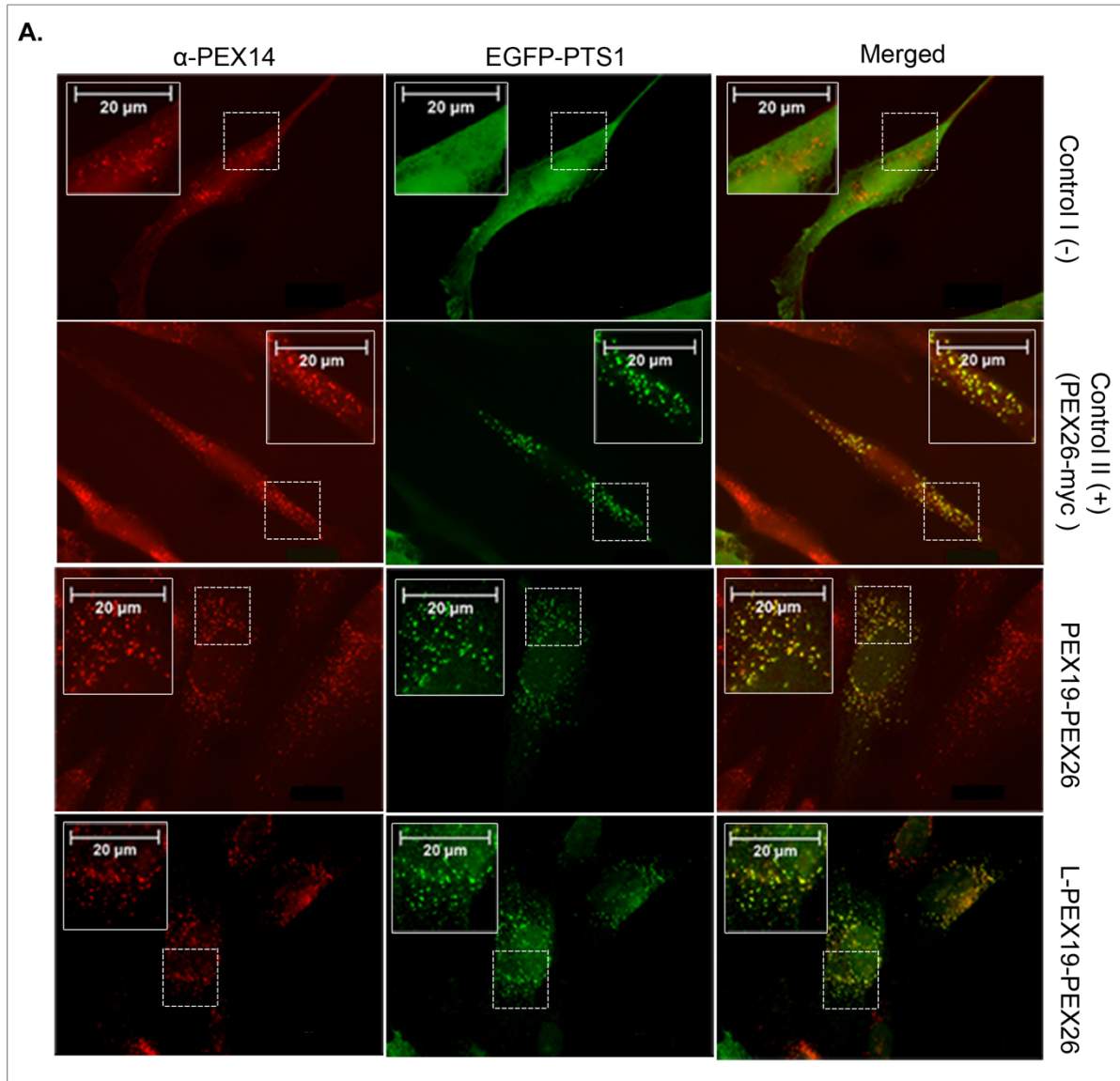


Figure 5.14: The PEX26-PEX19 complex is able to complement PEX26-deficient human fibroblasts. PBD059 cells were transfected with purified proteins. One fraction of the purified proteins was labelled with *Alexa488* to test the functionality of labelled complex. The labelled and unlabelled proteins diluted to 4 μ M for electroporation of PEX26-deficient human fibroblasts. After 14 hours' cultivation, the cells are immunostained with antibodies against a peroxisome marker PEX14 (α -PEX14) and a marker of peroxisome matrix EGFP-SKL(PTS1) (α -EGFP). After immunostaining, matrix protein import in transformed cells are assessed by fluorescence microscopy. Dashed square shows magnified area of images that is placed on the upper left corner of each images. **[A]** First row: negative control (-) of the fibroblasts are transformed with empty vector; pCDNA.3.1.zeo. Second row: positive control (+) of the fibroblasts transformed with a myc-PEX26 (cloned in pCDNA.3.1.zeo) vector. Third row: Fibroblasts transfected with purified complex of PEX19- PEX26. Last row: Fibroblasts transfected with PEX19-PEX26 complex which were labelled using *Alexa488* (DOL: 20%). **[B]** Quantification of data from two independent identical experiment including^[A]. Graphic shows percentage of co-localised cells against four different experimental groups. The quantification of transformation rates calculated regarding 500 fibroblasts from each experimental group, while the complementation rates based on the transformed cells. The statistical quantifications as well as significances of complementation of each group were calculated using *Prism* based on *mean squared deviation* and represented on bar plot.

5.8. Flow cytometry analysis of PEX26 associations with LUVs

We could show that the PEX19-PEX26 binary complex can restore *in vivo* PEX5 guided matrix protein import in PEX26-deficient fibroblasts, thus we conclude that it is functional under *in vivo* conditions. To test whether the PEX19-PEX26 binary complex is functional under *in vitro* conditions as well, we mimicked peroxisomes using Ni-NTA large unilamellar vesicles (LUVs) and assessed the PEX26 membrane integration through flow cytometry analysis. Flow cytometry analysis is mostly used to determine quantity or physical parameters like size or size differences of LUVs or cells^[123]. Thus, we have labelled purified nPEX3^T (*Thx-His6-Thr-TEV-PEX3₂₆₋₃₇₃*) and PEX19-PEX26 binary complex using *Alexa488* on free thiol groups of cysteines (see Figure 5.15: A and B). After labelling step, we measured labelled nPEX3^T and PEX19-PEX26 using *Nanodrop 2000* (Thermo Scientific) in order to acquire absorption spectrum in the range of 220-600 nm. These were used to calculate (see Section 4.5.1) the degree of labelling (DOL) of each protein (see Figure 5.15: A and B). In these spectra, the absorption values at 280 nm correspond to the UV absorption of proteins through their aromatic side chains, whereas the absorption at 495 nm originated from the labelling of the proteins through *Alexa488*. Accordingly, the DOLs of the proteins were calculated to 26% and 20% for nPEX3^T and PEX19-26, respectively (see Figure 5.15: A and B). Thereafter, we prepared Ni-NTA-LUVs consisting of 65.8% Egg-PC, 28.2% Egg-PE and 6% Ni-DGS. The size of the peroxisomes varies between 100 and 1000 nm under *in vivo* conditions. Based on this we extruded our LUV using 400 nm MWCO (molecular weight cut off) membranes and confirmed their size using DLS (dynamic

light scattering) measurement (see Figure 5.15: C). According to this measurement, the LUVs showed a distribution in 100 to 1000 nm range with an average diameter of 228 nm with size deviation of ± 112 nm. After preparation of the LUVs, they are divided into six sets of experimental groups and treated as in following Table 5.4.

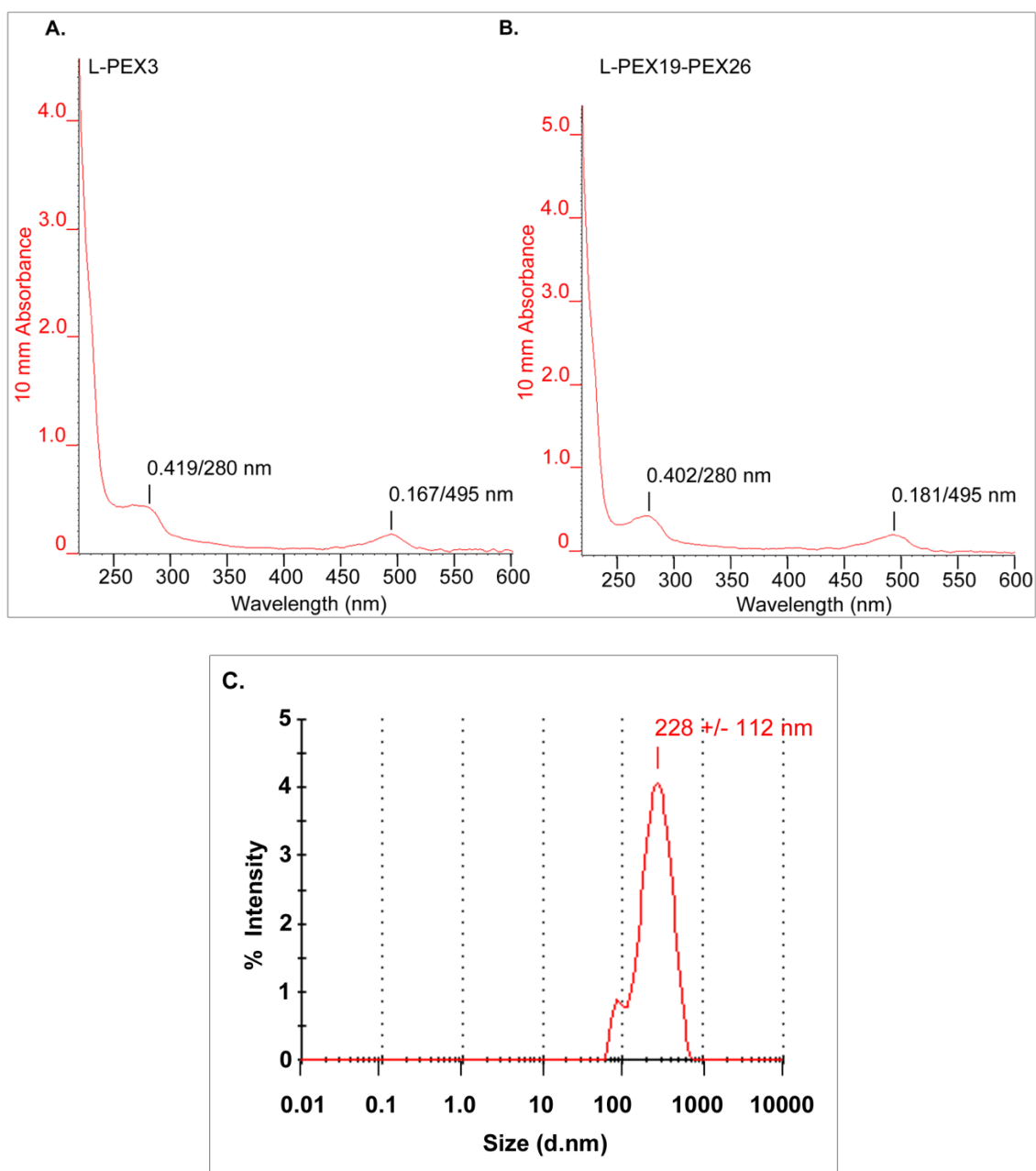


Figure 5.15: The absorption spectrum (220-600 nm) of labelled nPEX3^T and PEX19-PEX26, as well as DLS analysis of LUVs used in PEX26 membrane integration experiment. The absorbances of two peaks corresponding to 280 and 495 nm were used for the calculation of DOL. The degree of labelling (DOL) was calculated using the formula explained in Section 4.5.1. **[A]** Absorption spectrum of labelled nPEX3^T (DOL: 26%) and **[B]** L-PEX19-PEX26 (DOL: 20%) which were used in integration experiments. **[C]** The size distribution of LUVs measured using DLS and varied between 100 to 1000 MWCO range with an average diameter of 228 nm with size deviation of ± 112 nm

Table 5.4: The six identical fractions of LUVs and seven incubation steps for the assessment of PEX26-LUV-membrane integration using flow cytometry analysis

	(I)	(II)	(III)	(IV)	(V)	(VI)	(VII)
A	BSA/LUVA-S ₀	LUVA-S ₀	-	-	-	-	FC
B	BSA/LUVA-S ₀	LUVA-S ₀	nPEX3L	LUVA-S ₀	-	-	FC
C	BSA/LUVA-S ₀	LUVA-S ₀	PEX3L	LUVB-S ₀	-	-	FC
D	BSA/LUVA-S ₀	LUVA-S ₀	PEX19/26L	LUVA-S ₀	-	-	FC
E	BSA/LUVA-S ₀	LUVA-S ₀	PEX3	LUVA-S ₀	PEX19/26L	LUVA-S ₀	FC
F	BSA/LUVA-S ₀	LUVA-S ₀	PEX3	LUVA-S ₀	PEX19/26L	LUVB-S ₀	FC

Treatment of the Ni-NTA LUVs in six experimental groups including the steps; I: blocking with BSA, II: The washing step of blocked LUVs using LUVA-S₀, III: Incubation (except A) with appropriate proteins including nPEX3^TL (Labelled nPEX3^T for B and C), nPEX3^T(Unlabelled, for E and F) and PEX19-26L (Labelled PEX19-26 for D), IV: The second washing step using appropriate buffers; LUVA-S₀ (B, D, E and F) and LUVB-S₀(C), V: LUV-incubation with PEX19/26L (Labelled PEX19-26 for E and F), VI: The third washing step using appropriate buffers: LUVA-S₀ (E) and LUVB-S₀(F), VII: Flow cytometry (FC) analysis of all experimental groups

Prior to flow cytometry analysis, we incubated Ni-NTA-LUVs (A, Table 5.4) first with labelled nPEX3^T (*Thx-His6-Thr-TEV-PEX3₂₆₋₃₇₃*) (B, Table 5.4), that served as docking protein for the PEX19-PEX26 complex. To elucidate the type of interaction of PEX3 with the LUVs, we then eluted the proteins using 500 mM imidazole containing buffer (LUVB-S₀), that should break the *His₆-tag*-mediated interaction of nPEX3^T (C, Table 5.4). Afterwards we analysed the coupled as well as eluted Ni-NTA-LUVs in comparison with the non-coupled Ni-NTA-LUVs by acquisition through FITC-channel against FSC (forward side scatter) using *CytoFLEX* flow cytometer (Beckman Coulter). FITC channel (Fluorescein isothiocyanate, Ex/Em: 495 nm/519 nm) is one of the included channels in *CytoFLEX* which can only cover Ex/Em spectrum of *Alexa488* (Ex/Em: 499/520 nm). Furthermore, FITC-A distribution frame was divided into two regions as P1 and P2 which were defined based on non-coupled LUVs as negative control.

According to measurements, 4.5% of the non-coupled Ni-NTA-LUVs were found in the high FITC-intensity region, despite any conjugation with labelled proteins (see Figure 5.16: A). 85.8% of the Ni-NTA-LUVs were shifted to the high FITC-intensity range after conjugation with labelled nPEX3^T (see Figure 5.16: B). Moreover 61.6% of them shifted back to low intensity region after elution of labelled nPEX3^T after treatment with LUVB-

S_0 (500 mM imidazole) (see Figure 5.16: C). This indicates that Ni-NTA-LUVs can be successfully and reversibly coupled with nPEX3^T.

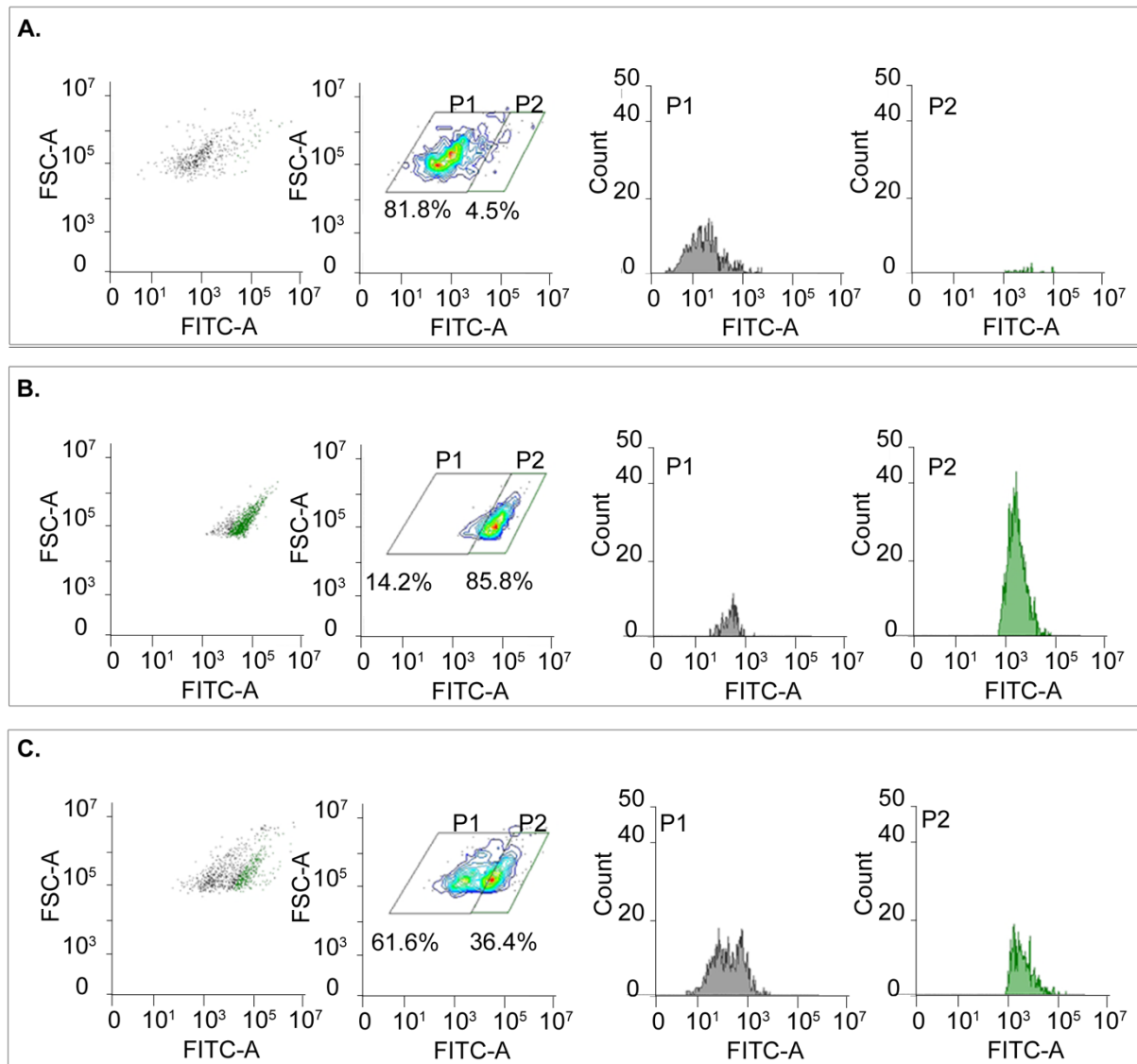


Figure 5.16: The distribution of FITC-A gating of Ni-NTA-LUVs coupled with labelled nPEX3^T. After the incubation steps I-VII, the LUVs were assessed by flow cytometry analysis. FITC-A distributions were divided into two regions (P1, P2) based on non-coupled LUVs in [A] as negative control. The distributions of 1000 events are shown using a *contour plot*. The highest density regions of the event distributions are coloured with red and the lowest ones with blue. **[A]** Distribution plot of non-coupled LUVs. This distribution resembles the negative control group and was used to define the P1 and P2 frames, which are identical for all groups. **[B]** Distribution plot of LUVs after coupling with nPEX3. LUVs were incubated with labelled nPEX3^T. **[C]**: Distribution plot of LUVs coupled with nPEX3^T after treatment with LUVB-S₀ (500 mM imidazole)

In order to investigate whether PEX26 could be inserted into a liposomal membrane, we incubated Ni-NTA-LUVs first directly with the PEX19-PEX26 complex as a negative

control (D, Table 5.4). A second fraction was incubated with unlabelled nPEX3^T and with the labelled PEX19-PEX26 complex (E, Table 5.4). The third fraction was incubated with unlabelled nPEX3^T and with labelled the PEX19-PEX26 complex and then treated with LUVB-S₀ (500 mM imidazole) (F, Table 5.4). According to flow cytometry analysis, 12.8% of Ni-NTA-LUVs interacted with PEX19-PEX26 in the absence of PEX3 (see Figure 5.17: D). Furthermore, 84.4% of Ni-NTA-LUVs that were coupled with unlabelled nPEX3^T interacted with labelled PEX19-PEX26 (see Figure 5.17: E). After incubation of these LUVs with LUVB-S₀ (500 mM imidazole), we observed a reduction of the FITC intensity by 31.3%. This indicates a release of unlabelled nPEX3^T together with labelled PEX19 as complex (see Figure 5.17: F). Accordingly, we quantified the intensities of FITC signals regarding the P2 from two independent experiments (see Figure 5.18). We subtracted the intensity of the positive control (12.8%) (see Figure 5.18: D) from the remaining intensity of 53.1% (see Figure 5.18: F) after treatment with imidazole buffer. Based on this, we conclude that nPEX3^T increased the integration of PEX26 to LUV membrane by 40.3%.

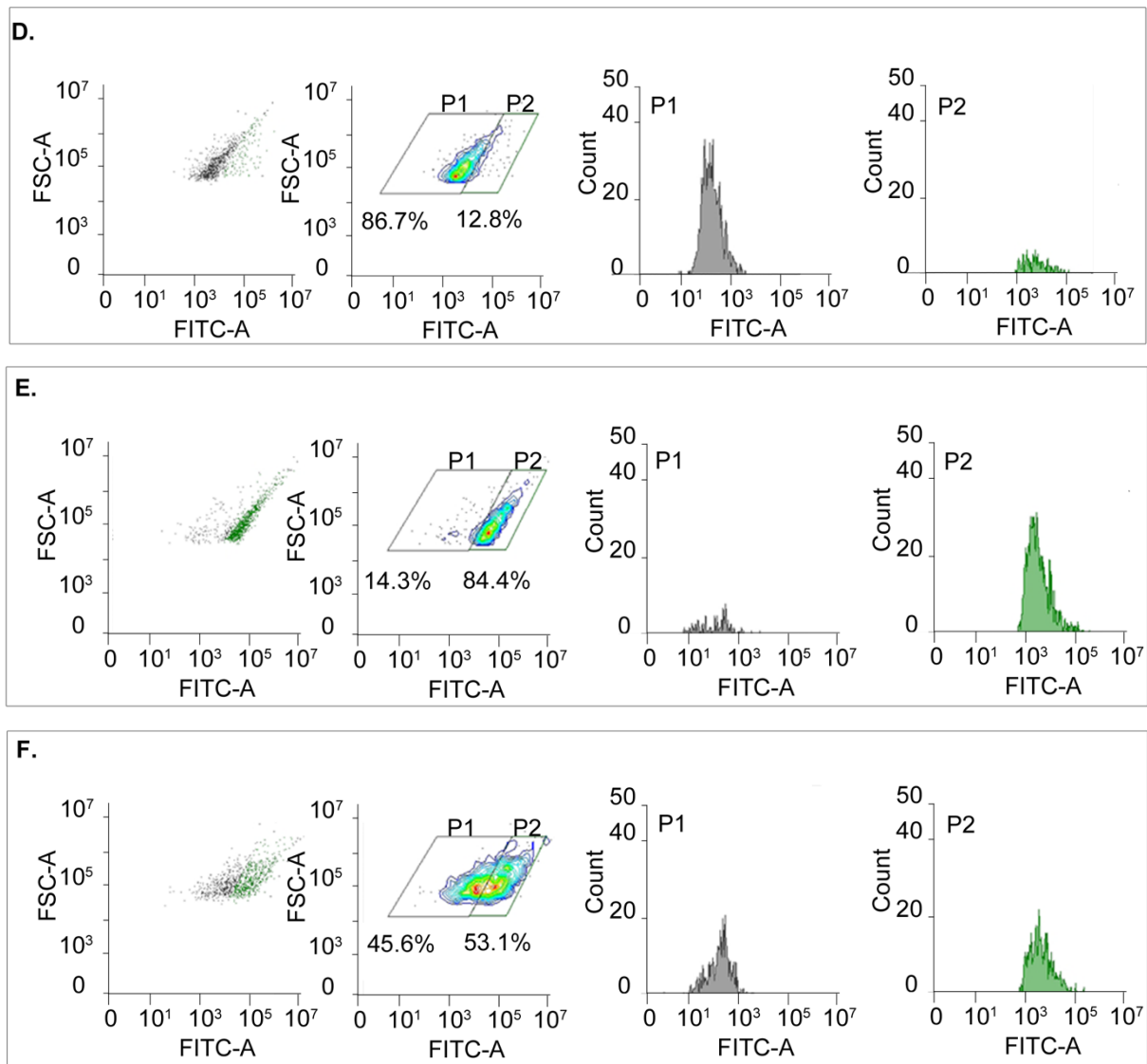


Figure 5.17: Distributions of FITC-A gating of Ni-NTA-LUVs coupled with labelled PEX19-PEX26. After incubation steps I-VII, the LUVs were assessed by flow cytometry. FITC-A distributions were divided into two regions (P1, P2) based on non-coupled LUVs in Figure 5.17 [A] as negative control. The distributions of 1000 events are shown using a *contour plot*. The highest density regions of the event distributions are coloured with red and the lowest ones with blue **[D]** The distribution plot of LUVs after incubation with PEX19-PEX26 coupled LUVs. This distribution illustrates the second negative control group for the experiment which reveals the background signal for PEX26 binding. **[E]** The distribution plot of LUVs previously coupled with unlabelled nPEX3^T and incubated with labelled PEX19-PEX26. **[F]** The distribution plot of LUVs treated as in E but eluted with LUVB-S₀ (500 mM imidazole)

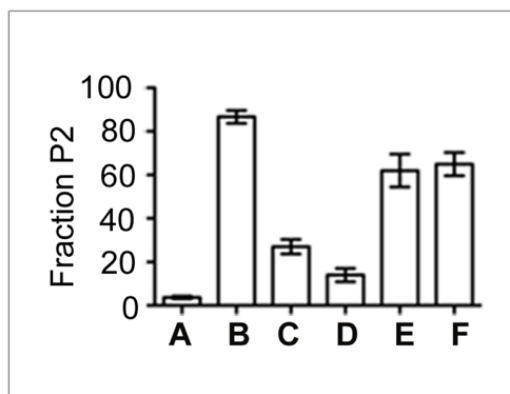


Figure 5.18: The quantification of flow cytometry data based on the percentages of FITC-A intensities. The quantification refers to the data obtained from four independent flow cytometry experiments shown in Figure 5.17 and 5.18 as well as in Table 5.4. Based on the FITC-A intensity, the graphic gives the levels (%) of the P2 fractions of the experimental groups A, B, C, D, E and F. Error bars represents \pm SEM (standard error of the mean).

5.9. Carbonate extraction of LUV-associated PEX26

Our flow cytometry analysis indicated, that a smaller amount of PEX26 interacted with LUVs independent from nPEX3 and a significant contribution of PEX3 to the binding of PEX26 to LUVs in a cell- and peroxisome-free system. However, the mode of the PEX26-interaction to LUVs needed to be more precisely analysed. In the next step we investigated the resistance of proteins to carbonate extraction from the prepared LUVs. Directly after flow cytometry analysis of LUV-protein interaction, these LUVs were subjected to sodium carbonate extraction using ultracentrifugation. Since LUVs should be bound to nPEX3^T through the affinity of lipid-Ni-NTA to *His*₆-tag of nPEX3^T, we expected that these LUVs (LUV+nPEX3^T) would be resistant to carbonate extraction. This was confirmed by western blot analysis, displaying a protein band at 55 kDa, detected with antibodies against PEX3 in the total (T) fraction before centrifugation and after, in the pellet (P) fractions, but not in the supernatant (S) (see Figure 5.19). Furthermore, the nPEX3^T signal remained unchanged in the pellet fractions of the first two conditions B and E described in Table 5.4 in Section 4.18 (see Figure 5.19). In contrast, the signal decreased after treatment with LUVB-S₀ (500 mM imidazole) (F, Table 5.4) Accordingly, we conclude that nPEX3^T binds to LUVs through *His*₆ affinity to Ni-NTA of LUVs, which was expectedly resistant to carbonate extraction.

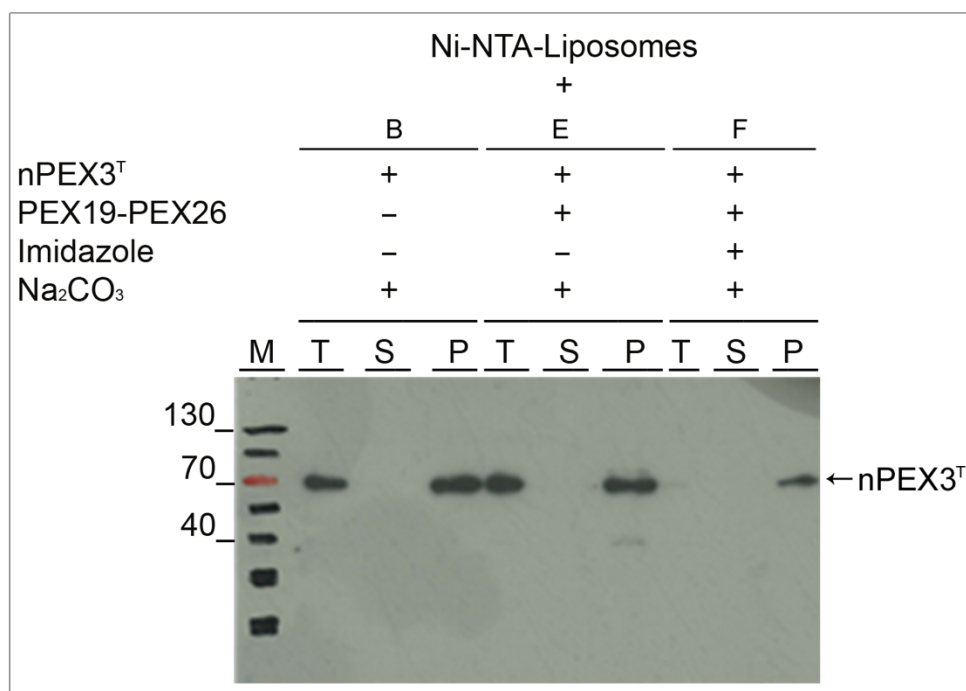


Figure 5.19: The Carbonate extraction of the nPEX3^T-LUV coupling

The experimental groups B, E and F mentioned in Section 4.18, were treated as described in the table 5.4 and subjected carbonate extraction subsequently to flow cytometry analysis. Total (T) as well as pellet (P) and supernatant(S) fractions, that were obtained after ultracentrifugation from the fractions B, E and F were further analysed with western blot using antibody against nPEX3^T. Theoretical molecular mass of nPEX3^T (*Trx-His6-Thr-TEV-nPEX3*): 57.3 kDa.

After confirming the binding manner of nPEX3^T to LUVs, we further analysed the PEX26 interaction. The LUVs, which were treated as described in the Table 5.4 (D, E and F) were subjected to carbonate extraction. Accordingly, all LUVs, which were coupled with nPEX3^T and subsequently incubated with PEX19-PEX26 (E and F, Table 5.4) or without nPEX3^T but only with PEX19-PEX26 (D, Table 5.4) were analysed in the next step for their resistance of PEX26 to carbonate extraction. These samples were also treated with Triton-X100, in comparison.

Accordingly, in negative control fraction D, PEX26 could be detected in all pellet fractions, whereas only faint signal was seen in the supernatant fraction of the Triton-X100 treatment (see Figure 5.20: D, Lane 4). Therefore, PEX26 showed a resistance to sodium carbonate, which could be considered as background this experiment. Moreover, it was extracted from the liposomal membrane after treatment with Triton-X100. This result showed that, PEX26 could integrate into LUV membrane in some extent also without PEX3.

The fraction E comprises the LUVs coupled with nPEX3^T in comparison to D, and incubated with PEX19-PEX26, which demonstrates a PEX26 signal consistently in all

pellet fractions. (see Figure 5.20: E). As expected, the signal appears also in the supernatant fraction after treatment with Triton-X100 (see Figure 5.20: E, 4. Lane). This result showed that presence of bound PEX3 on LUV membrane contributed to PEX26 integration in a higher extent than in fraction D.

The fraction F encompasses an additional LUVB-S₀ (500 mM imidazole) treatment step of fraction E, which demonstrates a PEX26 signal consistently in all pellet fractions as well (see Figure 5.20: F). The PEX26 signal appears also in the supernatant fraction after treatment with Triton-X100. This result suggests also that presence of bound PEX3 on LUV membrane contributed to PEX26 integration almost same as in E and in a higher extent than in fraction D. In addition, the LUVB-S₀ (500 mM imidazole) treatment in this fraction released the bound nPEX3^T portion to LUV membrane after the PEX26 integration stage. This excluded the unspecific i.e. non-integrated portions of PEX26 with LUV membrane through nPEX3^T-PEX19-PEX26 ternary complex.

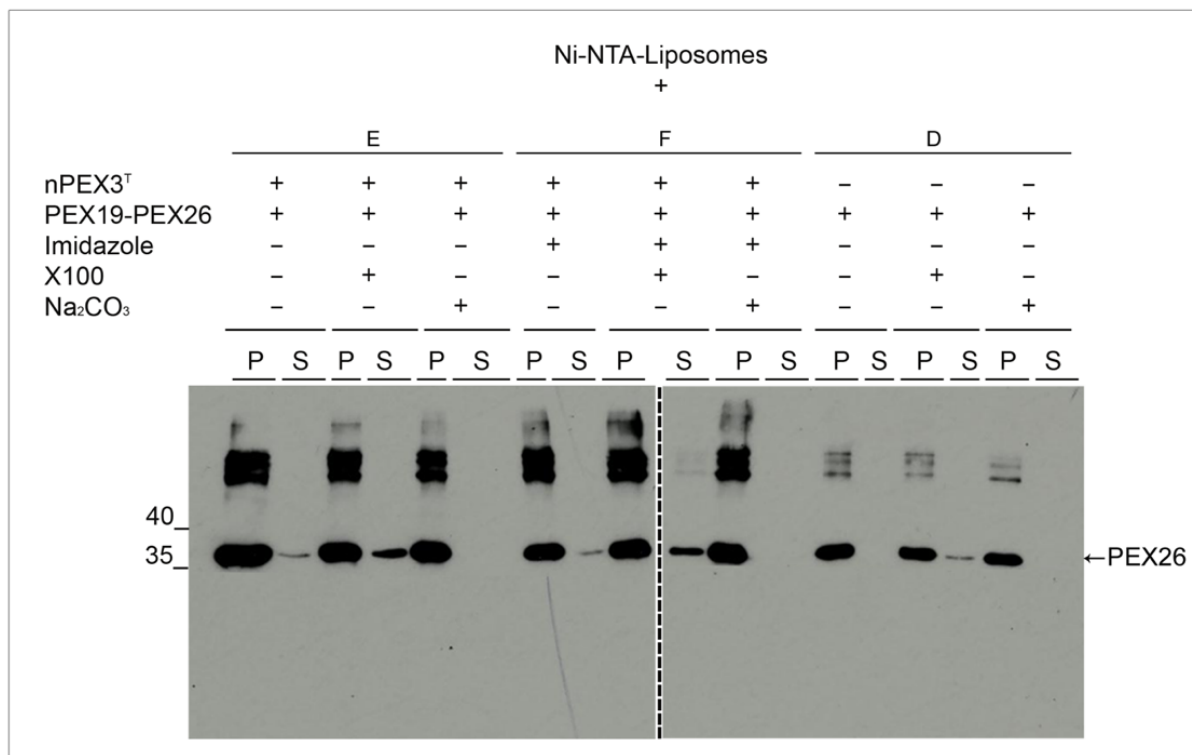


Figure 5.20: The Carbonate extraction of PEX26-LUV associations

Immediately after flow cytometry assessment, the LUVs of each groups are subjected to Na₂CO₃ extraction as well as treatment with Triton-X100(X100). Fraction^[D] contains Ni-NTA-LUVs that were incubated directly with the PEX19-PEX26 complex and considered as negative control group,^[E] coupled with nPEX3^T and subsequently incubated with PEX19-PEX26^[F] coupled with nPEX3^T and subsequently incubated with PEX19-PEX26 and then treated with LUVB-S₀ (500 mM imidazole) as well. The pellet (P) and supernatant(S) fractions, which were obtained after ultracentrifugation, from the fractions D, E and F were further analysed with

western-blot analysis using antibodies against PEX26. Theoretical molecular mass of PEX26: 33.9 kDa.

Furthermore, we quantified the relative ECL signal for the PEX26 levels after carbonate extraction (see Figure 5.21). The obtained data originated from two identical LUV-PEX26 integration experiments (n=2) based on the ECL signal levels of PEX26 after carbonate extractions subsequently to flow cytometry analysis. The relative ECL signal levels of PEX26 in each lane were calculated based on the highest signal (100%), that corresponds to the total pellet fraction of E (see Figure 5.20 and 5.21). Therefore quantification, the total ECL signal levels between the groups decreased in fractions E, F and D respectively. Fraction E demonstrated the highest level, which was reduced through LUVB-S₀ (500 mM imidazole) in fraction F, while fraction D showed the least level of PEX26-LUV integration. Accordingly, we conclude that nPEX3^T increases the PEX26 association to LUV membrane confirming its known mode of action as a docking protein for cargo loaded PEX19 i.e. PEX19-PEX26. In addition, the general course of ECL signal levels have almost same manner within all three groups. Thus, the ECL signal levels decreases within the groups as following: Total-pellet (T/P) > carbonate extraction-pellet (CO/P) > Triton-X100-pellet (TX/P) ≥ Triton-X100-supernatant (TX/S) ≥ total-supernatant (T/S) > carbonate extraction-supernatant (CO/S). Furthermore, the T/P and CO/P fractions comprise at least 90% of PEX26, whereas TX/P and TX/S have almost same levels. This result suggests that PEX26, which present in T/P fractions could be solubilised around 3-8-fold through Triton-X100 treatment, however Na₂CO₃ treatment has no effect on PEX26 association to LUV membrane (see Figure 5.21: CO/P and CO/S fractions).

In conclusion, these results showed that PEX26-LUV association is resistant to Na₂CO₃, but not to Triton-X100 treatment, therefore we suggest that this association indicates an integration of PEX26 into LUV membrane, which should be further analysed precisely through additional studies.

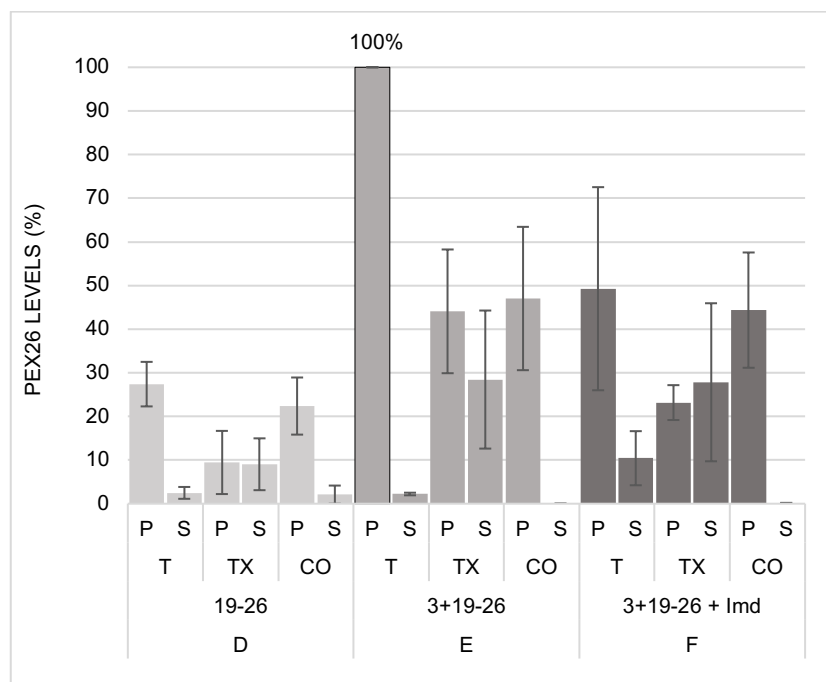


Figure 5.21: The quantification of relative ECL signal for the PEX26 levels after carbonate extraction. The quantification comprises the fractions D, E and F as described in see Section 5.8. The fraction [D] contains Ni-NTA-LUVs that were incubated directly with the PEX19-PEX26 complex and considered as negative control group. [E] contains Ni-NTA-LUVs that were coupled with nPEX3^T and subsequently incubated with PEX19-PEX26. [F] contains Ni-NTA-LUVs that were coupled nPEX3^T and subsequently incubated with PEX19-PEX26 and then treated with LUVB-S₀ (500 mM imidazole). The pellet (P) and supernatant(S) fractions, which were obtained after ultracentrifugation, from the fractions D, E and F were further analysed with western-blot analysis using antibodies against PEX26. The relative ECL signal levels of PEX26 in each lane were calculated based on the highest signal (100%), that corresponds to the total pellet fraction of E. The obtained data originated from average values of two identical LUV-PEX26 integration experiments (n=2) based on the ECL signal levels of PEX26 after carbonate extractions subsequently to flow cytometry analysis. Error bars represents \pm SEM (standard error of the mean).

6. Discussion

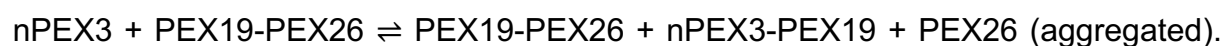
We showed that the recombinant expression of nPEX3, PEX19 and PEX26 resulted in the formation of the functional heteromeric complexes nPEX3-PEX19-PEX26 and PEX19-PEX26. Furthermore, the PEX19-PEX26 complex could restore peroxisomal matrix protein import in PEX26-deficient fibroblasts. This complex was analysed by native MS in order to figure out the stoichiometry of the monomers. Accordingly, native MS indicated a binary complex formation of PEX19 and PEX26. In addition, when the binary complex was further analysed using XL-MS to uncover its interacting segments, the neighbouring cross-linked peptides of PEX19 and PEX26 were revealed. This result indicated a high probability of an interaction between these segments that would promote the PEX19-PEX26 complex formation. Moreover, we demonstrated the association of PEX26 with LUVs in a nPEX3^T dependent manner using a flow cytometry-based approach. This association was further elucidated using carbonate extraction and indicated a PEX26 integration into the LUV membrane. The individual aspects of these results are discussed in greater detail in the following sections.

6.1. Recombinant PEX26 and PEX19 form a binary complex

Recombinant overproduction of membrane proteins often results in the appearance of soluble or insoluble aggregates during purification steps, which cannot be further analysed. Additionally, employing a detergent in these purification steps interferes with the equilibrium of thermodynamic states of proteins, $P_{\text{unfolded}} \rightleftharpoons P_{\text{native}}$ through binding to the hydrophobic regions of proteins and thus supporting the unfolded state^[142]. Based on these facts, we overproduced PEX26 together with its native receptor, the chaperon-like protein PEX19 in order to analyse PEX26 and its interactions with PEX19. The following purification step employing IMAC showed that *His*₆-tagged PEX19 eluted together with untagged full-length PEX26. This result was considered as a preliminary indication of a PEX19-PEX26 complex. However, we weren't able to make any assumptions on the stoichiometry of both proteins (binary or oligomeric) in this complex. Subsequently, the SEC analysis assigned the PEX19-PEX26 complex to 169 kDa in size, while the calculated theoretical size of the complex was 66.70 kDa (PEX19: 32.81, PEX26: 33.89 kDa). Based on this, we assumed that the 169 kDa complex comprised a heterodimeric complex formed by a highly extended conformation of monomeric PEX19 complexing with monomeric PEX26. Supporting this, several studies using protease protection assays indicated that PEX19 has a very

flexible N-terminal half and thus a very extended conformation^[73]. In addition, another former study reported a size of 95.2 kDa for PEX19 based on SEC analysis of monomeric PEX19^[28]. Confirming this, our SEC analysis of purified PEX19 showed that monomeric PEX19 could be assigned to 98 kDa and the monomeric nPEX3 (PEX3₂₆₋₃₇₃: 39.6 kDa) to 50 kDa (see Figure 6.1, A: a: PEX19, b: nPEX3 and d: PEX19-PEX26). Furthermore, the nPEX3-PEX19 complex was assigned to 152.1 kDa by the SEC chromatogram (see Figure 6.1, B: a: PEX19, b: nPEX3 and f: PEX3-PEX19).

Moreover, after addition of nPEX3 to PEX19-PEX26 with a molar ratio of 1:1, the size of an nPEX3-PEX19-PEX26 complex was assigned to 206.9 kDa (see Figure 6.1, C: a: PEX19, b: nPEX3 and e: PEX3-PEX19-PEX26). Therefore, the nPEX3 addition to the PEX19-PEX26 complex shifted the total size of the ternary complex by about 38 kDa indicating a more tightly assembled conformation than with the nPEX3-PEX19 complex (see Figure 6.1, D). Accordingly, we suggested that cargo loaded PEX19 (PEX19-PEX26) binds to its receptor protein PEX3 more tightly than PEX19 without cargo. However, the interactions between cargo (PEX26) and PEX19 get weaker over time resulting in a PEX3-PEX19 complex, which is more precisely explained by the equilibrium:



We assume that the nPEX3-PEX19 complex has a longer half-life than the PEX3-PEX19-PEX26 complex.

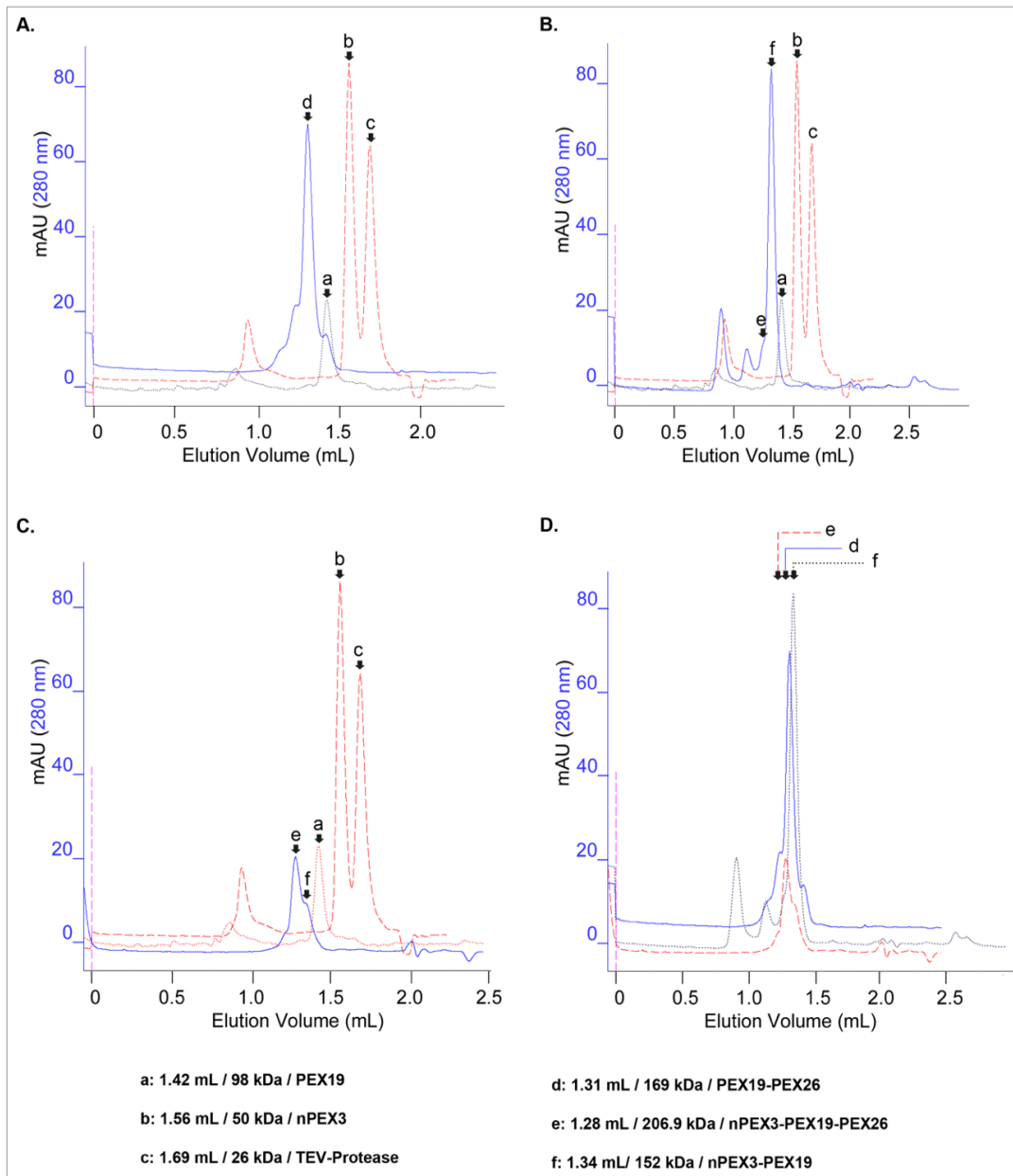


Figure 6.1: Comparisons of the SEC analysis of nPEX3, PEX19-PEX26 and nPEX3-PEX19-PEX26. Comparison of **[A]** PEX19-26(d) binary complex, **[B]** nPEX3-PEX19 complex formation (e and f), **[C]** ternary complex formation of nPEX3-PEX19-PEX26(e) through titration using a molar ratio of 1:1 with the monomeric nPEX3(b) and PEX19(a). **[D]** Comparison of all three heteromeric complexes of PEX19-26(e), nPEX3-PEX19(f) and nPEX3-PEX19-PEX26(d). The comparison of the elution volumes and corresponding masses of purified proteins and protein complexes: nPEX3-PEX19-PEX26: 206.9 kDa/1.28 mL, PEX19-PEX26: 169.1 kDa/1.31 mL and nPEX3: 50.4 kDa/1.56 mL. Molecular mass of the proteins PEX19: 32.8 kDa PEX26: 33.9 kDa, nPEX3: 39.6 kDa.

Moreover, we observed monomeric PEX19, as well as various high molecular sizes of PEX26 comprising 419 kDa and 241 kDa (see Section 5.2, Figure 5.3, C: peaks a and b) but not monomeric PEX26. Regarding this, a recent study suggests that PEX26 forms homodimers in the peroxisomal membrane after PEX19- and PEX3-mediated insertion^[63]. Accordingly, these dimers form further multi-subunit complexes with

PEX13, PEX14 and the PEX1-PEX6 AAA+ complex in the peroxisomal membrane. This study is in agreement with our observation that recombinant PEX26 forms high molecular aggregates in case PEX26 is not stabilised through PEX19.

As defined by the Kyte-Doolittle hydrophobicity scale, every amino acid has a hydropathy index, which can vary between -4.5 to 4.5 proportionally regarding their hydrophobicity. The GRAVY score is calculated by adding the hydropathy index for each amino acid and dividing it by the length of the sequence^[116]. As a TA membrane protein, PEX26 basically consist of three segments: firstly, a cytosolic N-terminal segment (aa 1-250), secondly a highly hydrophobic single-pass transmembrane segment (aa 251-269) and thirdly a hydrophilic luminal segment (aa 270-305)^[62, 133]. According to the positive GRAVY score of 0.047, full-length PEX26 is a highly hydrophobic membrane protein^[124]. This is in agreement with our observation that it is probably impossible to purify monomeric PEX26 in its full-length form (aa 1-305). In conclusion, we suggest that recombinant PEX26 is stabilised by PEX19 forming a heterodimeric binary complex from both monomeric proteins. SEC analysis showed an equilibrium of the binary complex formation $\text{PEX19-PEX26} \rightleftharpoons \text{PEX19} + \text{PEX26}$ (aggregates) (see Section 5.2, Figure 5.3, C: peaks a and b) which was further analysed using native-MS.

6.2. Native-MS confirms the binary PEX19-PEX26 complex

Further analysis of the complex using native-MS revealed its final stoichiometry supporting our hypothesis that recombinant PEX19 and PEX26 form a binary complex. However, we observed in one of two independent experiments a nonspecific 300 kDa-adduct of PEX19 and concluded that this as an adduct caused in the ionization step. A common phenomenon in native MS experiments is the formation of nonspecific adducts during ionization^[125]. Our explanation for this phenomenon is residual imidazole in the samples, which has a high gas basicity i.e. relative low gas acidity at the concentrations > 1 mM, and may lead to reduction in charge states of protein complex ions. This increases the kinetic stabilities of the protein complex and makes it more resistant to in-source dissociation^[134]. Furthermore, native-MS simulation of ternary complex formation between recombinant PEX3 and PEX19-PEX26 provided evidence that PEX19 binds favourably to PEX3 rather than to PEX26 (see Section 5.5, Figure 5.11) Based on this result we suggested the following equilibrium for PEX3, PEX19 and PEX26 complexes:

$n\text{PEX3} + \text{PEX19-PEX26} \rightleftharpoons \text{PEX19-PEX26} + n\text{PEX3-PEX19} + \text{PEX26 (degraded)}$

We simulated the relative intensities of PEX19-PEX26 in presence or absence of PEX3. Thereby, we observed approximately 83% decrease of PEX19-PEX26 upon PEX3 addition, based on two independent experiments (I: 80%, II: 87%) in average (see Figure 5.11). On one side, this simulation is based on relative intensities of ionized proteins considering the fact that ionization efficiency influences the acquired composition of proteins, thus, the peak intensities are not directly proportional to protein abundances in the samples. On the other side, since we based our simulation on the change of relative peak intensities of PEX19-PEX26 complex in presence or absence of PEX3, this experiment provides evidence regarding the complex kinetics in the peroxisomal membrane import machinery. In addition, protein interactions and complexes kinetics were already characterized using mass spectrometry^[135]. However, the mass spectrometry analysis of protein interactions gives reliable and reproducible results for some complexes, but not for all of them. Thus, these analyses in some of the cases are limited concerning its reliability and reproducibility^[125]. Therefore, our results represent a reproducible and reliable experiment which agree with data obtained with more established results regarding the PEX3, PEX19 and PEX26 complexes.

6.3. XL-MS reveals the interacting segments of the PEX19-PEX26 complex

In order to analyse the interacting segments of PEX19-PEX26 as well as of PEX3-PEX19, we employed the XL-MS method using an appropriate cross-linker, BS³ in our experiments. Chen et al. (2014), had previously characterized four further segments of PEX19, alpha-b, -c, -d and -e, which are highly conserved in human, yeast and *N.crassa*^[55]. This study had also characterized all these segments as well as alpha-1 regarding the hydrophobicity and acidity of residues within the segments. Accordingly, the segments comprising alpha-b, -c, -d, -e and -1 were classified as amphipathic, while alpha-a was acidic and hydrophobic, which was also the binding segment of PEX3. Moreover, they suggested that PEX19-dependent PMP import required alpha-d for insertion of TA proteins into peroxisomal membranes. Furthermore, Schueller et al. (2010), had reported that a PEX19 fragment comprising the segment 161-283 was sufficient for recognition of PEX26^[58]. Based on this, our XL-MS analysis revealed that seven residues of PEX19: G1, K34, K60, K90, K130, K138 and K245 were cross-linked to lysine at position 292 of PEX26 (Table 6.1). K292 is located on one of the predicted

binding site (BSII) of PEX19 in PEX26, which is also close neighbour to BSI including the TMS of PEX26, whereas six of seven PEX19 peptides are located to the flexible N-terminal half and one on the rigid core of PEX19^[58,62]. This means that all cross-linked residue pairs are located within the radius of 24 Å and accessible from the cross-linker BS³ in the binary complex of PEX19-PEX26^[104].

Accordingly, the first cross-links of PEX19 occurred at the N-terminus with the side chains of glycine, which was the residual amino acid after cleavage of *His*₆ from full length PEX19 and was not natively included in its sequence. The cross-linker BS³ reacts selectively with primary amines of lysines, as well as with the N-terminus of proteins. Therefore, this cross-linked residue indicated that the N-terminus of PEX19 is located within a radius of 24 Å and accessible for the cross-linker BS³ in the binary complex of PEX19-PEX26^[104]. The second cross-link occurred with a side chain of lysine on the alpha-a segment of PEX19. This segment is also included in the crystal structure of nPEX3^[28]. Chen et al. (2014), characterized this segment both, as partly hydrophobic and acidic^[55]. The third cross-link occurred with a side chain of lysine in the disordered segment of PEX19 between alpha a and very near of b, while the fourth one was directly on the segment alpha b. Moreover, Chen et al. (2014), characterized alpha-b as an amphipathic segment^[55]. This indicates clearly the participation of alpha-b with its hydrophobic side chains to the interaction of PEX26. The fifth cross-link of PEX19 occurred with a side chain of lysine on the alpha-d segment of PEX19. Alpha-d was characterized as an amphipathic segment and reported as a required segment for TA insertion into peroxisomal membranes^[55]. The sixth cross-link of PEX19 occurred with a side chain of lysine in the disordered segment of PEX19 between alpha d and e. Both segments were characterised as amphipathic. The last cross-link of PEX19 occurred with a side chain of lysin in the alpha-4 segment of PEX19. Alpha-4 was included in the crystal structure of PEX19^[58]. Moreover, the identified PMP binding pocket of PEX19 comprises a hydrophobic cavity, which was formed through participation of all four structurally clarified alpha-helices (alpha-1-4). Emmanouilidis et al. (2016), suggested that PMPs are stabilized in this hydrophobic cavity through interaction of their aliphatic groups with the farnesyl-rest of PEX19^[15]. Additionally, recent studies suggested that farnesylation is required for an efficient recognition of cargo proteins^[126]. Accordingly, we suggested that the flexible N-half of PEX19 participates strongly to stabilisation and insertion of PEX26 through hydrophobic interactions of its flexible N-half, i.e. alpha helices a-e. In addition, since the PEX19-

PEX26 complex was produced recombinantly in *E. coli*, our PEX19 is non-farnesylated. Based on this, we concluded that our XL-MS data are in accordance with all three studies and reveal the interacting segment within the flexible N-terminal half of PEX19 and PEX26, as shown in Table 6.1.

Table 6.1: The List of cross-linked peptides of the PEX19 and PEX26.

Segment (PEX19)	Position/ Peptide (PEX19)	Position/Peptide (PEX26)
N-terminus	1 / * G MAAAEEGCSVGAEADRELEELLESALDDFDK	292 / K AAF S R
alpha a	34 / AK P SPAPPSTTTAPDASGPQ K	292 / K AAF S R
near alpha a and b	61 / SPGD TAK DALFASQ EK	292 / K AAF S R
alpha b	90 / FFQELFDSELASQATAEF EKAMK	292 / K AAF S R
alpha d	131 / VGSDMTSQQEFTSCL K ETLSGLAK	292 / K AAF S R
near alpha d and e	139 / ETL SGLAK NATDLQNSSM S EEEL T K	292 / K AAF S R
alpha 4	246 / ICEQFEAETPTDSET TQK AR	292 / K AAF S R

Summary of the cross-linked peptides of PEX19 and PEX26 that were identified using *pLink*. The cross-linked peptides of PEX19 are classified based on putative and solved secondary structural elements including alpha-a, -b, d, e and -4. According to XL-MS experiments, PEX26 was could be cross-linked only at lysine 292, which is included in the peptide **KAAF****S****R**. All cross-linked lysine residues are shown in red. One of the cross-links of PEX19 occurs through a glycine (***G**) residue which is cross-linked through a primary amine due to the free N-terminus of PEX19 to residue lysine 292 of PEX26.

Additionally, PEX26 contains four lysines in PEX19-BS I and BSII (K253, K254, K282 and K292). Two of these (K253 and K254) are part of the TMS of PEX26, while the other two are in the PEX19-BSII of PEX26. Since cross-links of PEX26 only occurred on lysine 292 in the second PEX19 binding site (BSII), we concluded that the three remaining lysines in these regions were not accessible to our cross-linker BS³ or protected through a hydrophobic PEX19 interaction. However, this suggestion is limited to some extent, based to the fact that the residue pairs, which are located within the radius of 24 Å, were able to form cross-links through BS³ [104]. In conclusion, we propose a model of PEX26 import assembly based on our XL-MS data (see Figure 6.2) and showed that PEX19 and PEX26 form a binary complex. In addition, our results suggested that the farnesylation of PEX19 is not required for PEX26 stabilisation or recognition of membrane proteins.

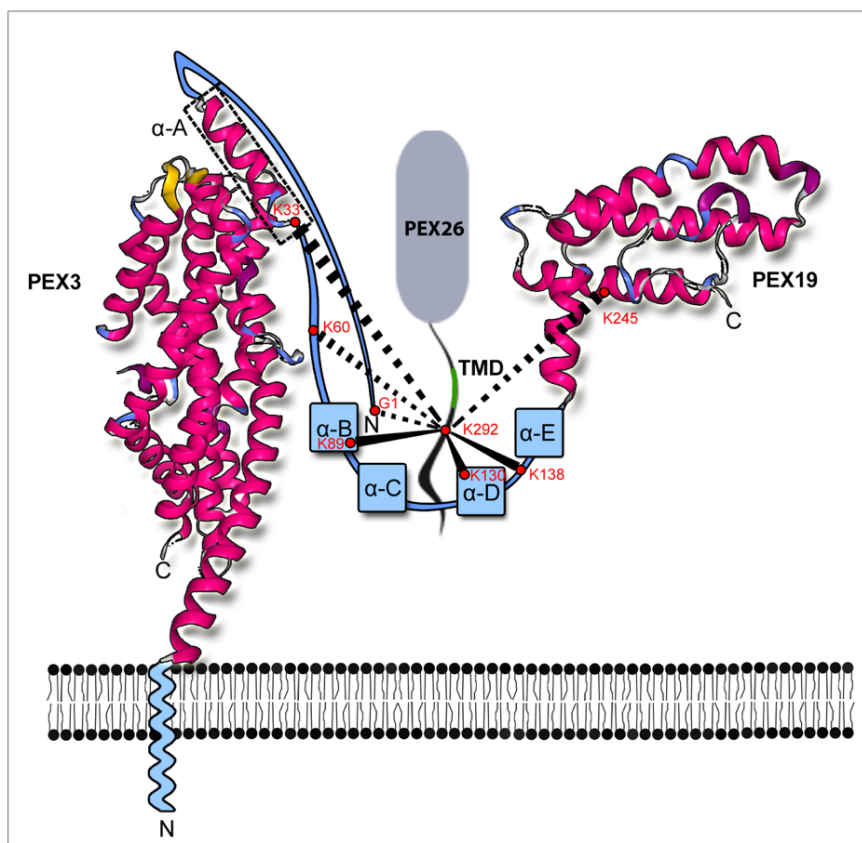


Figure 6.2: A proposed assembly model of the PEX26 import into the peroxisomal membrane. A representative model of PEX26 import through interactions of PEX3 and PEX19 based on the results of this study. PEX26 is a hydrophobic protein, which is stabilised already at translation step by its chaperone-like receptor protein PEX19. The cargo loaded PEX19 binds to its docking protein PEX3 to import PEX26 into the peroxisomal membrane. According to the Table 6.1, the cross-linked segments of PEX19 and PEX26 are shown using Fischer Projection. All cross-links have the same distance between two lysins, which corresponds to the length of the BS³ spacer as 11.4 Å, which used in cross-linking steps for XL-MS experiments. The purple coloured segments encompass the clarified structures of PEX19 and PEX3, while the blue segments illustrate unclarified structural elements of all three proteins.

Moreover, these results are in agreement with a recent study on PEX26, in which Guder et al. (2019) described the required segments for the PEX26-PEX19 interaction using BRET analysis. They identified two similar heptad-repeats segments, which are required for homo-oligomerization of PEX26 in the peroxisomal membrane. These two segments comprised amino acids 227-251 (motif 1) and amino acids 278-301 (motif 2). The TMS of PEX26 locates between these two segments. Furthermore, they reported that motif 1 was not required, while motif 2 was essential for the PEX19 interaction. Our XL-MS results also suggest that PEX19 is cross-linked to lysine 292 of PEX26, which is part of the identified motif 2.

6.4. The PEX19-PEX26 complex complemented PEX26-deficient cells

In order to analyse whether our binary complex comprising non-farnesylated PEX19 and PEX26 was functional in restoration of the multioligomeric exportomer complex comprising PEX1-PEX6 and PEX26, we subjected the complex to an import assay using PEX26-deficient fibroblasts from a patient with ZS phenotype (PBD059, assigned to CG8). This cell line showed the most severe defect in matrix protein import caused by a homozygous frame shift mutation at T77 of PEX26^[23].

Matsumoto et al. (2003) performed previously complementation studies using the CHO mutant PEX26-deficient cell line ZP167^[46]. The co-expression of *Flag-PEX26* and *PEX6-HA* in this cell line showed colocalisation of PEX6 with PEX26, but barely with PEX1^[46]. Weller et al. (2005) suggested that PEX26 binds PEX6 directly, while the PEX26 interaction to PEX1 occurs in a PEX6-dependent manner. Furthermore, PEX1 and PEX6 form a heterodimeric AAA ATPase complex, that regulated the recycling of PEX5 to the cytosol^[24]. Accordingly, PEX26 expression in ZP167 cells showed the same phenotype as wild-type CHO cells, indicating re-establishment of the export complex of PEX1 and PEX6 and thus successful EGFP-PTS1 import^[46]. In our complementation analysis regarding the peroxisomal matrix protein import (PTS1), we showed that the electroporation of cell line PBD059 with the purified binary PEX19-PEX26 complex was able to complement the PEX26-deficient cell line in same range as in the positive control group.

Based on the results from previous studies and from our analysis, we suggested that the binary complex formed through PEX19 stabilisation of PEX26 was able to insert PEX26 into the peroxisomal membrane. Thereby, PEX26 was able to recruit PEX6 and PEX1, respectively to the peroxisomal membrane re-establishing the multioligomeric exportomer complex consisting of PEX1, PEX6 and PEX26. The re-activated exportomer complex was able to export the ubiquitinated PEX5 to the cytosol, resulting in a continuation of matrix protein import into peroxisomes. However, a very recent study showed that a splice variant of PEX26 lacking the TMS was recruited to a PEX13-PEX14 complex in a PEX19-dependent manner without membrane insertion and thus the membrane insertion of PEX26 is not required for PEX6 and PEX1 recruitment to peroxisomal membranes^[63]. According to this study, the splice variant of PEX26 formed homodimers exposed to the cytosol. These dimers were able to recruit the PEX1-PEX6 complex to the peroxisomal membrane establishing the heterooligomeric exportomer complex. Since we elucidated the

membrane integration i.e. functionality of the full-length variant of PEX26 (TMS included), our results were not controversial to this study.

6.5. Flow cytometry indicates nPEX3^T-dependent PEX26 association with LUVs

In order to analyse the membrane insertion of PEX26 into LUVs, we designed an experiment with two main steps. First, we attached labelled (*Alexa488*) PEX3 to the LUVs, which consisted of 65.8% Egg-PC, 28.2% Egg-PE and 6% Ni-DGS. The reason, why we employed lipid-coupled Ni-NTA was the fact that our nPEX3^T was lacking the TMD. Full length PEX3 is not amenable to purification, therefore we used in our analysis a *His*₆ tagged PEX3₂₆₋₃₇₃ (nPEX3^T: Thx-His₆-Thr-TEV-nPEX3₂₆₋₃₇₃). To mimic a docking protein for membrane protein import, nPEX3^T was attached to the peroxisomal membrane through Ni-*His*₆-affinity (see Figure 6.3, A). We confirmed this step testing the FITC (Fluorescein isothiocyanate, Ex/Em: 495 nm/519 nm) intensity of LUVs before and after imidazole treatment. Accordingly, the FITC intensity changed from 85.8 % to 36.4% after imidazole treatment. This suggested that our nPEX3^T could bind to LUVs in an affinity dependent manner. However, we concluded that the imidazole treatment was not able to completely elute nPEX3^T from LUVs. We explained this difference with unspecific interactions of nPEX3^T with LUVs and with the residual FITC signal of untreated LUVs. Moreover, based on our experimental design the labelled nPEX3^T was only used to confirm binding to the LUVs. Since we only focused on the insertion of labelled PEX26 into LUVs and used unlabelled nPEX3^T in further steps of the experiment, the remaining PEX3 wasn't a factor which would interfere with the fluorescence results.

Secondly, in order to test if the binary complex formed through PEX19 stabilisation of PEX26 is able to insert PEX26 into liposomal membrane, we incubated the labelled binary complex with the LUVs attached to nPEX3^T (see Figure 6.3, B). Of note, since the PEX19-PEX26 binary complex is only amenable to be purified as a complex, the labelling using *Alexa488* involved both of the proteins. The calculated DOL of the proteins nPEX3^T and PEX19-PEX26 were calculated to 26% and 20 %, respectively. The second step of the analysis showed 84.4 % FITC intensity for LUVs coupled with labelled PEX19-PEX26 before and 53.1 % after imidazole treatment. This result suggested a 31.3 % reduction of the FITC signal which we explained through elution of unlabelled nPEX3^T together with bound PEX19-PEX26 or with labelled PEX19 after imidazole treatment. This is in agreement with previous studies that sPEX3

(PEX3₄₀₋₃₇₃) formed a very stable complex with PEX19^P(PEX19₁₄₋₃₃)^[28]. After evaluation of the flow cytometry analysis, we concluded that the remaining FITC signal of 53.1% originated from the LUVs bound to labelled PEX26 as well as to unspecific interactions of PEX19-PEX26 with LUVs. We quantified the FITC signal with 12.8 % from unspecific interactions (positive control group), in which we incubated LUVs only with labelled PEX19-PEX26 but not with the docking protein nPEX3^T. That means that 40.3 % of the FITC signal originated from LUVs coupled only with labelled PEX26 (or PEX26-PEX19). In conclusion, the contribution of nPEX3^T to PEX26 integration was significant using LUVs in a cell- and peroxisome-free system. However, the mode of PEX26 interaction with LUVs needed to be more precisely analysed.

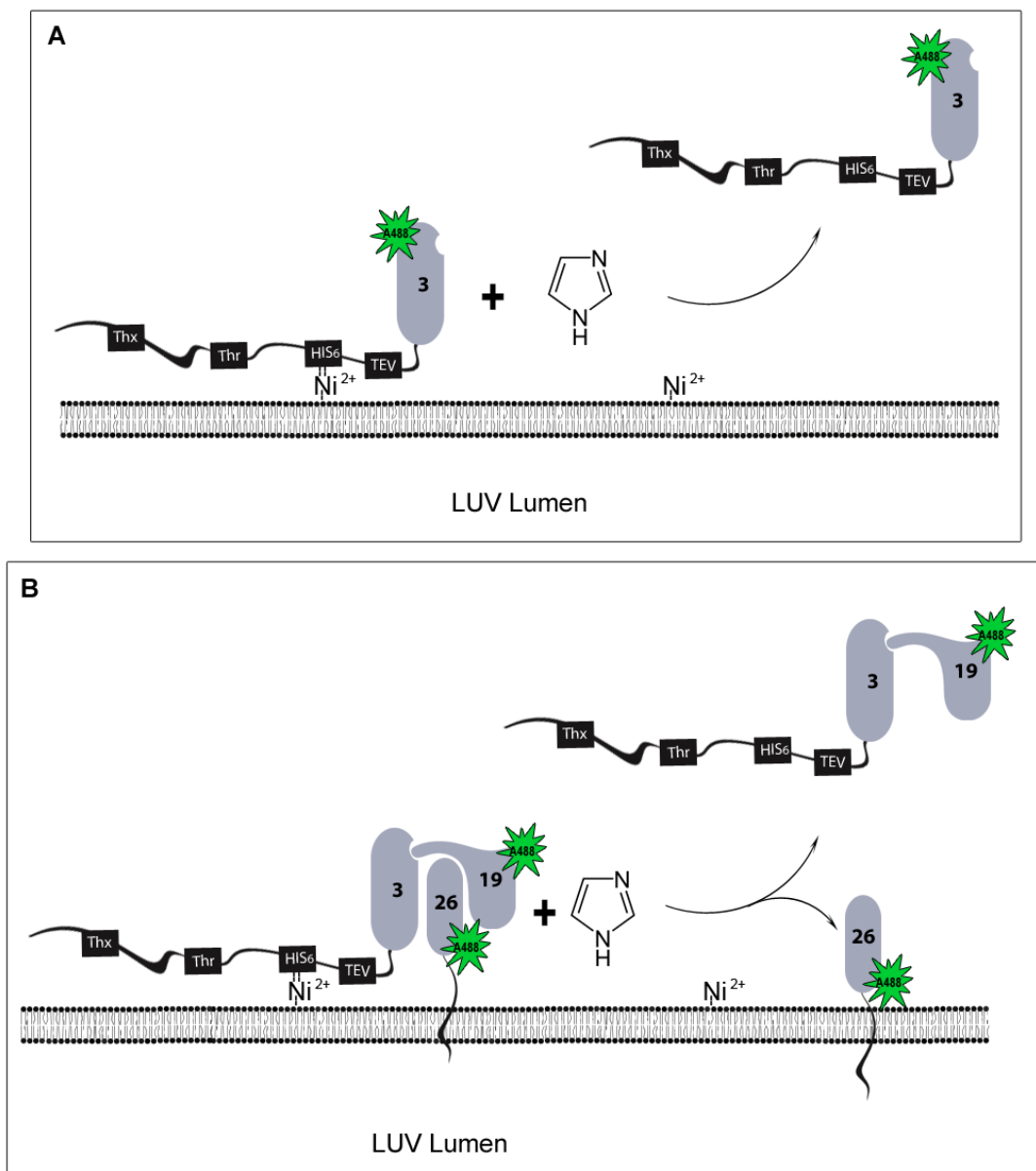


Figure 6.3: PEX26 integration into the LUV membrane using *His*₆-tagged PEX3 (nPEX3^T) as a docking protein The representation of PEX26 integration into the LUV (Ni²⁺) membrane as described in Section 5.8. In the first step **[A]**, labelled (A488) nPEX3^T (3) is attached to the

membrane through its *His*₆-tag affinity. In order to confirm this attachment, LUVs were treated with imidazole and measured before and after this treatment by flow cytometry analysis (B and C respectively, see Section 5.8). The uncoupled LUVs were used as a control for this step (A, see Section 5.8). In the second step **[B]**, LUVs attached with nPEX3^T (3) are coupled with the labelled (A488) PEX19-PEX26 complex (19 and 26) and treated with imidazole in order to release the PEX3-PEX19 complex from the LUV membrane (E and F respectively, see Section 5.8). After imidazole treatment, the remaining signal of labelled PEX26 was measured by flow cytometry. As a control for this step LUVs were coupled with the labelled PEX19-PEX26 complex without the step of nPEX3^T-attachment (D, see Section 5.8).

6.6. Carbonate extraction confirms PEX26 insertion into the LUV membrane

In order to further analyse the membrane association of PEX26, the LUVs from all steps including the negative and positive controls were subjected to carbonate extraction using ultracentrifugation. In the first part of the integration experiment, we attached nPEX3^T to the LUVs through *His*₆-Ni affinity and scrutinized this through imidazole elution. After carbonate extraction, we analysed the fractions using western blot analysis. Accordingly, the fractions including nPEX3^T or nPEX3^T coupled with PEX19-PEX26 contained nPEX3^T in the pellet fraction (see Section 5.9, Figure 5.20, B and E). Furthermore, the fraction including nPEX3^T coupled with PEX19-PEX26 that were treated with imidazole showed a nPEX3^T band only in the pellet fraction, but with less intensity in comparison to the previous step without imidazole treatment (see Section 5.9, Figure 5.20, F). This reduction provides evidence for the reversible mode of binding between nPEX3^T and LUVs through imidazole affinity. Moreover, the flow cytometry analysis confirmed this step through FITC signal reduction from 85.8 % to 36.4% after imidazole treatment. After confirmation of nPEX3^T-LUV attachment, in the second step, we examined the PEX26 insertion through carbonate extraction followed by western blot analysis (see Section 5.9, Figure 5.22). This blot comprises all experimental groups, including LUV attached to nPEX3^T as well as LUVs without nPEX3^T after PEX19-PEX26 incubation. According to this, we observed that PEX26 showed similar intensity levels in all three experimental groups. However, the intensity range was decreased in E, F and D, respectively. This indicated that nPEX3^T increased the association of PEX26 with the LUV membrane. This confirms the results of flow cytometry analysis as well. Regarding every individual experimental groups, PEX26 intensity increased in the supernatant fractions which were treated previously with Triton-X100, while it was unchanged in the supernatant fraction treated with Na₂CO₃, before. In conclusion, we suggested that PEX26, which was present as a complex with PEX19 was integrated into liposomal membranes in a nPEX3^T-dependent manner and

resistant to carbonate extraction. This result indicates a transmembrane integration of PEX26 into LUV membranes. This however, needs to be further confirmed also in respect of correct assembly and topology. Accordingly, a pegylation or IASD assay could be considered to elucidate the correctness of the PEX26 insertion, based on the cysteine (C263) in the TMS of PEX26. However, PEX26 is not a cysteine-less protein and contains six cysteines in total [137-138], that have to be mutated for further analysis by the pegylation or IASD assay. Furthermore, these mutations could affect the native conformation of PEX26 as well as its interaction with PEX19.

7. Outlook

PEX19 as a chaperone-like cytosolic PMP receptor, can stabilize PMPs during their translation *in vivo* [73]. This work demonstrates co-expression of recombinant *PEX19* and *PEX26* that gave rise to their native-like complex formation in *E. coli*. In addition, this complex could be purified for further structural and functional analysis. However, it was not amenable for X-ray crystallography analysis. Therefore, further approaches such as Nuclear Magnetic Resonance (NMR) analysis should be considered for a total clarification of the PEX19-PEX26 complex structure^[141]. This would also be helpful to provide more precise information about the PEX26 insertion into the peroxisomal membrane or for PEX3-PEX19-PEX26 assembly.

XL-MS Analysis of PEX19-PEX26 provided information about the assembly of the PEX19 and PEX26-segments and showed a high participation of PEX19-N-terminal half in this complex. Moreover, this information might be helpful as a supplement for prospective structural studies of the recombinant PEX19-PEX26 complex based on NMR or X-ray crystallography studies or for structural predictions.

The functional analysis using PEX26-deficient fibroblasts demonstrated that the recombinant PEX19-PEX26 complex able to restore peroxisomal matrix protein import through the PTS1 pathway. However, further import assays are required in order to confirm this for PTS2 pathway. Based on this, other PEX19-PMP candidates such as PEX2, PEX11, PEX13, PEX16, PMP22, PMP34 and PMP70 might be considered for further elucidation of functionality in our assay^[25-26]. This can also be considered for LUV integration experiments, in which our assay provided evidence about PEX26 integration into LUV membranes based on flow cytometry and carbonate extraction.

8 References

1. Rhodin J. (1954). Correlation of Ultrastructural Organization and Function in Normal and Experimentally Changed Proximal Tubule Cells of the Mouse Kidney. Doctorate. Thesis, Karolinska Institutet, Stockholm
2. De Duve C. The separation and characterization of subcellular particles. *Harvey Lect.* 1965;59:49-87.
3. Wanders RJ, Waterham HR. Biochemistry of mammalian peroxisomes revisited. *Annu Rev Biochem.* 2006;75:295-332.
4. Wiese S, Gronemeyer T, Ofman R, et al. Proteomics characterization of mouse kidney peroxisomes by tandem mass spectrometry and protein correlation profiling. *Mol Cell Proteomics.* 2007;6(12):2045-57.
5. El-bassyouni HT, Abdel maksoud SA, Salem FA, Badr el-deen R, Abdel aziz H, Thomas MM. Evidence of oxidative stress in peroxisomal disorders. *Singapore Med J.* 2012;53(9):608-14.
6. Schrader M, Fahimi HD. Peroxisomes and oxidative stress. *Biochim Biophys Acta.* 2006;1763(12):1755-66.
7. Islinger M, Voelkl A, Fahimi HD, Schrader M. The peroxisome: an update on mysteries 2.0. *Histochem Cell Biol.* 2018;150(5):443-471.
8. Schrader M, Fahimi HD. The peroxisome: still a mysterious organelle. *Histochem Cell Biol.* 2008;129(4):421-40.
9. Lachtermacher MB, Seuánez HN, Moser AB, Moser HW, Smith KD. Determination of 30 X-linked adrenoleukodystrophy mutations, including 15 not previously described. *Hum Mutat.* 2000;15(4):348-53.
10. Rezanka T. Very-long-chain fatty acids from the animal and plant kingdoms. *Prog Lipid Res.* 1989;28(3):147-87.

11. Wang B, Van veldhoven PP, Brees C, et al. Mitochondria are targets for peroxisome-derived oxidative stress in cultured mammalian cells. *Free Radic Biol Med.* 2013;65:882-894.
12. Wanders RJ, Ferdinandusse S, Brites P, Kemp S. Peroxisomes, lipid metabolism and lipotoxicity. *Biochim Biophys Acta.* 2010;1801(3):272-80.
13. Francisco T, Rodrigues TA, Dias AF, Barros-barbosa A, Bicho D, Azevedo JE. Protein transport into peroxisomes: Knowns and unknowns. *Bioessays.* 2017;39(10)
14. Braverman N, Dodt G, Gould SJ, Valle D. An isoform of pex5p, the human PTS1 receptor, is required for the import of PTS2 proteins into peroxisomes. *Hum Mol Genet.* 1998;7(8):1195-205.
15. Emmanouilidis L, Gopalswamy M, Passon DM, Wilmanns M, Sattler M. Structural biology of the import pathways of peroxisomal matrix proteins. *Biochim Biophys Acta.* 2016;1863(5):804-13.
16. Natsuyama R, Okumoto K, Fujiki Y (2013) Pex5p stabilizes Pex14p: a study using a newly isolated pex5 CHO cell mutant, ZPEG101. *Biochem J* 449: 195– 207. 16.
17. Shiozawa K, Konarev PV, Neufeld C, Wilmanns M, Svergun DI (2009) Solution structure of human Pex5-Pex14-PTS1 protein complexes obtained by small angle X-ray scattering. *J Biol Chem* 284: 25334–25342. 17.
18. Purdue PE, Yang X, Lazarow PB. Pex18p and Pex21p, a novel pair of related peroxins essential for peroxisomal targeting by the PTS2 pathway. *J Cell Biol.* 1998;143(7):1859-69.
19. MeineckeM, Cizmowski C, Schliebs W, Kruger V, Beck S, et al., (2010) The peroxisomal importomer constitutes a large and highly dynamic pore. *Nat Cell Biol* 12: 273–277. 19.

-
20. Eckert JH, Johnsson N. Pex10p links the ubiquitin conjugating enzyme Pex4p to the protein import machinery of the peroxisome. *J Cell Sci.* 2003;116(Pt 17):3623-34.
21. Agne B, Meindl NM, Niederhoff K, et al. Pex8p: an intraperoxisomal organizer of the peroxisomal import machinery. *Mol Cell.* 2003;11(3):635-46.
22. Tamura S, Matsumoto N, Takeba R, Fujiki Y. AAA peroxins and their recruiter Pex26p modulate the interactions of peroxins involved in peroxisomal protein import. *J Biol Chem.* 2014;289(35):24336-46.
23. Weller S, Cajigas I, Morrell J, et al. Alternative splicing suggests extended function of PEX26 in peroxisome biogenesis. *Am J Hum Genet.* 2005;76(6):987-1007.
24. Saffert P, Enenkel C, Wendler P. Structure and Function of p97 and Pex1/6 Type II AAA+ Complexes. *Front Mol Biosci.* 2017;4:33.
25. Sacksteder, K.A., J.M. Jones, S.T. South, X. Li, Y. Liu, and S.J. Gould. 2000. PEX19 binds multiple peroxisomal membrane proteins, is predominantly cytoplasmic, and is required for peroxisome membrane synthesis. *J. Cell Biol.* 148:931–944.
26. Jones JM, Morrell JC, Gould SJ. PEX19 is a predominantly cytosolic chaperone and import receptor for class 1 peroxisomal membrane proteins. *J Cell Biol.* 2004;164(1):57-67.
27. Brosius U, Gärtner J. Cellular and molecular aspects of Zellweger syndrome and other peroxisome biogenesis disorders. *Cell Mol Life Sci.* 2002;59(6):1058-69.
28. Schmidt F, Treiber N, Zocher G, et al., Insights into peroxisome function from the structure of PEX3 in complex with a soluble fragment of PEX19. *J Biol Chem.* 2010;285(33):25410-7.
29. Lazarow P.B., Y. Fujiki, Biogenesis of peroxisomes, *Annu. Rev. Cell Biol.* 1 (1985) 489–530.

-
30. Sugiura A, Mattie S, Prudent J, McBride HM. Newly born peroxisomes are a hybrid of mitochondrial and ER-derived pre-peroxisomes. *Nature*. 2017;542(7640):251-254.
31. Schrader M, Costello JL, Godinho LF, Azadi AS, Islinger M. Proliferation and fission of peroxisomes - An update. *Biochim Biophys Acta*. 2016;1863(5):971-83.
32. Cichocki BA, Krumpke K, Vitali DG, Rapaport D. Pex19 is involved in importing dually targeted tail-anchored proteins to both mitochondria and peroxisomes. *Traffic*. 2018;19(10):770-785.
33. Jansen RLM, Van der klei IJ. The peroxisome biogenesis factors Pex3 and Pex19: multitasking proteins with disputed functions. *FEBS Lett*. 2019;593(5):457-474.
34. Agrawal G, Shang HH, Xia ZJ, Subramani S. Functional regions of the peroxin Pex19 necessary for peroxisome biogenesis. *J Biol Chem*. 2017;292(27):11547-11560.
35. Gabaldón T. Peroxisome diversity and evolution. *Philos Trans R Soc Lond, B, Biol Sci*. 2010;365(1541):765-73.
36. Lowe M, Barr FA. Inheritance and biogenesis of organelles in the secretory pathway. *Nat Rev Mol Cell Biol*. 2007;8(6):429-39.
37. Hua R, Kim PK. Multiple paths to peroxisomes: Mechanism of peroxisome maintenance in mammals. *Biochim Biophys Acta*. 2016;1863(5):881-91.
38. Smith JJ, Aitchison JD. Peroxisomes take shape. *Nat Rev Mol Cell Biol*. 2013;14(12):803-17.
39. Kim P. Peroxisome Biogenesis: A Union between Two Organelles. *Curr Biol*. 2017;27(7):R271-R274.
40. Hua R, Gidda SK, Aranovich A, Mullen RT, Kim PK. Multiple Domains in PEX16 Mediate Its Trafficking and Recruitment of Peroxisomal Proteins to the ER. *Traffic*

-
41. Steinberg SJ, Dodt G, Raymond GV, Braverman NE, Moser AB, Moser HW. Peroxisome biogenesis disorders. *Biochim Biophys Acta*. 2006;1763(12):1733-48.
42. Fujiki Y, Yagita Y, Matsuzaki T. Peroxisome biogenesis disorders: molecular basis for impaired peroxisomal membrane assembly: in metabolic functions and biogenesis of peroxisomes in health and disease. *Biochim Biophys Acta*. 2012;1822(9):1337-42.
43. Corzo D, Gibson W, Johnson K, et al. Contiguous deletion of the X-linked adrenoleukodystrophy gene (ABCD1) and DXS1357E: a novel neonatal phenotype similar to peroxisomal biogenesis disorders. *Am J Hum Genet*. 2002;70(6):1520-31.
44. Itzkovitz B, Jiralerspong S, Nimmo G, et al. Functional characterization of novel mutations in GNPAT and AGPS, causing rhizomelic chondrodysplasia punctata (RCDP) types 2 and 3. *Hum Mutat*. 2012;33(1):189-97.
45. Fujiki Y. Peroxisome biogenesis and human peroxisome-deficiency disorders. *Proc Jpn Acad, Ser B, Phys Biol Sci*. 2016;92(10):463-477.
46. Matsumoto N, Tamura S, Furuki S, et al. Mutations in novel peroxin gene PEX26 that cause peroxisome-biogenesis disorders of complementation group 8 provide a genotype-phenotype correlation. *Am J Hum Genet*. 2003;73(2):233-46.
47. Dodt G, Gould SJ. Multiple PEX genes are required for proper subcellular distribution and stability of Pex5p, the PTS1 receptor: evidence that PTS1 protein import is mediated by a cycling receptor. *J Cell Biol*. 1996;135(6 Pt 2):1763-74.
48. Ghaedi K, Honsho M, Shimozawa N, Suzuki Y, Kondo N, Fujiki Y. PEX3 is the causal gene responsible for peroxisome membrane assembly-defective Zellweger syndrome of complementation group G. *Am J Hum Genet*. 2000;67(4):976-81.
49. Matsuzono Y, Kinoshita N, Tamura S, et al. Human PEX19: cDNA cloning by functional complementation, mutation analysis in a patient with Zellweger syndrome, and potential role in peroxisomal membrane assembly. *Proc Natl Acad Sci USA*. 1999;96(5):2116-21.

50. Mariappan M, Mateja A, Dobosz M, Bove E, Hegde RS, Keenan RJ. The mechanism of membrane-associated steps in tail-anchored protein insertion. *Nature*. 2011;477(7362):61-6.
51. Borgese N, Brambillasca S, Soffientini P, Yabal M, Makarow M. Biogenesis of tail-anchored proteins. *Biochem Soc Trans*. 2003;31(Pt 6):1238-42.
52. Wang F, Brown EC, Mak G, Zhuang J, Denic V. A chaperone cascade sorts proteins for posttranslational membrane insertion into the endoplasmic reticulum. *Mol Cell*. 2010;40(1):159-71.
53. Costello JL, Schrader M. Unloosing the Gordian knot of peroxisome formation. *Curr Opin Cell Biol*. 2018;50:50-56.
54. Costello JL, Castro IG, Camões F, et al. Predicting the targeting of tail-anchored proteins to subcellular compartments in mammalian cells. *J Cell Sci*. 2017;130(9):1675-1687.
55. Chen Y, Pieuchot L, Loh RA, et al., Hydrophobic handoff for direct delivery of peroxisome tail-anchored proteins. *Nat Commun*. 2014;5:5790.
56. Horie C, Suzuki H, Sakaguchi M, Mihara K. Characterization of signal that directs C-tail-anchored proteins to mammalian mitochondrial outer membrane. *Mol Biol Cell*. 2002;13(5):1615-25.
57. Kuroda R, Ikenoue T, Honsho M, Tsujimoto S, Mitoma JY, Ito A. Charged amino acids at the carboxyl-terminal portions determine the intracellular locations of two isoforms of cytochrome b5. *J Biol Chem*. 1998;273(47):31097-102.
58. Schueller N, Holton SJ, Fodor K, et al., The peroxisomal receptor Pex19p forms a helical mPTS recognition domain. *EMBO J*. 2010;29(15):2491-500.
59. Hattula K, Hirschberg D, Kalkkinen N, Butcher SJ, Ora A. Association between the intrinsically disordered protein PEX19 and PEX3. *PLoS ONE*. 2014;9(7):e103101.

-
60. Imanaka T., Shinina Y., Takano Y., Hashimoto T., Osumi T., Insertion of the 70kDa peroxisomal membrane protein into peroxisomal membrane in vivo and in vitro, *J. Biol. Chem.*, 271: 3706-3713, 1996
61. Diestelkötter P., Just W.W., In vitro insertion of the 22kDa peroxisomal membrane protein into isolated rat liver peroxisomes., *J. Biol. Chem.*, 123: 1717-1725, 1993
62. Halbach A, Landgraf C, Lorenzen S, et al., Targeting of the tail-anchored peroxisomal membrane proteins PEX26 and PEX15 occurs through C-terminal PEX19-binding sites. *J Cell Sci.* 2006;119(Pt 12):2508-17.
63. Guder P, Lotz-havla AS, Woidy M, et al. Isoform-specific domain organization determines conformation and function of the peroxisomal biogenesis factor PEX26. *Biochim Biophys Acta Mol Cell Res.* 2019;1866(3):518-531.
64. Yagita Y, Hiromasa T, Fujiki Y. Tail-anchored PEX26 targets peroxisomes via a PEX19-dependent and TRC40-independent class I pathway. *J Cell Biol.* 2013;200(5):651-66.
65. Rao M, Okreglak V, Chio US, Cho H, Walter P, Shan SO. Multiple selection filters ensure accurate tail-anchored membrane protein targeting. *Elife.* 2016;5
66. Chio US, Cho H, Shan SO. Mechanisms of Tail-Anchored Membrane Protein Targeting and Insertion. *Annu Rev Cell Dev Biol.* 2017;33:417-438.
67. Costello JL, Zalckvar E, Kemp S, et al. Peroxisomes: new insights into protein sorting, dynamics, quality control, signalling and roles in health and disease. *Histochem Cell Biol.* 2019;151(4):283-289.
68. Borgese N, Fasana E. Targeting pathways of C-tail-anchored proteins. *Biochim Biophys Acta.* 2011;1808(3):937-46.
69. Soukupova M, Sprenger C, Gorgas K, Kunau WH, Dodt G. Identification and characterization of the human peroxin PEX3. *Eur J Cell Biol.* 1999;78(6):357-74.A,

70. Shimozawa N, Tsukamoto T, Suzuki Y, Orii T, Fujiki Y. Animal cell mutants represent two complementation groups of peroxisome-defective Zellweger syndrome. *J Clin Invest.* 1992;90(5):1864-70.
71. Schmidt F, Dietrich D, Eylestein R, Groemping Y, Stehle T, Dodt G. The role of conserved PEX3 regions in PEX19-binding and peroxisome biogenesis. *Traffic.* 2012;13(9):1244-60.
72. Mayerhofer PU, Kattenfeld T, Roscher AA, Muntau AC. Two splice variants of human PEX19 exhibit distinct functions in peroxisomal assembly. *Biochem Biophys Res Commun.* 2002;291(5):1180-6.
73. Shibata H., Kashiwayama Y., Imanaka T., Kato H. Domain architecture and activity of human Pex19p, a chaperone-like protein for intracellular trafficking of peroxisomal membrane proteins. *J. Biol. Chem.* 2004;279:38486–38494.
74. Emmanouilidis L, Schütz U, Tripsianes K, et al. Allosteric modulation of peroxisomal membrane protein recognition by farnesylation of the peroxisomal import receptor PEX19. *Nat Commun.* 2017;8:14635.
75. Fransen M, Wylin T, Brees C, Mannaerts GP, Van veldhoven PP. Human pex19p binds peroxisomal integral membrane proteins at regions distinct from their sorting sequences. *Mol Cell Biol.* 2001;21(13):4413-24.
76. Nyathi Y, Wilkinson BM, Pool MR. Co-translational targeting and translocation of proteins to the endoplasmic reticulum. *Biochim Biophys Acta.* 2013;1833(11):2392-402.
77. Nilsson I, Lara P, Hessa T, Johnson AE, Von heijne G, Karamyshev AL. The code for directing proteins for translocation across ER membrane: SRP cotranslationally recognizes specific features of a signal sequence. *J Mol Biol.* 2015;427(6 Pt A):1191-201.

78. Ngosuwan J, Wang NM, Fung KL, Chirico WJ. Roles of cytosolic Hsp70 and Hsp40 molecular chaperones in post-translational translocation of presecretory proteins into the endoplasmic reticulum. *J Biol Chem*. 2003;278(9):7034-42.
79. Kohl C, Tessarz P, Von der malsburg K, Zahn R, Bukau B, Mogk A. Cooperative and independent activities of Sgt2 and Get5 in the targeting of tail-anchored proteins. *Biol Chem*. 2011;392(7):601-8.
80. Chartron JW, Suloway CJ, Zaslaver M, Clemons WM. Structural characterization of the Get4/Get5 complex and its interaction with Get3. *Proc Natl Acad Sci USA*. 2010;107(27):12127-32.
81. Borgese N, Coy-vergara J, Colombo SF, Schwappach B. The Ways of Tails: the GET Pathway and more. *Protein J*. 2019;38(3):289-305.
82. Abell BM, Pool MR, Schlenker O, Sinning I, High S. Signal recognition particle mediates post-translational targeting in eukaryotes. *EMBO J*. 2004;23(14):2755-64.
83. Mayerhofer PU, Bañó-polo M, Mingarro I, Johnson AE. Human Peroxin PEX3 Is Co-translationally Integrated into the ER and Exits the ER in Budding Vesicles. *Traffic*. 2016;17(2):117-30.
84. Lee J, Kim DH, Hwang I. Specific targeting of proteins to outer envelope membranes of endosymbiotic organelles, chloroplasts, and mitochondria. *Front Plant Sci*. 2014;5:173.
85. Hillenkamp F, Tsarbopoulos A, Gross ML. Focus on desorption ionization and macromolecular mass spectrometry. *J Am Soc Mass Spectrom*. 2008;19(8):1041-4.
86. Lindenstrauss AG, Pavlovic M, Bringmann A, Behr J, Ehrmann MA, Vogel RF. Comparison of genotypic and phenotypic cluster analyses of virulence determinants and possible role of CRISPR elements towards their incidence in *Enterococcus faecalis* and *Enterococcus faecium*. *Syst Appl Microbiol*. 2011;34(8):553-60.

-
87. Borgese N, Brambillasca S, Colombo S. How tails guide tail-anchored proteins to their destinations. *Curr Opin Cell Biol.* 2007;19(4):368-75.
88. Mann M, Wilm M. Error-tolerant identification of peptides in sequence databases by peptide sequence tags. *Anal Chem.* 1994;66(24):4390-9.
89. Hernández H, Robinson CV. Determining the stoichiometry and interactions of macromolecular assemblies from mass spectrometry. *Nat Protoc.* 2007;2(3):715-26.
90. Morgner N, Robinson CV. Massign: an assignment strategy for maximizing information from the mass spectra of heterogeneous protein assemblies. *Anal Chem.* 2012;84(6):2939-48.
91. Marty MT, Baldwin AJ, Marklund EG, Hochberg GK, Benesch JL, Robinson CV. Bayesian deconvolution of mass and ion mobility spectra: from binary interactions to polydisperse ensembles. *Anal Chem.* 2015;87(8):4370-6.
92. Susa AC, Xia Z, Tang HYH, Tainer JA, Williams ER. Charging of Proteins in Native Mass Spectrometry. *J Am Soc Mass Spectrom.* 2017;28(2):332-340.
93. Wells JM, Mcluckey SA. Collision-induced dissociation (CID) of peptides and proteins. *Meth Enzymol.* 2005;402:148-85.
94. Benesch JL, Robinson CV. Mass spectrometry of macromolecular assemblies: preservation and dissociation. *Curr Opin Struct Biol.* 2006;16(2):245-51.
95. Fan SB, Meng JM, Lu S, et al. Using pLink to Analyze Cross-Linked Peptides. *Curr Protoc Bioinformatics.* 2015;49:8.21.1-19.
96. Leitner A, Walzthoeni T, Kahraman A, et al. Probing native protein structures by chemical cross-linking, mass spectrometry, and bioinformatics. *Mol Cell Proteomics.* 2010;9(8):1634-49.

-
97. Rivera-santiago RF, Sriswasdi S, Harper SL, Speicher DW. Probing structures of large protein complexes using zero-length cross-linking. *Methods*. 2015;89:99-111.
98. Mullis K, Faloona F, Scharf S, Saiki R, Horn G, Erlich H. Specific enzymatic amplification of DNA in vitro: the polymerase chain reaction. *Cold Spring Harb Symp Quant Biol*. 1986;51 Pt 1:263-73.
99. Sanger F. Determination of nucleotide sequences in DNA. *Biosci Rep*. 1981;1(1):3-18.
100. Cuatrecasas P, Wilchek M, Anfinsen CB. Selective enzyme purification by affinity chromatography. *Proc Natl Acad Sci USA*. 1968;61(2):636-43.
101. Smith PK, Krohn RI, Hermanson GT, et al. Measurement of protein using bicinchoninic acid. *Anal Biochem*. 1985;150(1):76-85.
102. Laemmli UK. Cleavage of structural proteins during the assembly of the head of bacteriophage T4. *Nature*. 1970;227(5259):680-5.
103. Renart J, Reiser J, Stark GR. Transfer of proteins from gels to diazobenzylxymethyl-paper and detection with antisera: a method for studying antibody specificity and antigen structure. *Proc Natl Acad Sci USA*. 1979;76(7):3116-
104. Leitner A, Walzthoeni T, Aebersold R. Lysine-specific chemical cross-linking of protein complexes and identification of cross-linking sites using LC-MS/MS and the xQuest/xProphet software pipeline. *Nat Protoc*. 2014;9(1):120-37.
105. Kim JA, Cho K, Shin MS, et al. A novel electroporation method using a capillary and wire-type electrode. *Biosens Bioelectron*. 2008;23(9):1353-60.
106. Osborn M, Weber K. Immunofluorescence and immunocytochemical procedures with affinity purified antibodies: tubulin-containing structures. *Methods Cell Biol*. 1982;24:97-132.

-
107. Wozniak-knopp G, Bartl S, Bauer A, et al. Introducing antigen-binding sites in structural loops of immunoglobulin constant domains: Fc fragments with engineered HER2/neu-binding sites and antibody properties. *Protein Eng Des Sel.* 2010;23(4):289-97.
108. Schmidt C, Robinson CV. A comparative cross-linking strategy to probe conformational changes in protein complexes. *Nat Protoc.* 2014;9(9):2224-36.
109. Givan AL. Flow cytometry: an introduction. *Methods Mol Biol.* 2011;699:1-29.
110. Harding SE, Horton JC, Jones S, Thornton JM, Winzor DJ. COVOL: an interactive program for evaluating second virial coefficients from the triaxial shape or dimensions of rigid macromolecules. *Biophys J.* 1999;76(5):2432-8.
111. Goto Y, Calciano LJ, Fink AL. Acid-induced folding of proteins. *Proc Natl Acad Sci USA.* 1990;87(2):573-7.
112. Hermanson GT. *Bioconjugate techniques.* Academic Press; San Diego: 1996.
113. Picot J, Guerin CL, Le van kim C, Boulanger CM. Flow cytometry: retrospective, fundamentals and recent instrumentation. *Cytotechnology.* 2012;64(2):109-30.
114. Fujiki Y, Hubbard AL, Fowler S, Lazarow PB. Isolation of intracellular membranes by means of sodium carbonate treatment: application to endoplasmic reticulum. *J Cell Biol.* 1982;93(1):97-102.
115. Harris ES, Rouiller I, Hanein D, Higgs HN. Mechanistic differences in actin bundling activity of two mammalian formins, FRL1 and mDia2. *J Biol Chem.* 2006;281(20):14383-92.
116. Kyte J, Doolittle RF. A simple method for displaying the hydropathic character of a protein. *J Mol Biol.* 1982;157(1):105-32.

117. Matsuzono Y, Fujiki Y. In vitro transport of membrane proteins to peroxisomes by shuttling receptor Pex19p. *J Biol Chem.* 2006;281(1):36-42.
118. Pinto MP, Grou CP, Fransen M, Sá-miranda C, Azevedo JE. The cytosolic domain of PEX3, a protein involved in the biogenesis of peroxisomes, binds membrane lipids. *Biochim Biophys Acta.* 2009;1793(11):1669-75.
119. Kebarle, P., Verkerk, U.H.: Electrospray: from ions in solutions to ions in the gas phase, what we know now. *Mass Spectrom. Rev.* 28, 898–917 (2009)
120. Mann K, Edsinger E. The *Lottia gigantea* shell matrix proteome: re-analysis including MaxQuant iBAQ quantitation and phosphoproteome analysis. *Proteome Sci.* 2014;12:28.
121. UniProt: a worldwide hub of protein knowledge. *Nucleic Acids Res.* 2019;47(D1):D506-D515.
122. Purcell S, Neale B, Todd-brown K, et al., PLINK: a tool set for whole-genome association and population-based linkage analyses. *Am J Hum Genet.* 2007;81(3):559-75.
123. Basiji DA, Ortyn WE, Liang L, Venkatachalam V, Morrissey P. Cellular image analysis and imaging by flow cytometry. *Clin Lab Med.* 2007;27(3):653-70, viii.
124. Wilkins MR, Gasteiger E, Bairoch A, et al. Protein identification and analysis tools in the ExPASy server. *Methods Mol Biol.* 1999;112:531-52.
126. Rucktäschel R, Thoms S, Sidorovitch V, et al. Farnesylation of pex19p is required for its structural integrity and function in peroxisome biogenesis. *J Biol Chem.* 2009;284(31):20885-96.
127. Kane JF. Effects of rare codon clusters on high-level expression of heterologous proteins in *Escherichia coli*. *Curr Opin Biotechnol.* 1995;6(5):494-500.
2015;16(8):832-52.

-
128. Höhfeld J, Veenhuis M, Kunau WH. PAS3, a *Saccharomyces cerevisiae* gene encoding a peroxisomal integral membrane protein essential for peroxisome biogenesis. *J Cell Biol.* 1991;114(6):1167-78.
129. Will GK, Soukupova M, Hong X, et al. Identification and characterization of the human orthologue of yeast Pex14p. *Mol Cell Biol.* 1999;19(3):2265-77.
131. Bianchi AA, Baneyx F. Hyperosmotic shock induces the sigma32 and sigmaE stress regulons of *Escherichia coli*. *Mol Microbiol.* 1999;34(5):1029-38.
132. Gardner BM, Castanzo DT, Chowdhury S, et al. The peroxisomal AAA-ATPase Pex1/Pex6 unfolds substrates by processive threading. *Nat Commun.* 2018;9(1):135.
133. Fujiki Y, Nashiro C, Miyata N, Tamura S, Okumoto K. New insights into dynamic and functional assembly of the AAA peroxins, Pex1p and Pex6p, and their membrane
134. Hunter CL, Mauk AG, Douglas DJ. Dissociation of heme from myoglobin and cytochrome b5: comparison of behavior in solution and the gas phase. *Biochemistry.* 1997;36(5):1018-25.
135. Bich C, Baer S, Jecklin MC, Zenobi R. Probing the hydrophobic effect of noncovalent complexes by mass spectrometry. *J Am Soc Mass Spectrom.* 2010;21(2):286-9.
136. Berman HM, Westbrook J, Feng Z, et al. The Protein Data Bank. *Nucleic Acids Res.* 2000;28(1):235-42.
137. Krumpke K, Rapaport D. An assay to monitor the membrane integration of single-span proteins. *Methods Mol Biol.* 2013;1033:301-6.
138. Howe V, Brown AJ. Determining the Topology of Membrane-Bound Proteins Using PEGylation. *Methods Mol Biol.* 2017;1583:201-210.

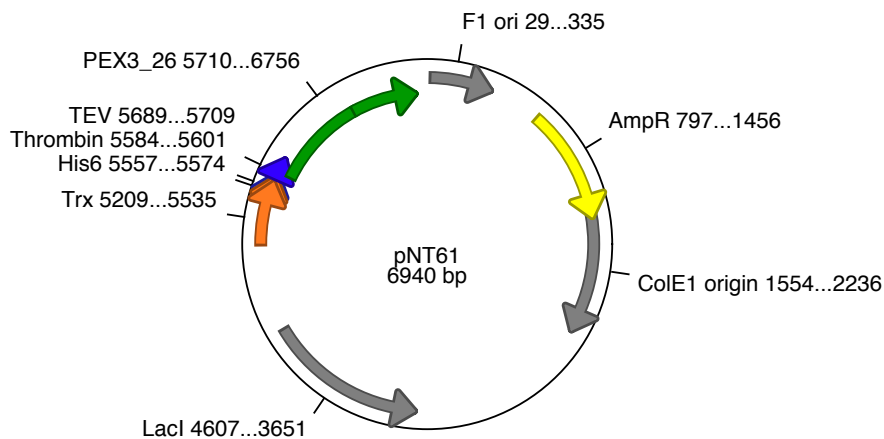
139. Buentzel J, Vilardi F, Lotz-havla A, Gärtner J, Thoms S. Conserved targeting information in mammalian and fungal peroxisomal tail-anchored proteins. *Sci Rep.* 2015;5:17420.
140. Schuldiner M, Metz J, Schmid V, et al. The GET complex mediates insertion of tail-anchored proteins into the ER membrane. *Cell.* 2008;134(4):634-45.
141. Göbl C, Madl T, Simon B, Sattler M. NMR approaches for structural analysis of multidomain proteins and complexes in solution. *Prog Nucl Magn Reson Spectrosc.* 2014;80:26-63.
142. González flecha FL. Kinetic stability of membrane proteins. *Biophys Rev.* 2017;9(5):563-572.
143. Sharon M, Robinson CV. The role of mass spectrometry in structure elucidation of dynamic protein complexes. *Annu Rev Biochem.* 2007;76:167-93

9. Appendix

9.1. pNT61: PEX3(26-373) in pET32a

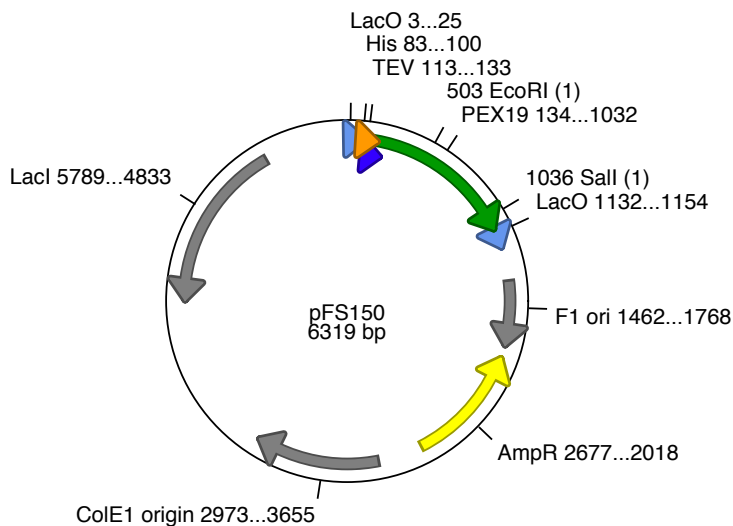
Protein Sequence: NH₂-[Trx-His₆-Thr-TEV-PEX3₂₆₋₃₇₃]-COOH

Mutation: C235S



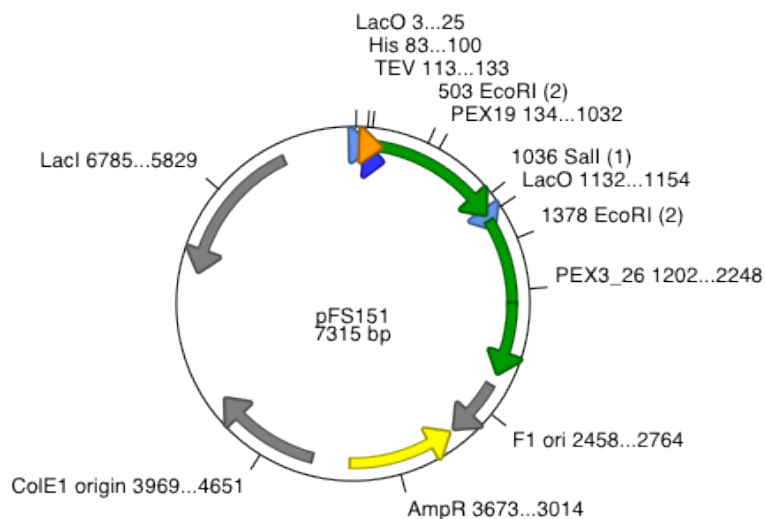
9.2. pFS150: PEX19(1-299) in pETDuet

Protein Sequence: NH₂-[His₆-TEV-PEX19₁₋₂₉₉]-COOH



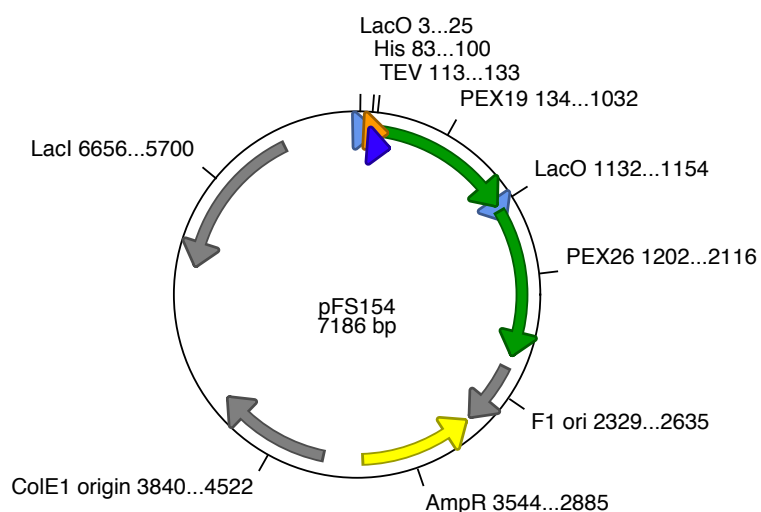
9.3. pFS151: PEX19(1-299)-PEX3(26-373) in pETDuet

Protein Sequence: NH₂-[His₆-TEV-PEX19₁₋₂₉₉]-[PEX3₂₆₋₃₇₃]-COOH



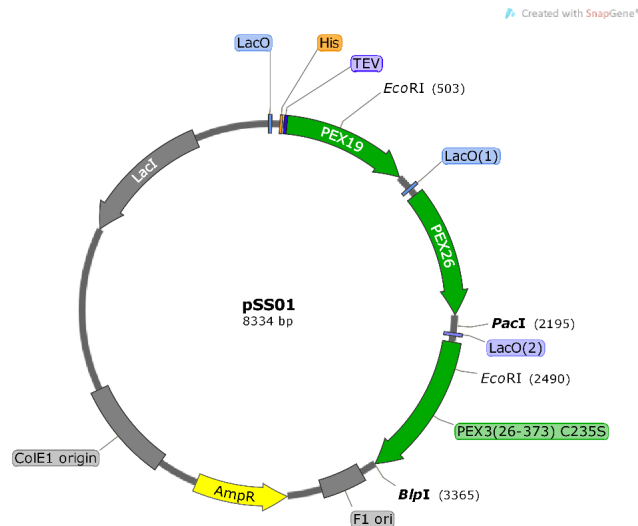
9.4. pFS154: PEX19(1-299)-PEX26(1-305) in pETDuet

Protein Sequence: NH₂-[His₆-TEV-PEX19₁₋₂₉₉]-[PEX26₁₋₃₀₅]-COOH



9.5 pSS01: PEX19(1-299)-PEX26(1-305)- PEX3(26-373) in pETDuet

Protein Sequence: NH₂-[His₆-TEV-PEX19₁₋₂₉₉]-[PEX26₁₋₃₀₅]-[PEX3₂₆₋₃₇₃]-COOH



9.6 PEX3_HUMAN

MLRSVWNFLKRHKKKCIFLGTVLGGVYILGKYGQKKIREIQEREA AEYIAQARRQYH
 FESNQRTCNMTVLSMLPTLREALMQQLNSESLTALLKNRPSNKLEIWEDLKII SFTRS
 TVAVYSTCMLVLLRVQLNIIGGYIYLDNAAVGKNGTTILAPPDVQQQYLSSIQHLLG
 DGLTELITVIKQAVQKVLGSVSLKHSLSLLDLEQKLKEIRNLVEQHKSSSWINKDGSK
 PLLCHYMPDEETPLAVQACGLSPRDITTIKLLNETRDMLESPDFSTVLNTCLNRGF
 SRLLDNMAEFFRPTEQDLQHGNSMNSLSSVSLPLAKIPIVNGQIH SVCSETPSHFV
 QDLLTMEQVKDFAANVYEFSTPQQLEK^[121]

9.7 nPEX^T (Trx-His6-Thr-TEV-nPEX3)

MSDKIIHLTDDSFDTDVLKADGAILVDFWAEWCGPCKMIAPILDEIADEYQGKLTVAK
 LNIDQNP GTAPKYGIRGIPTLLLFKNGEVAATKVGALSKGQLKEFLDANLAGSGSGH
 MHHHHHSSGLVPRGSGMKETA AAKFERQHMDSPDLGTD DDDKAMENLYFQGV
 YILGKYGQKKIREIQEREA AEYIAQARRQYHFESNQRTCNMTVLSMLPTLREALMQQ
 LNSESLTALLKNRPSNKLEIWEDLKII SFTRSTVAVYSTCMLVLLRVQLNIIGGYIYLD
 NAAVGKNGTTILAPPDVQQQYLSSIQHLLGDGLTELITVIKQAVQKVLGSVSLKHSL
 LLDLEQKLKEIRNLVEQHKSSSWINKDGSKPLLSHYMPDEETPLAVQACGLSPRDI

TTIKLLNETRDMLESPDFSTVLNNTCLNRGFSRLLDNMAEFFRPTEQDLQHGNMNS
LSSVSLPLAKIPIVNGQIHSVCSETPSHFVQDLLTMEQVKDFAANVYEFSTPQQLE
K^[121]

9.8 nPEX (PEX3_{25(G*)-373})

G*VYILGKYGQKKIREIQEREA AEYIAQARRQYHFESNQRTCNM TVLSMLPTLREAL
MQQLNSESLTALLKNRPSNKLEIWEDLKII SFTRSTVAVYSTCMLVLLRVQLNIIGGY
IYLDNAAVGKNGTTILAPPDVQQQYLSSIQHLLGDGLTELITVIKQAVQKVLGVSLSK
HLSLLDLEQKLKEIRNLVEQHKSSSWINKDGSKPLL SHYMMMPDEETPLAVQACGL
SPRDITTIKLLNETRDMLESPDFSTVLNNTCLNRGFSRLLDNMAEFFRPTEQDLQHGN
SMNSLSSVSLPLAKIPIVNGQIHSVCSETPSHFVQDLLTMEQVKDFAANVYEFSTP
QQLEK^[121] * Residue due to TEV-protease cleavage.

9.9 PEX19_HUMAN

MAAAEEGCSVGAEADRELEELLESALDDFDKAKPSPAPPSTTTAPDASGPQKRSP
GDTAKDALFASQEKFQELFDSELASQATAEF EKAMKELAE EEPHLVEQFQKLSEA
AGRVGSDMTSQQEFTSCLKETLSGLAKNATDLQNSSMSEEELTKAMEGLGMDEG
DGEGNILPIMQSIMQNLLSKDVL YPSLKEITEKYPEWLQSHRESLPPEQFEKYQEQH
SVMCKICEQFEAETPTDSETTQKARFEMVLDLMQQQLQDLGHPPKELAGEMPPGLN
FDLDALNLSGPPGASGEQCLIM^[121]

9.10 PEX26_HUMAN

MKSDSSTSAAPLRGLGGPLRSSEPVRAPARAPAVDLL EEAADLLVHLD FRAALE
TCERAWQSLANHAVA EEPAGTSLEVKCSLCVVG IQALAEMDRWQEVLSWVLQYYQ
VPEKLPPKVLELCILLYSKMQEPGAVLDVVGAWLQDPANQNLPEYGALAEFHVQRV
LLPLGCLSEAEELVVGSAAFGEERRLDVLQAIHTARQQKQEHS GSEEAQKPNLEG
SVSHKFLSLPMLVRQLWDSAVSHFFSLPFKKSLLAALILCLLVVRFDPASPSSLHFLY
KLAQLFRWIRKAAFSRLYQ LRIRD^[121]

Table 9.1: Q-TOF Ultima and Synapt G1 Settings

Setting	Q-ToF Ultima	Synapt G1
Acceleration	200	-
Acceleration1	-	50-70
Acceleration2	-	150-200
Analyser	-	V mode
Aperture1	0	0
Aperture2	-	70-100
Aperture3	15	-
Bunching Factor	4-7 4	at max. $m/z > 4000$
Capillary	1.3	1.3
Collision Energy	30	-
Collision Energy Trap	-	30
Collision Energy Transfer	-	30
Cone Gas Flow	20-40	80
Detector / MCP	2100	1750
Extraction Cone	-	3
Entrance	65	75
Ion Energy	1.4-2	1
Offset 1	-1.3	-
RF lens 1	120	-
RF lens 2	0	-
Sampling Cone	60-80	60
Source Temperature[°C]	20	20
Source Gas Flow[ml/min]	-	30
Transfer DC Entrance	-	5
Transfer DC Exit	-	15
Transport	3	-
Transport1	-	70
Transport2	-	70
Trap DC Bias	-	15
Trap DC Entrance	-	5
Trap DC Exit	-	5
Trap Gas Flow[ml/min]	-	3
Tube lens	150	-

Table 9.2: HPLC gradient for MS analysis

	QExactive™Plus				Orbitrap™XL			
Solvent A	0.1% FA				4% DMSO, 0.1% FA			
Solvent B	86% MeCN, 0.1%FA				48% MeOH, 30% MeCN, 4% DMSO, 0.1% FA			
	In-gel		In-solution		AP-MS		In-gel	
	Retention time[^l min]	Solvent B[^l %]	Retention time[^l min]	Solvent B[^l %]	Retention time[^l min]	Solvent B[^l %]	Retention time[^l min]	Solvent B[^l %]
	0	4	0	4	0	4	0	1
	5	4	5	4	25	4	5	1
	35	40	140	39	75	40	35	65
	10	95	155	54	80	95	40	95
	45	95	160	95	85	95	45	95
	46	4	165	95	86	4	46	1
	60	4	166	4	100	4	60	1
			180	4				

Table 9.3: Proteomic analysis instrument parameters

Setting	QExactive™Plus	Orbitrap™XL
Source voltage	1.5 kV	1.5 kV
Capillary temperature	200°C	200°C
MS mass-range	375-1750 <i>m/z</i>	375-1750 <i>m/z</i>
Resolution	70000 at 200 <i>m/z</i>	60000
AGC target MS	3 10 ⁶	5 10 ⁵
Max. Injection time MS	60 ms	500 ms
MSMS fragmentation	HCD	CID
Normalised collision energy	28	35
AGC target MS2	1 10 ⁵	3 10 ⁴
Max. Injection time MS2	120 ms	100 ms
Isolation width	3 <i>m/z</i> , cross-links 2 <i>m/z</i>	2 <i>m/z</i>
Resolution MS2	35000	-
Dynamic exclusion time	45 sec	45 sec
Min charge allowed	2	2

Table 9.4: *pLink* cross-link search parameters

Setting	Value
enzyme.name	Trypsin
max_miss_site	3
mod.fixed.total	1
mod.fixed.1	Carbamidomethyl_C
mod.variable.total	1
mod.variable.1	_Oxidation_M_15.995
linker.total	1
linker.name1	BS ³
peptide_tol_total	1
peptide_tol1	2
peptide_tol_type1	Da
peptide_tol_base1	1.500000
peptide_tol_base_type1	Da
filter_peptide_tol_base	0,1.0028,2.0056,3.0084
filter_peptide_tol_lb	-8,-8,-8,-8
filter_peptide_tol_ub	8,8,8,8
filter_peptide_tol_type	ppm
evaluate_max	1

Acknowledgments

First and foremost, I would like to extend my deepest gratitude to my research guide Prof. Dr. Gabriele Dodt for introducing me to this exciting field of science and supporting me during these five years. She has given me invaluable guidance and all the freedom to pursue my research. I have learnt extensively from her, including how to raise new possibilities how to reach a problem by systematic thinking. Every time, many insightful and long discussions with her have promoted a shift in my analytical mindset, which I would be able to put into practice in my future scientific employment as well as in my private life.

My special word of thanks should go to my research co-guide Prof. Dr. Dirk Schwarzer offering his guidance, time and support throughout the review of this work.

I also wish to thank the members of my dissertation committee: Prof. Dr. Doron Rapaport and Prof. Dr. Ralf Jansen for generously offering their valuable time and effort to be members of my doctoral examination committee.

Special thanks to my colleague Saroj Pandey for his continuous collaborations during the laboratory experiments and commenting on earlier versions of the thesis and helping with the final preparations.

I would also like to express my gratitude to all members of Stehle's Group for giving me the possibility to use their analytical instruments as well as for their advices and help.

A special thanks to my friends: Ömer Ünal, Gülhanım Yerlikaya and Cansu Doğan for their help and moral support.

I owe my deepest gratitude to my brother Ersoy for his support, patience and sacrifice during these five years. Without him, I would not have been able to complete what I have done and become who I am.

My heartfelt thanks to my mother Emine and my father Cemil for their indirect contributions giving me love and moral support. They were always there for me during these five years, when I got any difficulties or whenever I needed it the most.

I would like to dedicate this work to my grandfather Ali Biçer, who has died on 6 February 2017. Without his love I would not be where I am today. His love and wisdom will accompany me in every stage of my life.

This is for you Dede!

Erman Koçak

Curriculum Vitae**Personal Information**

Name: Erman

Surname: Koçak

Date of Birth: 05.07.1982

Country of Birth: Turkey

Citizenship: German

E-mail: ermankocak@gmail.com

Education**09/2002- 07/2007**

Bachelor of Science Biochemistry

Ege University, Turkey

Bachelor Thesis: An amperometric biosensor for hydrogen peroxide (H₂O₂) based on Immobilization of Horseradish Peroxidase

08/2008-10/2009

German language preparation for DSH.

04/2010- 03/2013

Master of Science Biochemistry

University of Marburg, Germany

Master thesis: Study on proteomics of nematode membrane proteins by mass spectrometry identification in the laboratory of Prof. Dr. Günter Lochnit, Protein Analytic, University of Giessen

04/ 2014- 09/2019

PhD Candidate

University of Tübingen, Germany

Insight into the Intermolecular Interactions and Functionality of the Recombinant PEX19-PEX26 Complex

Zusammenfassung

Peroxisomale Membranproteine (PMPs) fungieren in verschiedenen Prozessen als Membranrezeptoren oder Dockingproteine. Sie sind in Peroxisomen hauptsächlich für den Import von Metaboliten und Matrixproteinen sowie für den Export des zytosolischen Importrezeptors PEX5 zuständig. PEX3 als eines der PMPs der Klasse II, dient als Dockingprotein für PEX19 in der peroxisomalen Membran. Das Fehlen von PEX3 oder PEX19 verursacht einen Verlust von Peroxisomen oder peroxisomalen „remnants“ und führt zum Abbau oder zur Fehllokalisierung von PMP auf andere Organellen wie zum Beispiel Mitochondrien. Hierbei, PEX19 ist ein „chaperone-Like“ Rezeptor für neu synthetisierte PMPs der Klasse I und sorgt dafür, dass PMPs an die peroxisomale Membrane dirigiert werden. Beispiele hierfür sind die PMPs, PMP22, PMP34 und PMP70 die am Transport von Metaboliten beteiligt sind oder die PMPs, PEX2, PEX10, PEX12 und PEX13, die das membranverankerte Docking-Translocation-Modul (DTM) für den Importrezeptor PEX5 bilden. Außerdem ist PEX19 durch den Import von PEX26 in die peroxisomale Membrane auch für Aufbau des Rezeptorexportmoduls (REM) essentiell.

PEX26 als eines dieser „tail-anchored“ PMPs fungiert im Export von PEX5, indem es den AAA-ATPase-Komplex (PEX1-PEX6) an die peroxisomale Membran rekrutiert und dadurch das REM bildet. Der Verlust an AAA-ATPase in *HeLa*-Zellen führt zur Anhäufung von monoubiquitiniertem PEX5, wodurch der Import von Matrixproteinen beeinträchtigt wird. Phänotypisch führt ein Mangel an PEX26 in Patienten der Komplementationsgruppe 8 zu einem Zellweger-Syndrom, das als die schwerwiegendste Form der peroxisomalen Erkrankungen gilt.

Die Überexpression von *PEX26-cDNA* in *E. coli* führte zu unlöslichem oder aggregiertem PEX26. Im Gegensatz dazu ergab dessen Co-Expression mit PEX19 einen stabilen und löslichen binären Komplex.

In der vorliegenden Arbeit wurden PEX19 und PEX26 als ein nativer und binärer Komplex durch ein Zwei-Promotor-*E.-coli*-System hergestellt und aufgereinigt. Dies lieferte uns einen nativen PEX19-PEX26 Komplex, der durch Gelfiltration und native MS analysiert werden konnte. Darüber hinaus haben wir interagierenden Segmente dieses binären Komplexes durch XL-MS unter Verwendung eines Cross-Linker, BS³ identifiziert. Dies ermöglichte uns die Nachbarschaft interagierender Segmente aufzuzeigen. Hinsichtlich der Funktionalität haben wir gezeigt, dass dieser binäre Komplex den Matrixproteinimport *in vivo* in PEX26-defizienten Fibroblasten

wiederherstellen konnte. Des Weiteren wurde PEX26 erfolgreich in die Ni-NTA-LUVs integriert, die zuvor mit nPEX3^T (Thx-His₆-Thr-TEV-nPEX3) gekoppelt wurden. Eine anschließende Analyse mittels Durchflusszytometrie ergab, dass nPEX3^T effektiv zur Integration von PEX26 in die LUV-Membrane beitrug. Die Membranassoziation von PEX26 wurde mittels Carbonatextraktion getestet und zeigte eine Integration von PEX26 in die LUVs.

